

A Measurement of $\Upsilon(1S)$, $\Upsilon(2S)$, and $\Upsilon(3S)$ Polarization at CDF

James Thome, James Russ¹

Carnegie Mellon University, USA

Abstract

Measurements of $\Upsilon(nS)$ polarization have been made, using 4.9 fb^{-1} of data obtained by the CDF II detector at the Tevatron. The analysis is performed in the s-channel helicity frame on Υ mesons having rapidity $|y| < 0.6$ and $2 < p_T \leq 40 \text{ GeV}/c$ via the decay channel $\Upsilon(nS) \rightarrow \mu^+ \mu^-$. A template method is used to correct for acceptance and trigger effects. The $\Upsilon(1S)$ polarization is small and longitudinal at low p_T . It is consistent with a constant at all p_T . The $\Upsilon(2S)$ and $\Upsilon(3S)$ behaviors are similar to each other within statistics. Both have small polarization at low p_T and move toward transverse polarization in the bin with $p_T > m(\Upsilon)$.

Contents

1	Introduction	2
1.1	Υ Spin Alignment and Decay Angular Distributions	4
2	Dataset and Event Selection	4
2.1	Υ Candidate Selection	5
2.2	Duplicate events	5
2.3	Υ Dimuon Triggers	5
3	Simulation	6
3.1	Monte Carlo Generation	6
3.2	Acceptance and Efficiency	6
3.3	Monte Carlo re-weighting	7
3.4	Angular Binning and p_T Resolution	9
3.5	Test of Monte Carlo using μ^+ distribution s in p_T and η	10

¹jthome@fnal.gov, russ@fnal.gov

4	$\Upsilon(nS)$ Polarization Analysis	11
4.1	Υ Mass PDFs from Simulation	12
4.2	Υ Mass Fits	13
4.2.1	Modifying the Monte Carlo Mass Fits	13
4.2.2	Angular Distributions and Yields	13
4.3	Υ Polarization Fitter	14
4.4	Toy Monte Carlo Tests of Fitter	15
4.5	$\Upsilon(nS)$ Polarization Results	15
4.5.1	$\Upsilon(1S)$ Polarization	15
4.5.2	$\Upsilon(2S)$ and $\Upsilon(3S)$ Polarization	16
5	Systematics	16
6	Comparison with Other Measurements	19
7	Summary	19
8	Appendix A - Details of Monte Carlo Mass Fits	57
9	Monte Carlo mass fit Results	58
10	Appendix B Signal and Background Yield Tables	64

1 Introduction

Vector meson production and polarization in hadronic collisions is usually discussed within the framework of non-relativistic QCD (NRQCD), following the Tevatron Run I observations of surprisingly large production cross sections for all three vector mesons J/ψ , $\psi(2S)$, and Υ . This theoretical framework separates the heavy flavor production into a perturbative short-distance process to produce the $Q\bar{Q}$ pair times a long-distance matrix element to create the vector meson (or, more generally, any quarkonium state). The short-distance process can include color-octet $Q\bar{Q}$ contributions as well as color singlet configurations because the long-distance matrix elements can absorb soft gluon emission terms. This *factorization* hypothesis lies at the core of the NRQCD analysis [1]. The long-distance part is expanded in powers of the heavy quark velocities, using the vacuum expectation values of appropriate 4-fermion operators with parametrized coefficients. These coefficients are *universal* in that they are the same for all quarkonium states. Fixing them from data in one process leads to predictions valid in all other quarkonium production processes.

Using the degrees of freedom available in the parametrization, NRQCD calculations can fit the Tevatron production cross sections for the three vector mesons [2, 4]. However, the theory predicts that vector meson polarization should become transverse

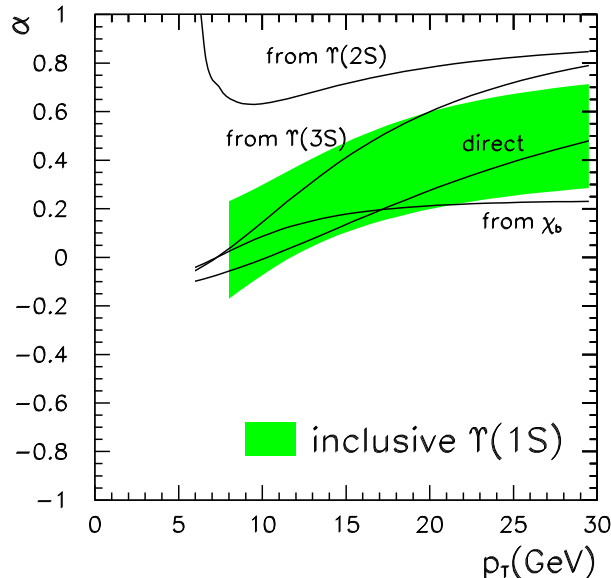


Figure 1: NRQCD prediction for $\Upsilon(1S)$ prompt polarization, including feed-down from higher bottomonium states.

in the perturbative regime, i.e., for large transverse momentum p_T of the vector meson. Recent CDF measurements of polarization for J/ψ and $\psi(2S)$ do not support this prediction [5, 11]. Other measurements, e.g., the fixed-target production ratio for the p-wave states χ_1/χ_2 [?] or J/ψ photoproduction at HERA [?], do not match NRQCD predictions well. Some theorists have proposed a different NRQCD expansion for c-quark states and b-quark states [6]. The NRQCD predictions for Υ polarization for Tevatron Run I, including feed-down effects from higher charmonium states, from Braaten and Lee [9] are shown in Figure 1.

Recently, different models of production that emphasize higher-order processes have been invoked to explain the vector meson production data. A model invoking a tower of gluon processes, leading to a sum of NLO amplitudes that enhances the LO color singlet amplitude, has been proposed [3]. This model gives a qualitative description of the CDF Run II measurements for J/ψ and $\psi(2S)$ production and polarization. A new color singlet calculation including terms up to α_S^5 has been used to model $\Upsilon(1S)$ production and polarization [7]. One of the features of this model is that the Υp_T will be balanced by one or more gluon jets.

All authors agree that polarization and production information on the Υ family are essential tests of NRQCD and alternative production models. This note describes the first step in that procedure for CDF data - a measurement of the $\Upsilon(nS)$ production polarization.

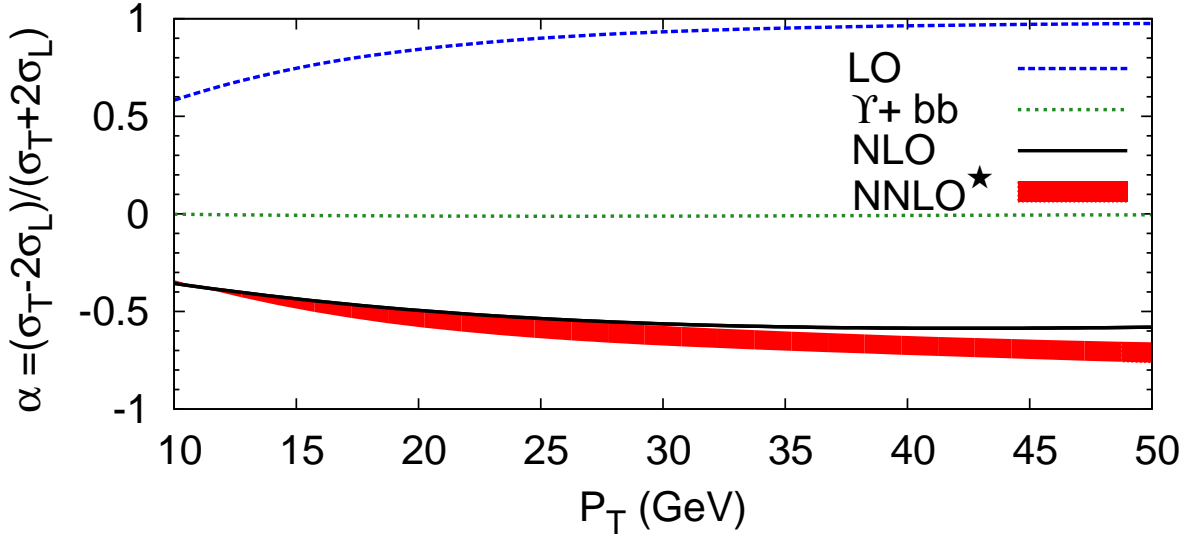


Figure 2: Color Singlet Model prediction for $\Upsilon(1S)$ prompt polarization, including NNLO terms from multigluon processes.

1.1 Υ Spin Alignment and Decay Angular Distributions

This analysis, like all proton collider polarization analyses to date, uses a quantization axis defined in the s-channel helicity frame. In this frame, the quantization axis is defined as the negative of the boost direction that takes the Υ from the laboratory frame to its rest frame, i.e., the negative of the Υ direction in the lab.

In the rest frame of the Υ meson, the μ^+ makes an angle θ^* with respect to the Υ direction in the lab frame. The angular distribution depends on the polarization parameter α , which lies in the interval -1 to 1 :

$$\frac{d\Gamma}{d\cos\theta^*} \propto 1 + \alpha \cos^2\theta^*. \quad (1)$$

If the Υ meson is fully polarized in the transverse direction, $\alpha = 1$. If it is fully aligned longitudinally, $\alpha = -1$. In our later discussion we use a related alignment parameter η that measures the fraction of longitudinal alignment. The two parameters are simply related:

$$\eta = \frac{1 - \alpha}{3 + \alpha} \quad (0 \leq \eta \leq 1). \quad (2)$$

2 Dataset and Event Selection

The $\Upsilon(nS)$ analysis uses data from runs 184062-287261, comprising 4.9 fb^{-1} of data. We omit runs prior to 184062 due to lower COT efficiency prior to the introduction of

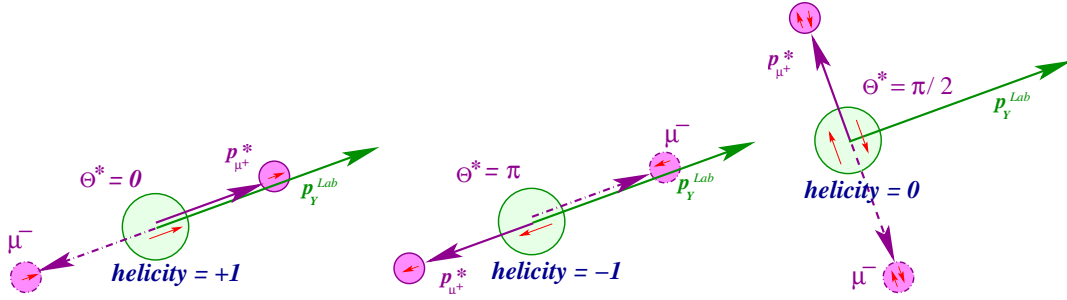


Figure 3: The diagrams of polarization angles with three different helicity states. When the helicity states are equally populated, Υ mesons have zero polarization. The little arrow on the top of each particle indicates its spin alignment.

oxygen into the gas mix, based on the polarization fluctuations seen in the J/ψ analysis documented in cdf8212. Runs are required to have 'good' status for COT, CMU, and CMP systems in the good run database produced by the DQM group. Other systems, including silicon and calorimeters, are not required to be marked 'good.'

2.1 Υ Candidate Selection

Candidate events are reconstructed using COT tracks linked to muon segments, both in Monte Carlo and data. Silicon hits are not required on the muons. Candidate events in data and Monte Carlo are required to pass the standard set of selection cuts for COT tracks and muon identification, described in detail in the Monte Carlo section below.

2.2 Duplicate events

Some events contain multiple combinations of tracks whose reconstructed masses fall within the appropriate range and which pass all the cuts required for Υ candidates. In these cases, like-signed muons from each event are compared and if they fall inside an isolation cone of radius 0.2, the second candidate using that track is considered a clone and is dropped. This occurs in less than 1% of events. If there are multiple muons in an event, each different combination of tracks in an event is tested against all trigger conditions. If it passes and is not classified as a clone of another event, that combination is treated as a valid Υ candidate and kept.

2.3 Υ Dimuon Triggers

This analysis utilizes only the UPSILON_CMUP_CMU trigger path to select Υ candidates. At L1, L1_TWO_CMU1.5_PT1.5 requires that two CMU muons have $p_T > 1.5\text{GeV}/c$ with a separation of two trigger towers if both muons are on the same side. The current L2 trigger, L2_CMUP1.5_PT3_&_CMU1.5_PT1.5 requires that at least one of the muons is a CMUP muon with $p_T > 3\text{GeV}/c$. Prior to Run 181839, L2

was set to automatically accept events passing L1, but as mentioned in section 2, we do not use date prior to Run 184062. The L3 trigger applied for this study is L3_UPSILON_CMUP_CMU. At this level, a CMUP muon is required to have $p_T > 4\text{GeV}/c$ and $\Delta x < 15\text{ cm}$. The other muon is required to have $p_T > 3\text{GeV}/c$ and $\Delta x < 30\text{ cm}$. Furthermore, the two-track mass is required to be between 8.0 and 12.0 GeV/c^2 and the muons are required to have opposite charge. When applying cuts to emulate the L3 trigger, we increase minimum p_T requirements by 0.05 GeV/c above the nominal trigger thresholds to reduce turn-on effects.

3 Simulation

This analysis utilizes a set of Monte Carlo templates which represent the shapes of purely transverse or longitudinal distributions as they would be observed by CDF. The acceptance and efficiency of the CDF apparatus act to modify the angular distribution and yield of Υ mesons. These effects vary with spin alignment. For these reasons, the template method employed in this analysis accounts for any such effects by applying the CDF detector simulation, production, and data-driven trigger efficiency function to the Monte Carlo events before the polarization fitter compares the distributions with data. The data-driven CMU trigger efficiency developed for the $B^0 \rightarrow \mu^+\mu^-$ search is applied in the construction of the templates to account for CDF dimuon trigger efficiencies [10]. The CMP efficiency measurement is described later in this note.

3.1 Monte Carlo Generation

The CDF simulation package, MCProduction, is used for Monte Carlo generation. Events are generated using FAKEEV according to a flat $p_T(\Upsilon)$ spectrum in each of several bins (eight, four, and four bins for $\Upsilon(1S)$, $\Upsilon(2S)$, and $\Upsilon(3S)$, respectively) covering the region $2 \leq p_T \leq 40$. The specific bin boundaries are listed in various tables, e.g., Table 5. The Υ events are generated flat in rapidity for $|y| < 0.8$ and uniform in ϕ . The generated Υ is decayed using the EvtGen package with a fully transverse (T) or fully longitudinal (L) polarization. Having been decayed, the events are passed to CDFSIM and Production to simulate detector response and reconstruction effects. The number of events generated per $p_T(\Upsilon)$ bin is the same for both polarizations. Differences in acceptance for T and L polarizations cause Monte Carlo yields for each template to be somewhat different.

3.2 Acceptance and Efficiency

Trigger effects modify the decay angular distribution of real events, and we utilize the data-driven trigger efficiency functions from the $B^0 \rightarrow \mu^+\mu^-$ search to incorporate such effects into the simulation. These functions characterize the efficiencies of dimuon and single-muon triggers as a function of trigger type and run number, as well as the type, p_T , η , and ϕ of each muon. Because the dimuon efficiencies provided in that study are

not tested for dimuon masses $> 6\text{GeV}/c^2$, we use the product of the two muons' L1 single-muon efficiencies. The two muons come from the decay of a high mass state, so there is very little chance that they will sample the same COT cell and have a correlated inefficiency. These efficiencies have been calculated using the CMU only, and because we utilize a CMUP trigger, we calculate an additional efficiency for the CMP and apply it in the same way. We find that the CMP efficiency is flat in η and varies with p_T as demonstrated in Figures 4 and 5. We fit the μ^+ and μ^- distributions separately, finding the PDFs in Equations 3 and 4 best describe CMP efficiency functions. Each event in our Monte Carlo sample is tested against the CMU and CMP efficiency functions and is kept or thrown out based on the calculated efficiency. Because these functions are based on muons with p_T less than $35\text{ GeV}/c$, we treat any muon with p_T in excess of that value as having exactly $35\text{ GeV}/c$ to avoid potentially nonphysical behavior of the efficiency function. The number of events for which this is an issue is vanishingly small.

$$\epsilon_{\mu^+}(p_T) = (0.969 + 0.0023 \times p_T + 0.000071 \times p_T^2) / \{1 + \exp[-9.84 \times (p_T - 3.93)]\} \quad (3)$$

$$\epsilon_{\mu^-}(p_T) = (0.975 + 0.0033 \times p_T + 0.000096 \times p_T^2) / \{1 + \exp[-9.83 \times (p_T - 3.91)]\} \quad (4)$$

The Monte Carlo events are processed in a FakeEvt + EvtGen, CdfSim, Trigsim++, Production sequence. We do not test the trigger bits set in Trigsim++ but use cuts to simulate the L1, L2, and L3 triggers. In order to apply the trigger efficiency as discussed above, one must apply a set of selection cuts that emulate the XFT requirements by quantizing phiSL6 in 1.25-degree segments and removing events in which both muons hit the same segment. The trigger tower requirement on muon ϕ separation is imposed by quantizing each muon's ϕ angle into 5-degree segments. Muon pairs must have at least two tower separation (gaps between adjacent segments count as a tower for this purpose) to satisfy the trigger tower requirement. Applying these cuts to data is redundant with hardware and therefore removes very few events. Trigger emulation requirements are listed in Table 3.2.

For data, trigger conditions are verified using TPrereqFast, and these events pass the same cuts as Monte Carlo.

3.3 Monte Carlo re-weighting

The Monte Carlo is generated with a flat p_T distribution in a given $p_T(\Upsilon)$ bin. However, the data has a smooth, continuous distribution which is not flat. Because the acceptance is p_T dependent and the Υ polarization itself is p_T -dependent, the use of a flat distribution can cause a systematic error in the measurement, especially for bins covering a large range of p_T . To avoid this, the Monte Carlo events are reweighted to match the data distribution after (polarization-dependent) acceptance and efficiency losses. This ensures that each bin has the appropriate p_T weight despite the flat generation. To account for the polarization dependence effects, we iterate the procedure:

Cuts	
Basic Offline Cuts	Require CMU or CMUP muons $n_{ctax} \geq 10$ $n_{ctst} \geq 10$ $ z_0 \leq 60\text{cm}$ $ \Delta z_0(\mu^+, \mu^-) \leq 5\text{cm}$ $ z_{SL} \geq 1.5\text{cm}$ $ z_{COTexit} \leq 155\text{cm}$ $\mu\mu$ Vertex Fit Prob ≥ 0.001 $\sigma L_{xy} \leq 0.025\text{cm}$
Trigger Cuts	CMU Muon: $p_T \geq 3.05\text{GeV}$, CMUdx $\leq 30\text{cm}$ At least 1 CMUP Muon CMUP Muon: $p_T \geq 4.05\text{GeV}$, CMUdx $\leq 15\text{cm}$ Each μ has matched XFT track Min. 2 trigger towers between hits

Table 1: Selection cuts required for data and Monte Carlo, as well as L3 trigger requirements imposed in the form of cuts.

(a) perform a polarization analysis using a flat $p_T(\Upsilon)$ spectrum; (b) compute the p_T -dependent acceptance and efficiency using the current polarization; (c) reweight the p_T spectrum to account for changes in acceptance and efficiency; (d) recompute the polarization to see if it is sensitive to the change; (e) iterate if there is a statistically significant change in the polarization.

The reweighting procedure uses a background-subtraction method to extract the signal $p_T(\Upsilon)$ distribution. The background under the signal peaks is estimated using a low-mass sideband below the 1S from 9.1-9.225 GeV/c^2 , a mid-mass sideband between 1S and 2S from 9.65-9.775 GeV/c^2 , and a high mass sideband above the 3S from 10.55-10.675 GeV/c^2 . The mass distribution in a given pT bin is fitted with a 3rd-order Chebyshev Polynomial background shape and the decay-angle-integrated mass probability distribution functions for each peak that are described in section 4.1. The sideband distributions determine the background p_T distribution. This background shape is extrapolated into the signal region and subtracted from the pT distribution in the signal region. The $\Upsilon(1\text{S})$ uses the nearby low-mass and mid-mass sidebands. The $\Upsilon(2\text{S})$ and (3S) use the mid-mass and high-mass sideband regions. Despite a large distance between those sidebands, the background pT spectrum over that range is stable, as demonstrated in Figure ??.

For the data, the p_T distribution for each state within a given $p_T(\Upsilon)$ bin is fitted with an exponential function that represents the probability that a detected event in that bin has a certain p_T . In the corresponding Monte Carlo p_T bins, the initially-flat p_T distribution is broken into ten sub-bins. A p_T weight function is determined from the exponential fit to data by evaluating the function at the center of each sub-bin.

Effects of p_T reweight on polarization			
p_T bin	η , no rwt	η , first rwt	η , second rwt
2-3	0.396 ± 0.02	0.395 ± 0.02	0.395 ± 0.02
3-4	0.340 ± 0.02	0.340 ± 0.02	0.340 ± 0.02
4-6	0.325 ± 0.02	0.355 ± 0.02	0.355 ± 0.02
6-8	0.367 ± 0.03	0.380 ± 0.03	0.380 ± 0.03
8-12	0.409 ± 0.04	0.410 ± 0.04	0.410 ± 0.04
12-16	0.311 ± 0.06	0.305 ± 0.06	0.306 ± 0.06
16-21	0.243 ± 0.08	0.235 ± 0.08	0.235 ± 0.08
21-40	0.376 ± 0.12	0.308 ± 0.12	0.307 ± 0.12

Table 2: The polarization may change significantly after a single reweight, but thereafter it is highly stable with respect to further iterations.

The Monte Carlo population is reweighted so that its p_T distribution accurately reflects the data distribution over the p_T interval while preserving the number of Monte Carlo events in the $p_T(\Upsilon)$ bin. The new, reweighted Monte Carlo templates are used to determine the next iteration of the polarization. The changes in polarization are listed in Table 2.

The effects of reweighting the Monte Carlo in dimuon rapidity were considered as well. The Monte Carlo y distribution integrated over p_T agrees well with that from data for $|y|_\Upsilon < 0.6$. No y reweighting is required. We use only p_T reweighting for the final measurement. The y distribution for data and Monte Carlo are shown in Fig. 7 and 8.

3.4 Angular Binning and p_T Resolution

To observe the dependence of Υ polarization on p_T , we place events into p_T and $\cos \theta^*$ bins. The Υ p_T binnings are listed in Tables 7, 8, and 9. The $\cos \theta^*$ distribution is folded about 0, using parity invariance in the decay, and the bins are chosen to have a width of 0.1 to ensure good statistics. The equivalence of the folding has been checked in two ways. First, we define the polarization angle from the negative muon instead of the positive one and saw that the polarization was the same. Second, we compare the negative $\cos \theta^*$ distribution with the positive one by overlaying the two halves on the same axis. For example, the folded angular distribution of the $\Upsilon(1S)$ is shown in Fig. 12.

We check the significance of migration effects by determining from Monte Carlo the resolution for p_T and $\cos \theta^*$ for the $\Upsilon(1S)$. This is done by comparing these quantities as measured using generator-level information against fully-reconstructed events. The results are featured in Figures 13 - 18. Because the shapes are not easily fit by a simple Gaussian, we produce an approximate width by folding the difference distributions about zero and then determining the region that contains 68% of the total yield for

$\Upsilon(1S) \cos \theta^*$ Resolution		
p_T bin	Percentile	Resolution
2-3	68.74	0.011
3-4	69.14	0.009
4-6	70.55	0.007
6-8	71.14	0.007
8-12	71.21	0.006
12-17	70.17	0.006
17-23	70.41	0.006
23-40	68.07	0.006

Table 3: $\cos \theta^*$ resolution determined from $\Upsilon(1S)$ Monte Carlo. The listed percentile indicates the portion of events within a region ending on a specific bin boundary.

$\Upsilon(1S) p_T$ Resolution		
p_T bin	Percentile	Resolution (GeV/c)
2-3	70.57	0.030
3-4	70.30	0.033
4-6	69.59	0.037
6-8	68.24	0.043
8-12	68.96	0.060
12-17	69.67	0.090
17-23	68.89	0.133
23-40	68.18	0.197

Table 4: $p_T(\Upsilon)$ resolution in GeV/c determined from $\Upsilon(1S)$ Monte Carlo. The listed percentile indicates the portion of events within a region ending on a specific bin boundary.

that bin. In the absence of a fit, we must choose a region that ends on a bin boundary. Therefore, we take the upper end of the bin containing the 68th percentile as the (slightly conservative) estimate. The results are shown in Tables 3 and 4.

3.5 Test of Monte Carlo using μ^+ distribution s in p_T and η

To check the validity of the Monte Carlo acceptance calculations we compare the measured distributions of μ^+ mesons from Υ decay to the polarization-weighted Monte Carlo predictions for the μ^+ . Unlike the polarization analysis, which fits for the background in each angle bin, the μ^+ comparisons rely on sideband subtraction for the data. At low p_T especially, there is a sizeable background subtraction. The background changes exponentially in normalization as one moves from the low sideband

to the high sideband. This means that assuming a linear average behavior for the background shape as one varies the dimuon mass may not be a completely satisfactory approximation. The effects of a non-linear behavior of the $p_T(\mu^+)$ distribution can be seen in Fig. 11. The average of the upper and lower distributions produces some peaks and dips at low muon p_T . A small residue of this behavior can be seen by comparing the background distributions to the sideband-subtracted $\mu^+ p_T$ distributions in Fig. 9. The η plots are not affected by this kind of background shape change. Overall the distributions match well in shape for all $p_T(\Upsilon)$. There is no indication of a mismatch between the polarization-weighted Monte Carlo predictions and the data distributions.

4 $\Upsilon(nS)$ Polarization Analysis

The $\Upsilon(nS)$ studies use a dimuon mass interval from 8.82-10.98 GeV/c². For a given state and a given p_T bin the polarization analysis requires a determination of the $\Upsilon(nS)$ yield in each $\cos\theta^*$ bin. We invoke parity conservation in the decay and organize the events in ten bins of $|\cos\theta^*|$ on the interval (0,1.). In each $|\cos\theta^*|$ bin we make a simultaneous fit for all three $\Upsilon(nS)$ peaks plus a Chebyshev polynomial background function. This process is repeated for each p_T bin. For the $\Upsilon(1S)$ analysis, we have 8 bins. Because the higher-mass states have lower yields, we don't use the $\Upsilon(2S)$ or $\Upsilon(3S)$ yields from the 1S binning, even though the mass fit includes all three states. For the $\Upsilon(2S)$ or $\Upsilon(3S)$ yields we rebin the data into four p_T bins and repeat the analysis procedure.

The background is unconstrained by physics considerations. Determining the best background description is somewhat tricky due primarily to the different background shapes in different bins of $\cos\theta^*$. We evaluated the utility of the following method [8]. We fit with a large number of Chebyshev polynomials and truncate the series when, scanning backward from the highest-order polynomial used, a parameter's significance surpassed a level chosen *a priori*. Using a significance level of 3 gave reasonable fits in most bins, but there were cases in which the polynomial level was clearly too low to fit the data even though the significance of individual terms was less than two σ . These bins typically had large χ^2 values for the fits.

We modified the strategy as follows. The mass distribution in each $\cos\theta^*$ bin was fit eight times, each with an increased number of Chebyshev polynomials. We looked for the best fit as the place where χ^2 stopped dropping by at least two units per additional term. In a few cases there was a second step at the large N end of the trials. In such cases we used the lower polynomial order as the best fit and assigned a background systematic to that particular bin as the difference between the two plateau levels. This systematic is added in quadrature with the statistical uncertainty of that bin. The maximum effect seen in any single bin was $1.0\sigma_{stat}$ in one case. Most bins had no systematic, and for those that did the systematic was usually less than $0.2\sigma_{stat}$. All the yields and uncertainties are listed in Tables 11-13 of Appendix B. Signal PDFs were determined from Monte Carlo studies and adjusted to match angle-integrated mass

plots, as described below.

We also checked the stability of the fit using a narrower mass range of $8.875 - 10.9 \text{ GeV}/c^2$. There is no sensitivity to the limits. The yields in some bins require a higher order Chebyshev polynomical because of clear curvature of the background. This is evident from Figure 27.

4.1 Υ Mass PDFs from Simulation

To determine the $\Upsilon(\text{nS})$ yields from data, we fit fixed signal shapes and polynomial backgrounds to the mass distributions in each p_T and $|\cos \theta^*|$ bin. We obtain the signal shapes by fitting Monte Carlo events for each $\Upsilon(\text{nS})$ state after processing through CdfSim and Production. Efficiency effects are developed from data and triggers are emulated with cuts. The resulting mass distributions are binned into histograms and are fit by a smooth functional form.

We studied many different fitting functions and their combinations to fit the upsilon mass distribution. The basic shapes are Gaussian (G), Crystal Ball (CB), Modified Crystal Ball (MCB) or Johnson SU function. The functional forms used and the paramters involved are shown in the following equations.

$$PDF_G = \frac{1}{\sqrt{2\pi\sigma^2}} \exp\left(-\frac{(x-\mu)^2}{2\sigma^2}\right) \quad (5)$$

$$PDF_{JSU} = \frac{\delta}{\lambda\sqrt{2\pi}\sqrt{\left(\frac{x-\xi}{\lambda}\right)^2 + 1}} \exp\left(-1/2 \left(\gamma + \delta \log\left(\left(\frac{x-\xi}{\lambda}\right) + \sqrt{\left(\frac{x-\xi}{\lambda}\right)^2 + 1}\right)\right)^2\right) \quad (6)$$

$$PDF_{CB} = \begin{cases} A \exp\left(-\frac{(x-Et)^2}{2\sigma^2}\right) & \frac{x-Et}{\sigma} > -\alpha \\ A\left(\frac{n}{\alpha}\right)^n \frac{\exp(-\alpha^2/2)}{\left(\frac{Et-x}{\sigma} + \frac{n}{\alpha} - \alpha\right)^n} & \frac{x-Et}{\sigma} \leq -\alpha \end{cases} \quad (7)$$

$$PDF_{MCB} = \begin{cases} A \left(\exp\left(-\frac{(x-Et)^2}{2\sigma^2}\right) + R \exp\left(-\frac{(x-Et)^2}{2(B\sigma)^2}\right)\right) & \frac{x-Et}{\sigma} > -\alpha \\ A\left(\frac{n}{\alpha}\right)^n \frac{\exp(-\alpha^2/2)}{\left(\frac{Et-x}{\sigma} + \frac{n}{\alpha} - \alpha\right)^n} & \frac{x-Et}{\sigma} \leq -\alpha \end{cases} \quad (8)$$

Single function shapes did not fit well, so we used combinations of functions: two and three Gaussians, JSU+G, JSU+2G, CB+G, JSU+CB. We chose JSU+CB as our fitting function, because among the candidate functions, it alone can fit all the data distributions successfully with no fit status errors from Minuit and with suitable χ^2 values. The other options all led to MINUIT fit errors, either an inaccurate error matrix or an error matrix that is not positive-definite. In all cases the JSU+CB function

described the Monte Carlo distributions well. The details of the mass fits, including the parameters for the fit functions for the individual angle bins and the angle-integrated distributions are given in Appendix A.

4.2 Υ Mass Fits

4.2.1 Modifying the Monte Carlo Mass Fits

We know that the CDF simulation package does not match the data mass distributions exactly. In most CDF B analyses, the Monte Carlo predictions track the relative p_T dependence of a mass distribution, are typically too narrow and tend to be shifted slightly. The data themselves are used to correct the Monte Carlo PDF parameters, using the integral mass distribution. In this case, we divide the Υ data into $p_T(\Upsilon)$ bins appropriate for analyzing the nS state in question: 8 bins for the 1S, 4 bins for the 2S, 3S. We describe the data by three $\Upsilon(nS)$ peaks and a polynomial background term, just like the fits in the individual $\cos \theta^*$ bins. The mass PDFs use the Monte Carlo-derived PDF described above but include a single scale factor to float the CB Gaussian width (σ in Eq. 6) and the JSU width parameter (λ in Eq. 5) for all three states and a global mass shift term to allow movement in the central value for the peaks (E_t for the CBF, ξ for the JSU). The mass differences between the three nS peaks are fixed at the PDG values. This procedure determines the *width scale factor* $s_{\text{fw}} = \text{width}(\text{data})/\text{width}(\text{Monte Carlo})$ and the *mass shift* for this p_T bin. These shifts are applied to the Monte Carlo mass PDFs in making the mass fits that determine the yields in a given $\cos \theta^*$ bin. The mass fits for the p_T bins are shown in Fig. 19 - 26. The fit χ^2 values, mass shift and scale factors are summarized in Tab. 5.

The mass shifts and scale factors in the 1S p_T bins in Tab. 5, excepting bin 8, are consistent with a single constant value at all p_T . The average mass shift and scale factor (over the first seven bins, weighted by bin population) is used for the subsequent yield fits for all nS states in all p_T bins.

The 21-40 GeV/c bin is somewhat inconsistent with other bins. Because we have no explanation for an upward shift in mass, we still apply the average mass shift and scale factor when fitting that bin. The actual fit value is used to determine a systematic error in that bin's polarization, as discussed in the Systematics section, and its effect is small.

4.2.2 Angular Distributions and Yields

When the adjusted mass pdfs are fit to the data in a given p_T , $\cos \theta^*$ bin, the only free parameters are the three yield parameters and the background parameters for the Chebyshev terms. There are 48 mass bins from 8.82 to 10.98 GeV/c^2 in each $\cos \theta^*$ bin. The maximum likelihood fit determines the yields and the MINOS uncertainties on these parameters provide the yield uncertainties for the data in that particular bin. These fits are shown in Figures 28 - 39. The fits all have acceptable χ^2 probabilities in the range of 2-96%. The yields are the inputs to the polarization fit, discussed in the

Mass Shifts and Scale Factors			
$p_T(\Upsilon)[\text{GeV}/c]$	Fit χ^2 (39 DoF)	Mass shift [GeV/c^2]	Width SF
2-3	38.5	-0.0025 ± 0.0004	1.21 ± 0.01
3-4	44.0	-0.0027 ± 0.0004	1.19 ± 0.01
4-6	85.8	-0.0022 ± 0.0003	1.18 ± 0.01
6-8	60.5	-0.0027 ± 0.0004	1.17 ± 0.01
8-12	63.8	-0.0027 ± 0.0005	1.22 ± 0.01
12-16	49.9	-0.0027 ± 0.0008	1.18 ± 0.02
17-21	30.8	-0.0025 ± 0.0014	1.19 ± 0.03
21-40	45.7	0.0042 ± 0.0026	1.29 ± 0.06
Mean (2-21)		-0.0025	1.186

Table 5: Mass shifts and width scale factors from fits in p_T bins.

next section. The order of the highest Chebyshev polynomial included in the base fit was determined by the procedure described in Section 4.1.

A number of bins in high $\cos \theta^*$ bins have inadequate statistics to form a good fit. These histograms are still included in Figures 28 - 39 and can be identified by the absence of a drawn fit function. These bins are, of course, omitted from the polarization fit.

4.3 Υ Polarization Fitter

After the mass-fit procedure, we have the yields and their uncertainties for each $\Upsilon(\text{NS})$ state in each $\cos \theta^*$ bin i . The theoretical signal function for $\cos \theta^*$ bin i is the polarization-weighted sum of the $T(p_T)$ and $L(p_T)$ templates for that bin in this p_T range:

$$E_i(p_T) = N(\eta; p_T)[(1 - \eta) \cdot T_i(p_T) + \eta \cdot L_i(p_T)]. \quad (9)$$

The normalization parameter $N(\eta; p_T)$ matches the total yield $Y(p_T)$ for the specific p_T bin to the η -dependent prediction from the templates:

$$N(\eta; p_T) = \frac{Y(p_T)}{(1 - \eta) \cdot \sum_i T_i(p_T) + \eta \cdot \sum_i L_i(p_T)}. \quad (10)$$

The number of signal events $N_i(p_T)$ in bin i , the uncertainty $\sigma_i(p_T)$, each taken from the mass fits in $\cos \theta^*$ bins, and $E_i(p_T)$ define a χ^2 function which is optimized to determine the polarization parameter η . This function is implemented in ROOT using MINUIT. The best fit parameter and its uncertainty, evaluated using MINOS errors, are quoted in Tables 7, 8, and 9 for each Υ state and p_T bin.

Input η	Mean Pull	σ_{pull}
0.2	0.085 ± 0.047	0.944 ± 0.034
0.4	0.026 ± 0.053	1.047 ± 0.038
0.6	-0.022 ± 0.049	0.981 ± 0.035
0.8	0.027 ± 0.050	0.990 ± 0.036

Table 6: Pull distribution mean and σ for each input polarization in the fourth (6-8 GeV/c) p_T bin.

4.4 Toy Monte Carlo Tests of Fitter

A study of possible bias in the fit function was done by making additional L and T Monte Carlo samples from which to build test samples with any desired polarization parameter η : a sample S having polarization η is $S(\eta) = \eta L + (1-\eta)T$. The size of the L and T samples *at generation* is equal. We chose sample sizes so that the number of events in the sample S after reconstruction and cuts was about 2000 events.

For simplicity, we chose to generate the test samples using only one run number. This had the unanticipated consequence of requiring an independent set of template files to be made with this same run number. The subtle variations in detector response with run number gave a misleading indication of a fitter pull when we used the standard templates. This points out the importance of using a proper luminosity-weighted set of runs for the actual templates used in the data analysis for optimal results. The size of the false pulls that we saw when we compared single-run-number samples to the complete templates was up to $0.5 \sigma_{statistical}$. We conclude that, having used the good run list for Monte Carlo and data, there is not likely to be any significant systematic uncertainty in polarization due to different acceptance between Monte Carlo templates and real data. The pulls are shown in Figure 40 and Table 6. We see no indication of a fitter bias.

4.5 $\Upsilon(nS)$ Polarization Results

4.5.1 $\Upsilon(1S)$ Polarization

The results of the $\Upsilon(1S)$ fits listed in Table 7 show a small longitudinal polarization independent of $p_T(\Upsilon)$, consistent with the CDF Run I result [15]. At the two highest p_T bins, the central values are slightly positive, but with significant uncertainties. The results are consistent with a constant polarization $\alpha = -0.108 \pm 0.014$ with $\chi^2 = 5.2$ for seven degrees of freedom. There is no clear trend toward transverse polarization in the s-channel helicity frame. The $\cos\theta^*$ distributions for 1S data and the results of these fits are included in Figure 41.

$\Upsilon(1S)$ Polarization				
$p_T(\Upsilon)[GeV/c]$	Data Yield	η	α	$\sigma_{syst}(\eta)$
2-3	38940 ± 291	0.4027 ± 0.0128	$-0.148^{+0.026}_{-0.026}$	N/A
3-4	37911 ± 281	0.3831 ± 0.0121	$-0.108^{+0.026}_{-0.025}$	N/A
4-6	48567 ± 308	0.3853 ± 0.0127	$-0.113^{+0.027}_{-0.026}$	N/A
6-8	25238 ± 216	0.3953 ± 0.0227	$-0.133^{+0.047}_{-0.046}$	N/A
8-12	22504 ± 200	0.3627 ± 0.0256	$-0.065^{+0.056}_{-0.054}$	N/A
12-16	7492 ± 121	0.3499 ± 0.0426	$-0.037^{+0.097}_{-0.091}$	N/A
16-21	3083 ± 81	0.2795 ± 0.0609	$0.126^{+0.156}_{-0.142}$	N/A
21-40	1510 ± 59	0.3852 ± 0.1039	$-0.112^{+0.234}_{-0.201}$	0.011

Table 7: Measured yields and polarization parameters for $\Upsilon(1S)$

$\Upsilon(2S)$ Polarization				
$p_T(\Upsilon)[GeV/c]$	Data Yield	η	α	σ_{syst}
2-4	19397 ± 270	0.3806 ± 0.0250	$-0.103^{+0.053}_{-0.052}$	N/A
4-6	14997 ± 222	0.3415 ± 0.0237	$-0.018^{+0.054}_{-0.052}$	N/A
6-12	16167 ± 211	0.2924 ± 0.0319	$0.095^{+0.078}_{-0.075}$	N/A
12-40	4155 ± 102	0.1785 ± 0.0586	$0.394^{+0.177}_{-0.161}$	N/A

Table 8: Measured yields and polarization parameters for $\Upsilon(2S)$

4.5.2 $\Upsilon(2S)$ and $\Upsilon(3S)$ Polarization

The $\Upsilon(2S)$ and $\Upsilon(3S)$ data are grouped into coarser p_T bins, as discussed earlier. These states are less strongly contaminated by feed-down from χ_b states because the production cross sections for the higher-mass χ_b states are small at the Tevatron. These polarizations are viewed as a better test of the NRQCD predictions. The polarization starts out somewhat negative at small p_T and moves positive at the largest p_T . The data are not consistent with a p_T -independent polarization. The $\cos\theta^*$ distributions for 2S data and the results of these fits are included in Figure 42 and tabulated in Table 8.

5 Systematics

The polarization is determined by the muon angular distribution. Anything which affects the yield as a function of angle in the Υ rest frame can generate a systematic uncertainty. We consider the following potential sources of systematic error:

1. Change in the mass PDF as a function of $\cos\theta^*$
2. Incorrect estimation of mass PDF from Monte Carlo information

$\Upsilon(3S)$ Polarization				
$p_T(\Upsilon)[GeV/c]$	Data Yield	η	α	σ_{syst}
2-4	9923 ± 280	0.3224 ± 0.0502	$0.025^{+0.119}_{-0.111}$	N/A
4-6	8187 ± 230	0.3046 ± 0.0417	$0.066^{+0.101}_{-0.095}$	N/A
6-12	10063 ± 221	0.3404 ± 0.0510	$-0.016^{+0.118}_{-0.109}$	N/A
12-40	3099 ± 110	0.1809 ± 0.0835	$0.387^{+0.258}_{-0.224}$	N/A

Table 9: Measured yields and polarization parameters for $\Upsilon(3S)$ (Yield numbers need to be updated)

3. Change in acceptance as a function of $\cos \theta^*$ due to muon efficiency function
4. Sensitivity to $p_T(\Upsilon)$ re-weighting function
5. Sensitivity to $\cos \theta^*$ bin width and resolution
6. Sensitivity to background parametrization
7. Change in templates due to unaccounted-for changes in apparatus performance during data-taking.
8. Averaging mass shifts and scale factors

The first item might arise because the muon momenta are nearly equal when $\cos \theta^* \sim 0$ and are quite asymmetric when $\cos \theta^* \sim \pm 1$. Multiple Coulomb scattering will be different in the two cases. Such effects are included in the Monte Carlo. Example mass fits to data shown in Fig. 28 in $\cos \theta^*$ bins, using Monte Carlo parametrizations, show no indication of a discrepancy within our statistical precision. Therefore, we assign no systematic uncertainty from this source.

For the second possible issue, as discussed in the section on Mass PDFs from Simulation, many studies of particle masses confirm that the Monte Carlo underestimates the actual width of the mass distribution for a particle peak, although it gets the p_T variation of the width correct. The studies outlined in that section showed excellent fits to the observed mass distribution integrated over all decay angles. We studied the effect of changing the histogram bin widths used for the Monte Carlo samples from the standard 10 MeV up to 30 MeV. No significant change in the integrated yields in data occurred when we used different Monte Carlo parametrizations. We assign no systematic uncertainty from this source.

Item three includes the effects of systematic uncertainties in the muon efficiency function, which translate into systematic uncertainties in the templates. We have looked at the effect on the Υ polarization of changing the muon efficiency function by $\pm 1\sigma_{syst}$. The largest change seen in Υ polarization parameter η in any bin was approximately 0.0006. This, being around 1% of the statistical uncertainty, is negligible as a source of systematic uncertainty.

We have also used a different p_T reweighting scheme than the one described above, wherein weights are assigned to Monte Carlo based strictly upon the data p_T distribution. The changes to polarization are negligible. We assign no systematic uncertainty due to p_T re-weighting shape.

In checking our resolution for $\cos \theta^*$, we determined that the polarization varies within statistical uncertainty when halving or doubling the bin width. Combining this with the result that our resolution is much smaller than the bin width used indicates that there should be no systematic uncertainty assigned due to angular bin migration effects.

In CDF9896, we reported polarization results measured using a method which utilized sideband subtraction to determine the $\Upsilon(1S)$ yields and polarization. The method described here constitutes a completely different approach. The polarization results from the two studies are consistent with the statistical changes in the data arising from differing methods and datasets. This indicates that there are no large systematics from the background subtraction. For this method, we have varied the width of the mass window from the standard 8.82-10.98 GeV/c^2 to 9.00-10.8 GeV/c^2 . There was no effect on the signal yields.

The variation of yield due to different orders of the background polynomial is a systematic uncertainty that varies bin by bin. In many bins there is no effect. As discussed in Section 4.1, we determine the systematic uncertainty in each $\cos\theta^*$ bin due to the fit choice. These values are listed in Appendix B Tables 11- 14. The systematic uncertainty is added in quadrature with the statistical uncertainty before making the polarization fit. To illustrate the procedure, we include two examples. The first is a bin to which we assign zero systematic. The second is a bin to which we assign the largest systematic seen in this sample. These are the seventh and sixth angle bins of the first $\Upsilon(1S)$ p_T bin, for which the mass fits are seen in Fig. 28. The data are in Table 10.

The variation of templates with run number was explored as part of the fitter bias study. Using probe samples made with a single run number to test templates made with the complete good run list showed potential biases of up to $0.5 \sigma_{\text{statistical}}$. This bias varies depending on the run number used and disappears when the template run distribution matches the probe run distribution. Because the templates were built using the good run list that describes the data luminosity distribution, any residual effect of run-dependent variations will be negligible.

As noted above, the mass shift and scale factor determined for the highest $\Upsilon(1S)p_T$ bin was inconsistent with the other bins. As we are unaware of any reason to expect an upward mass shift, we apply the weighted average of these values over the first seven bins to this bin. Using that as a baseline, we also conduct the analysis using the exact values determined for that bin. We find that the χ^2 of the mass fits in angular bins is stable between the two versions, and the resulting change in polarization (η) is 0.021. We assign half of this value as a systematic in that bin. No systematic is assigned to the 2S and 3S bins in this region because the highest p_T range for those states covers 12-40 GeV/c . This range begins well below the start of the $\Upsilon(1S)$ bin in question,

Order	Yield	σ_{stat}	χ^2/dof	Order	Yield	σ_{stat}	χ^2/dof
0	3794	81	408.0	0	4335	86	300.8
1	3544	81	115.8	1	4100	86	63.4
2	3611	82	80.8	2	4115	87	61.5
3	3736	86	48.5	3	4186	91	53.6
4	3743	87	48.3	4	4213	92	48.5
5	3744	88	48.3	5	4225	93	48.2
6	3782	93	46.5	6	4288	95	43.4
7	3775	93	45.6	7	4288	99	43.4
8	3737	85	44.1	8	4305	104	43.2

Table 10: Mass Yields, Uncertainties and χ^2 values versus Chebyshev order for $\Upsilon(1S)$ p_T bin 1, angle bins 7 (left) and 6 (right). The left side shows a rapid decrease of χ^2 with background order until $N=3$, then plateaus. No systematic is assigned. The right side shows a steady decrease until $N = 4$, then another step down at $N=6$. The two yields differ by 75 events. We use half that number as the systematic.

and it is populated primarily by events in the lower end of the p_T range. Therefore, the scale factor and mass shift for these states is better-described by the preceding $\Upsilon(1S)p_T$ bins.

6 Comparison with Other Measurements

This method of measuring the polarization was compared to the results from CDF9896, wherein an alternate method was employed. Over the same dataset (but using a newer runlist), the new method agrees well with the old, as seen in Figure 44.

The results of the polarization measurements using the full 4.9 fb^{-1} for the $\Upsilon(1S)$, $\Upsilon(2S)$, and $\Upsilon(3S)$ are illustrated in Figures 45, 46, and 47, respectively. Our result for $\Upsilon(1S)$ polarization agrees well with the CDF Run I result [15], as shown in Figure 48. The Run I result was for $|y| < 0.4$, while the NRQCD predictions were explicitly done to compare to that result, using the same y range. The $\Upsilon(1S)$ polarization measurement by D0 disagrees with the CDF results both for Run I and Run II. They report longitudinal polarization at low p_T and a trend toward transverse polarization at high p_T as indicated in Figure 49 [16]. On the other hand our result is consistent with the D0 result for the $\Upsilon(2S)$ polarization, shown in Figure 50. The D0 measurements cover the range $|y| < 1.8$, while these measurements use data in the range $|y| < 0.5$.

7 Summary

This measurement of $\Upsilon(1S)$ polarization shows very small polarization at all p_T in the s-channel helicity frame. A fit to a constant polarization gives $\langle \alpha \rangle = -0.108 \pm 0.014$

with a χ^2 of 5.2 for 7 degrees of freedom. This result is consistent with the CDF Run I measurement but disagrees at low p_T with the published D0 measurement. Our background measurements show significant variation with dimuon mass, whereas the D0 fits use smooth polynomial background estimates over a large mass interval. The respective rapidity coverage of each measurement also differs, with D0 covering $|y| < 1.8$ and this measurement covering $|y| < 0.6$. The results presented here disagree with the NRQCD prediction of transverse polarization for large p_T .

The gluon tower model of Ref. [3] predicts a longitudinal polarization and expects that it will be significantly longitudinal by $15\text{GeV}/c$. The multiple-interaction model of Ref. [7] also predicts longitudinal polarization, but starting at $p_T \sim 5 \text{ GeV}/c$, lower than we observe. This model incorporates multi-gluon processes, suggesting that the Υ states should have accompanying gluon jet activity.

Recent work by Lansberg and collaborators on the higher order effects in the color singlet model suggest that the $\Upsilon(1S)$ polarization may become longitudinal as p_T increases. This model is capable of handling both the cross section and the polarization of the Υ family and deserves careful study ??.

The 2S and 3S states are expected in NRQCD to be more strongly transverse than the 1S, due to reduced feed-down from higher mass χ_b and nS states. We observe larger polarizations for these states at the highest p_T . For $p_T < 10 \text{ GeV}/c$ the 2S and 3S states are essentially unpolarized. In this p_T region polarization effects due to feed-down from higher nS states to the 1S should be small, leaving only χ_b feed-down to affect the 1S polarization.

These results extend Υ polarization measurements to a transverse mass $m_T \leq 4m_\Upsilon$, fully into the perturbative regime. They do not follow the NRQCD expectations in the s-channel helicity frame. We are now performing a similar analysis using Collins-Soper templates to study the polarization in that quantization frame.

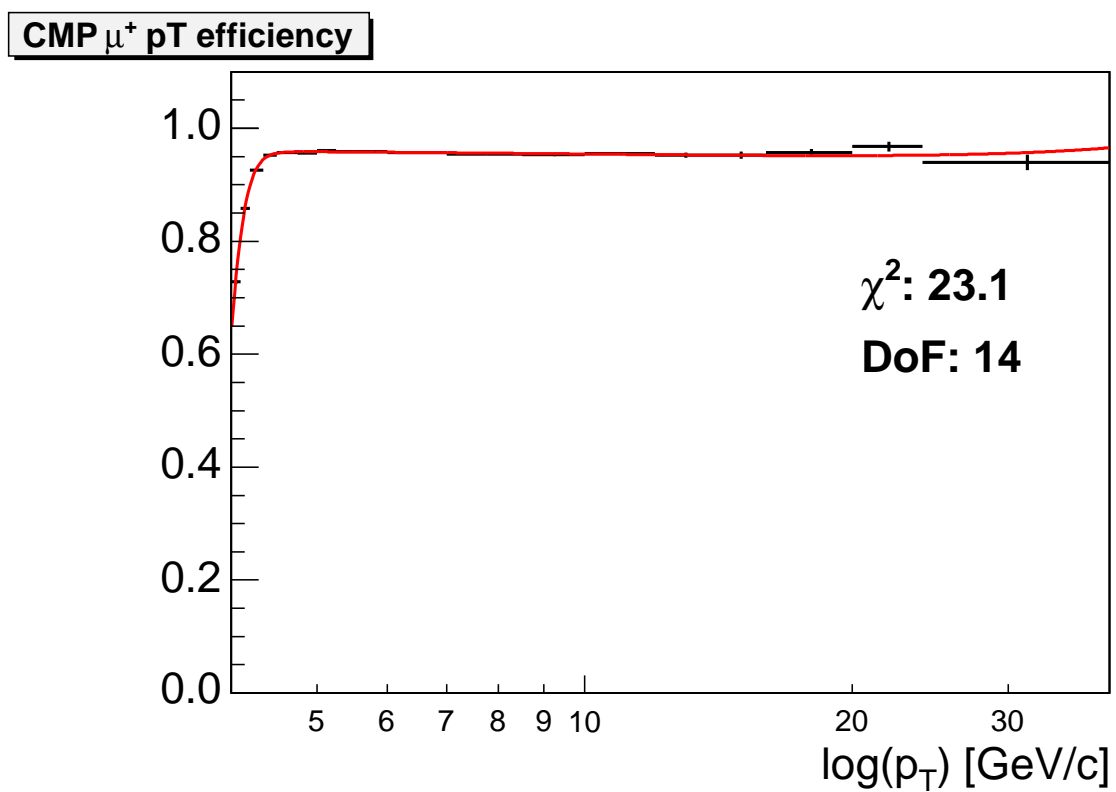


Figure 4: Measured CMP efficiency for μ^+ .

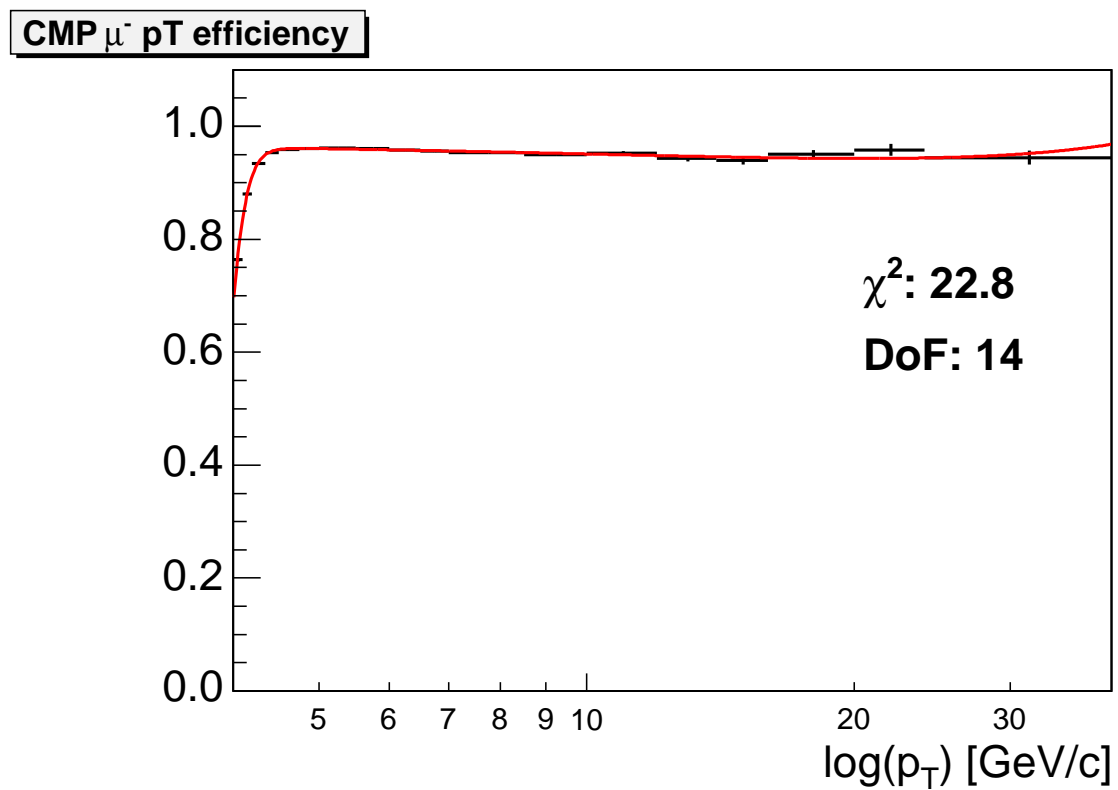


Figure 5: Measured CMP efficiency for μ^- .

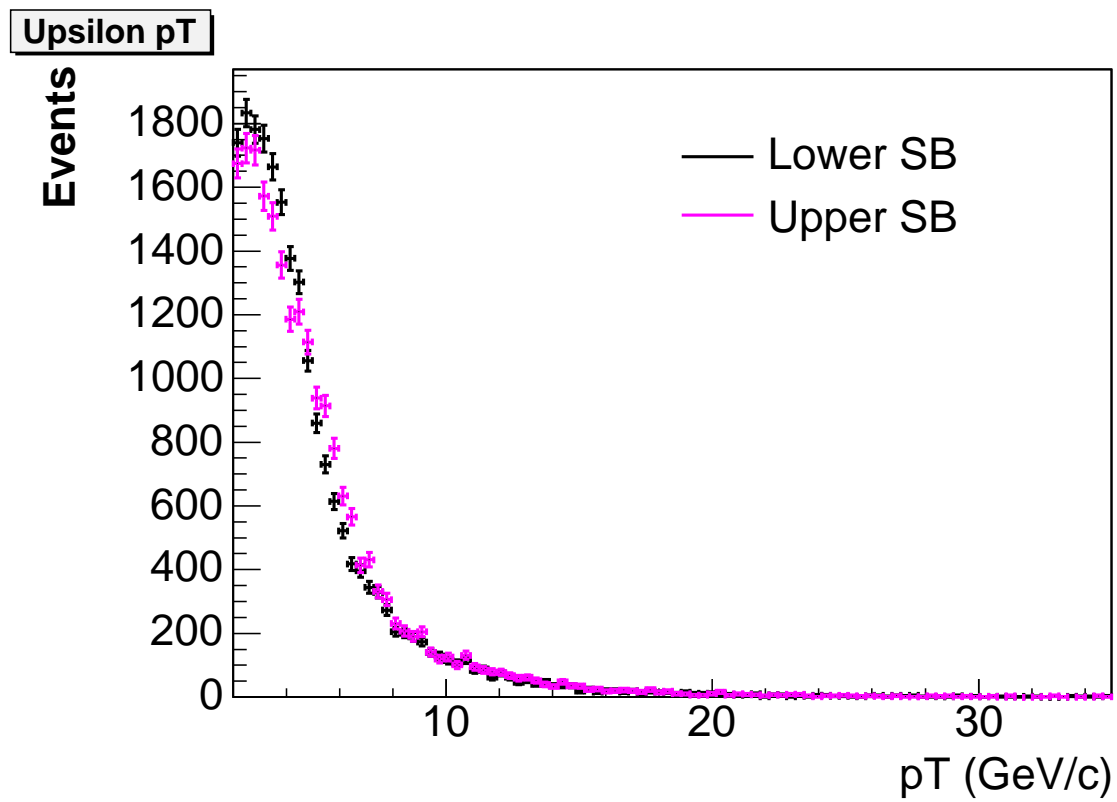


Figure 6: Υp_T of events in the sideband regions for the 2S and 3S states. The distributions are quite stable over that range.

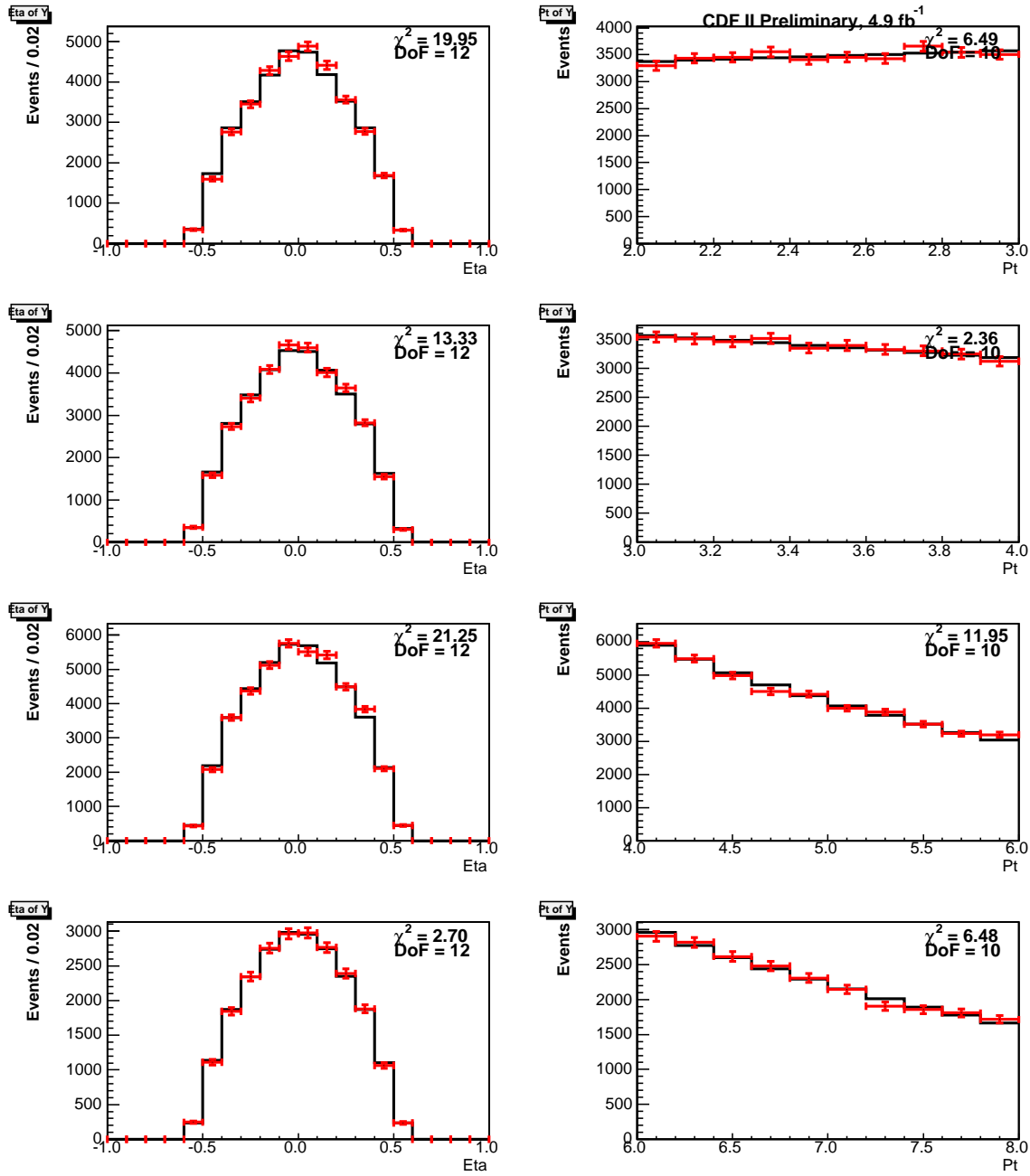


Figure 7: Sideband-subtracted data (points) and Monte Carlo (solid line) rapidity and p_T distributions of Υ , for the first four p_T bins, based on 4.9 fb^{-1} .

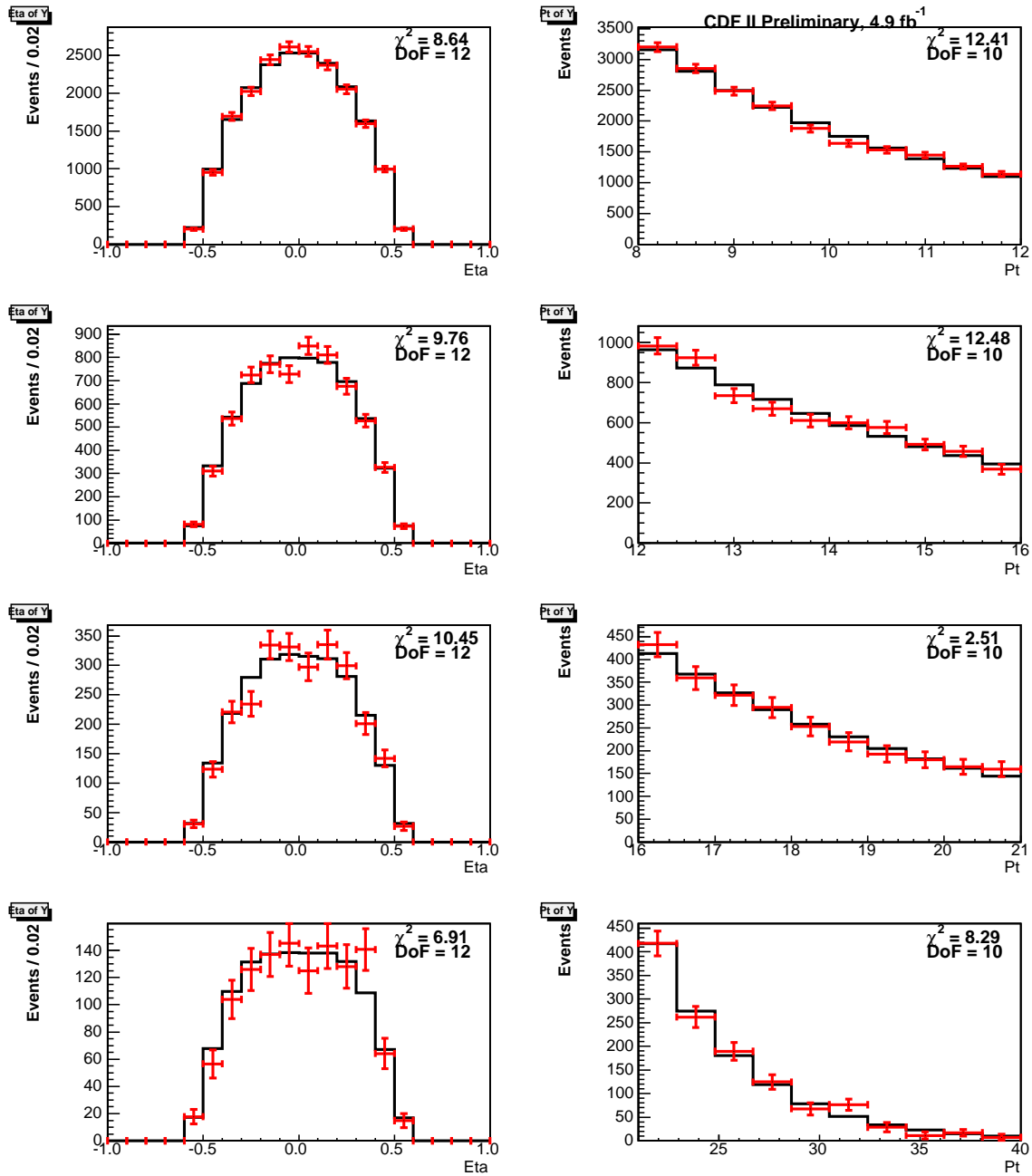


Figure 8: Sideband-subtracted data (points) and Monte Carlo (solid line) rapidity and p_T distributions of Υ , for the last four p_T bins, based on 4.9 fb^{-1} .

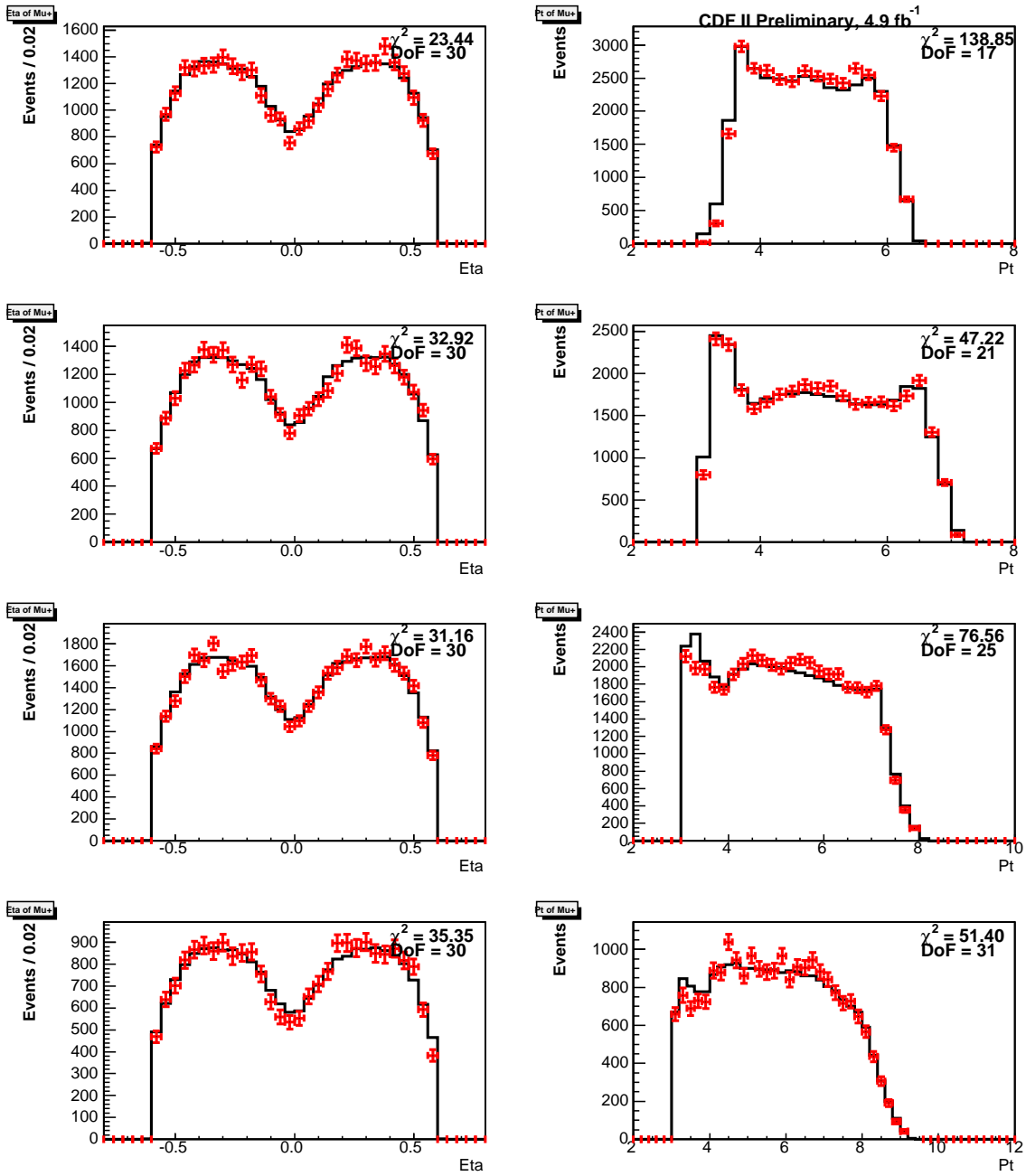


Figure 9: Sideband-subtracted data (points) and Monte Carlo (solid line) rapidity and p_T distributions of muons, for the first four p_T bins, based on 4.9 fb^{-1} .

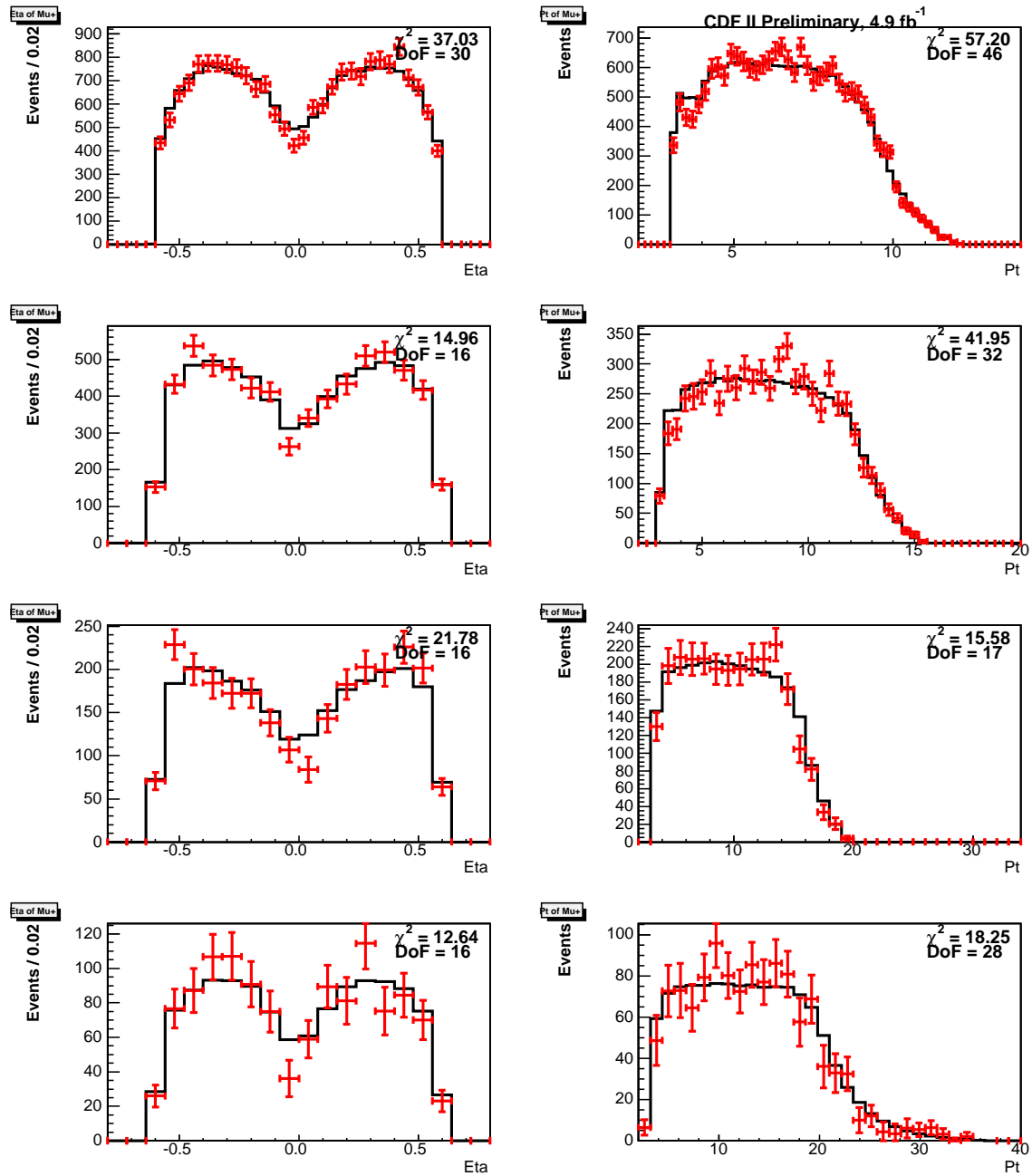


Figure 10: Sideband-subtracted data (points) and Monte Carlo (solid line) rapidity and p_T distributions of muons, for the last four p_T bins, based on 4.9 fb^{-1} .

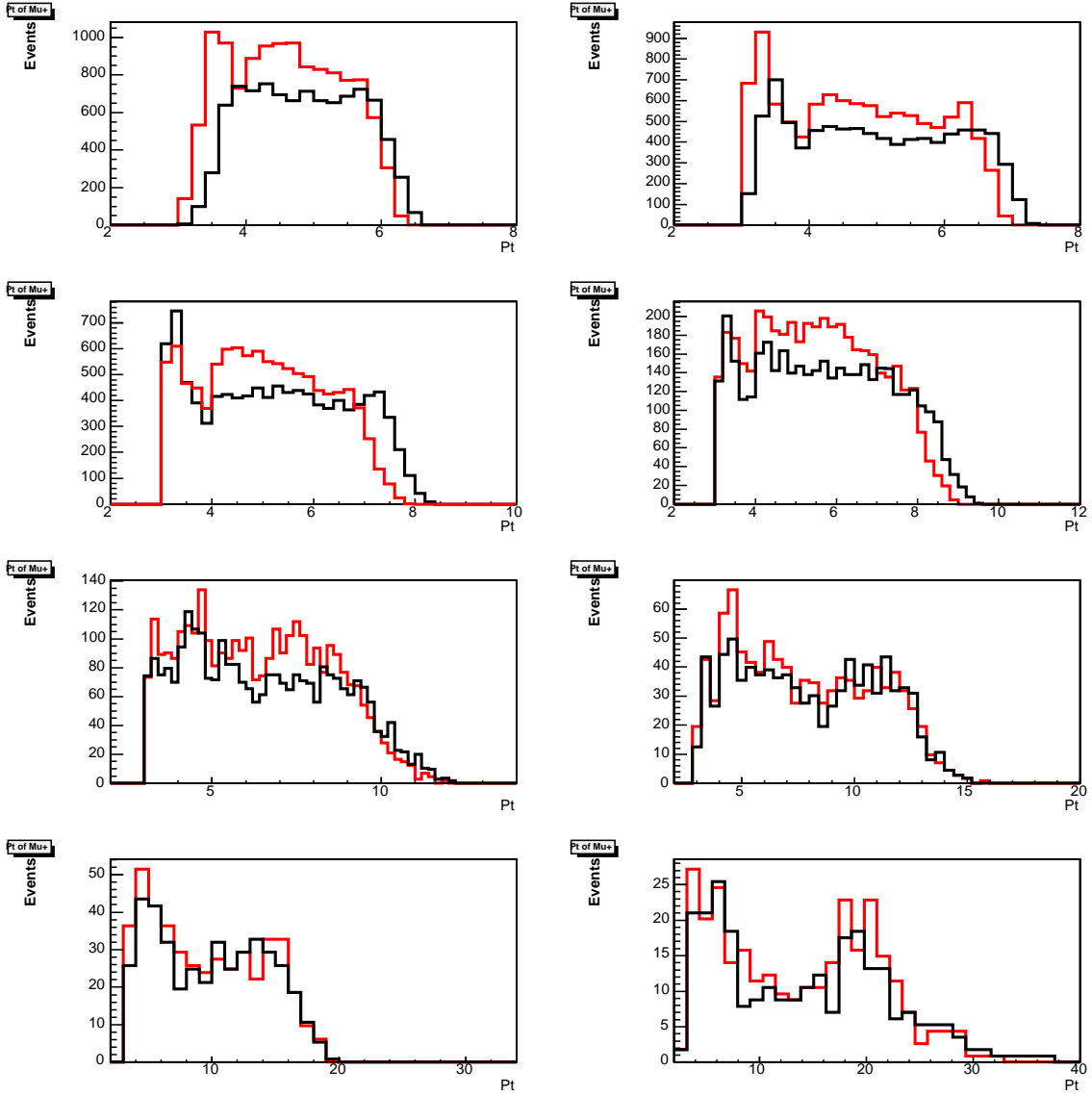


Figure 11: $\mu^+ p_T$ distributions for the sideband regions used for $\Upsilon(1S)$. The lower (“low-mass”) sideband is indicated by the red line, while the upper (“mid-mass”) sideband is shown in black.

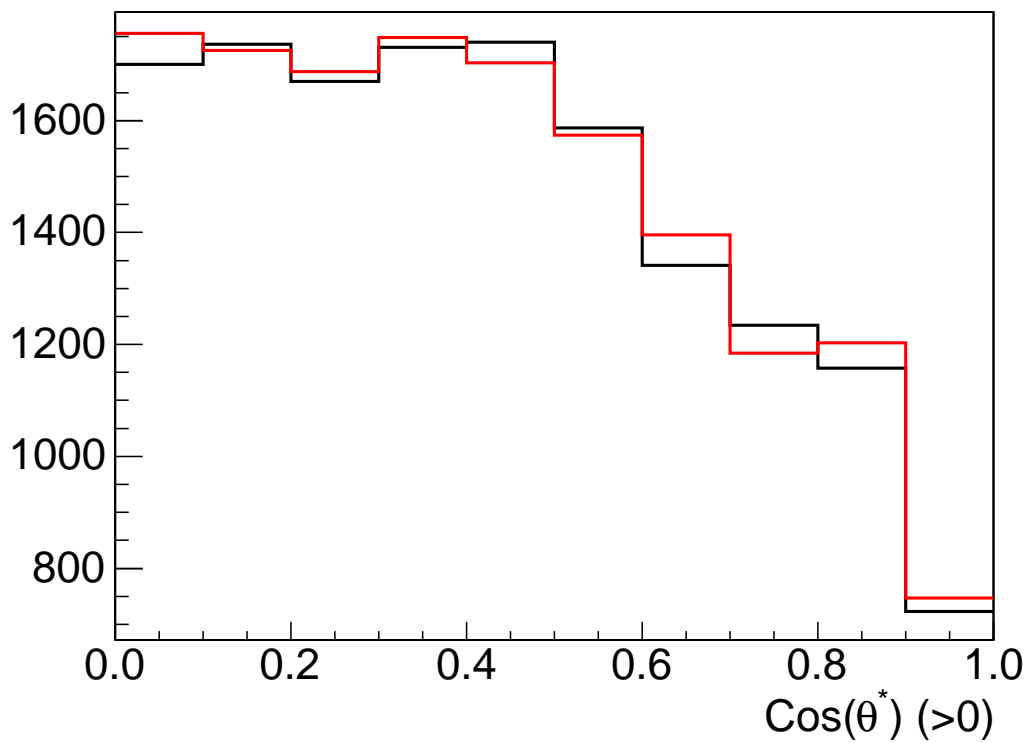


Figure 12: An example of the symmetry about zero of the angular distributions. This plot shows the signal-region angular distribution (including background) for the first p_T bin of the $\Upsilon(1S)$.

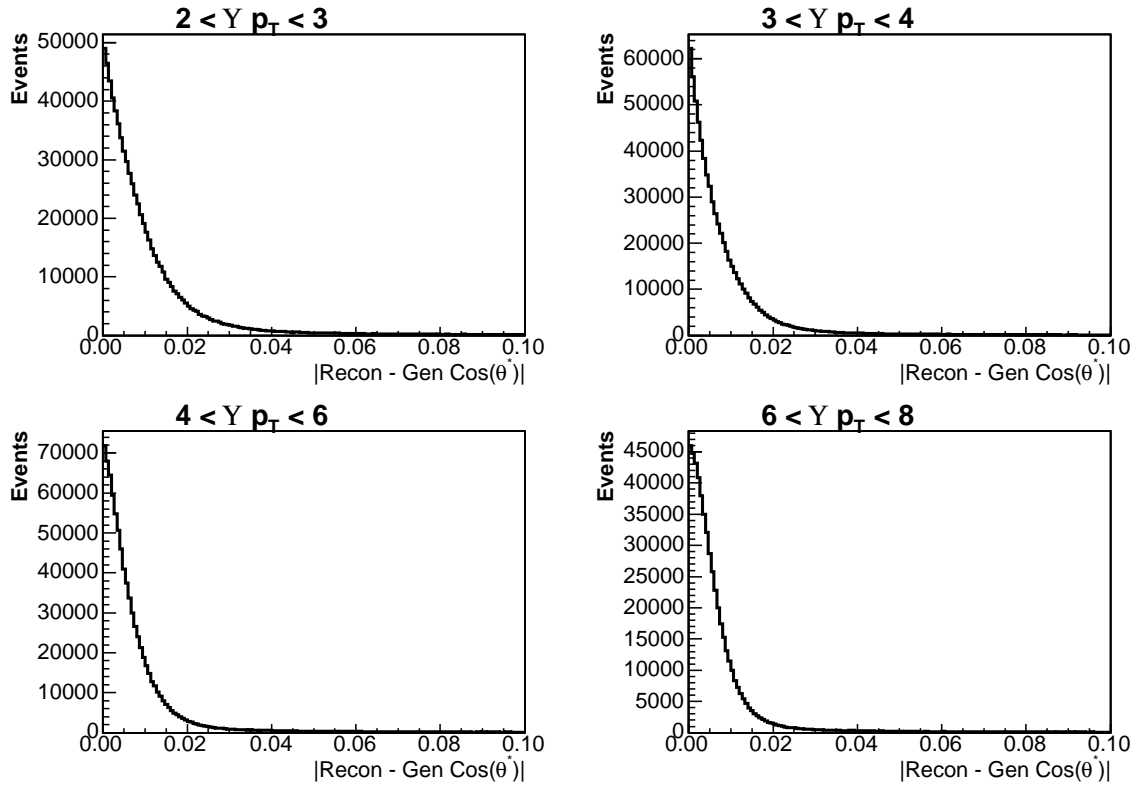


Figure 13: Absolute value of the difference between reconstructed $\cos \theta^*$ and generator values for the first four p_T bins. The resolution shown is much smaller than the bin sizes, so event migration effects are considered negligible.

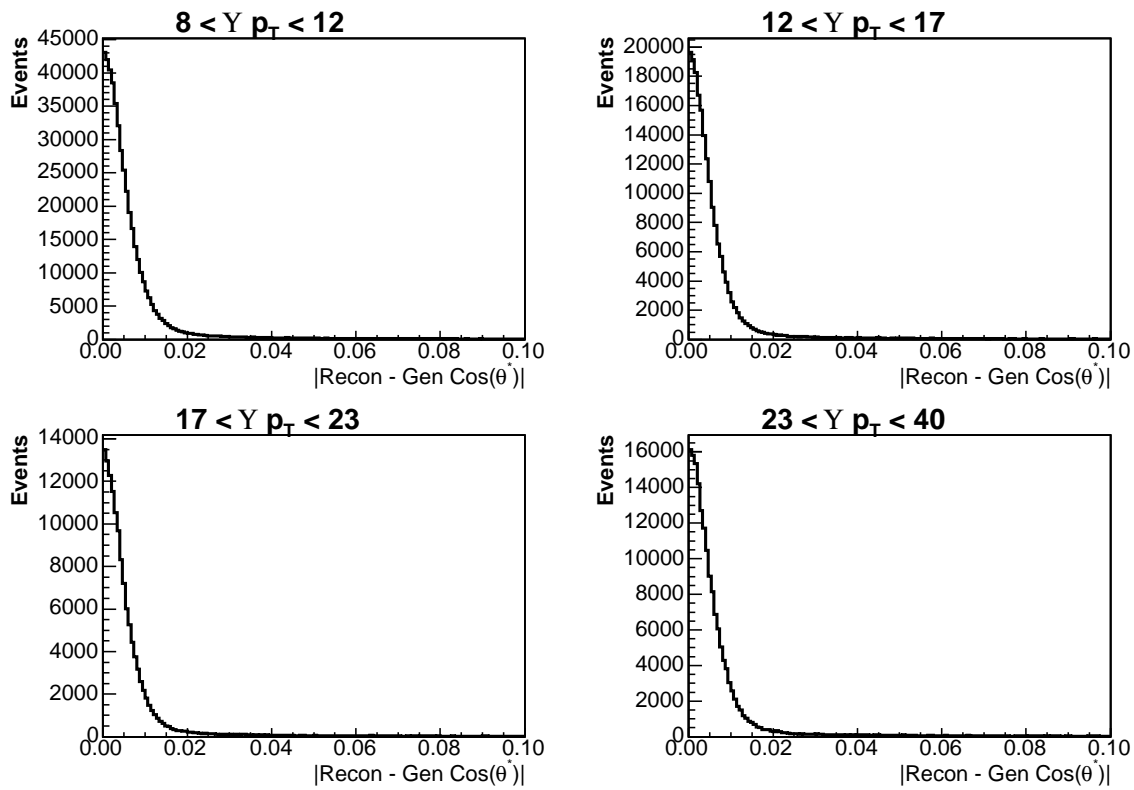


Figure 14: Absolute value of the difference between reconstructed $\cos \theta^*$ and generator values for the last four p_T bins. The resolution shown is much smaller than the bin sizes, so event migration effects are considered negligible.

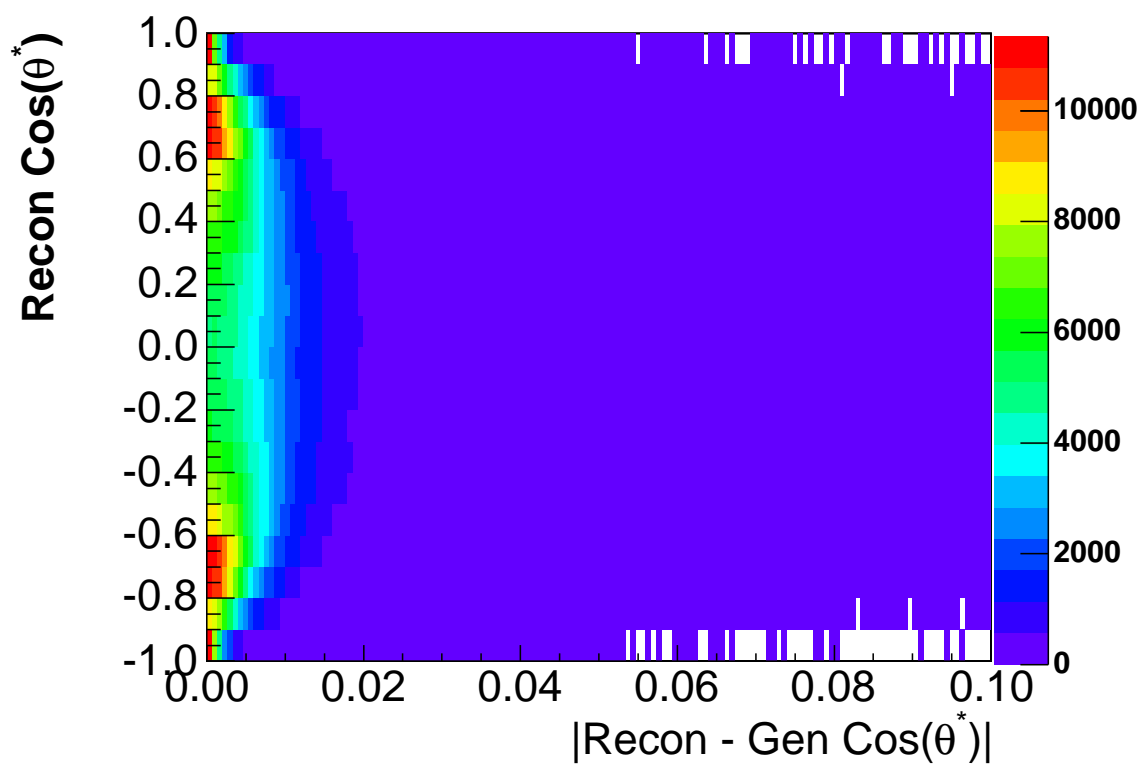


Figure 15: $\cos \theta^*$ resolution as it varies with $\cos \theta^*$ for T-polarized Monte Carlo.

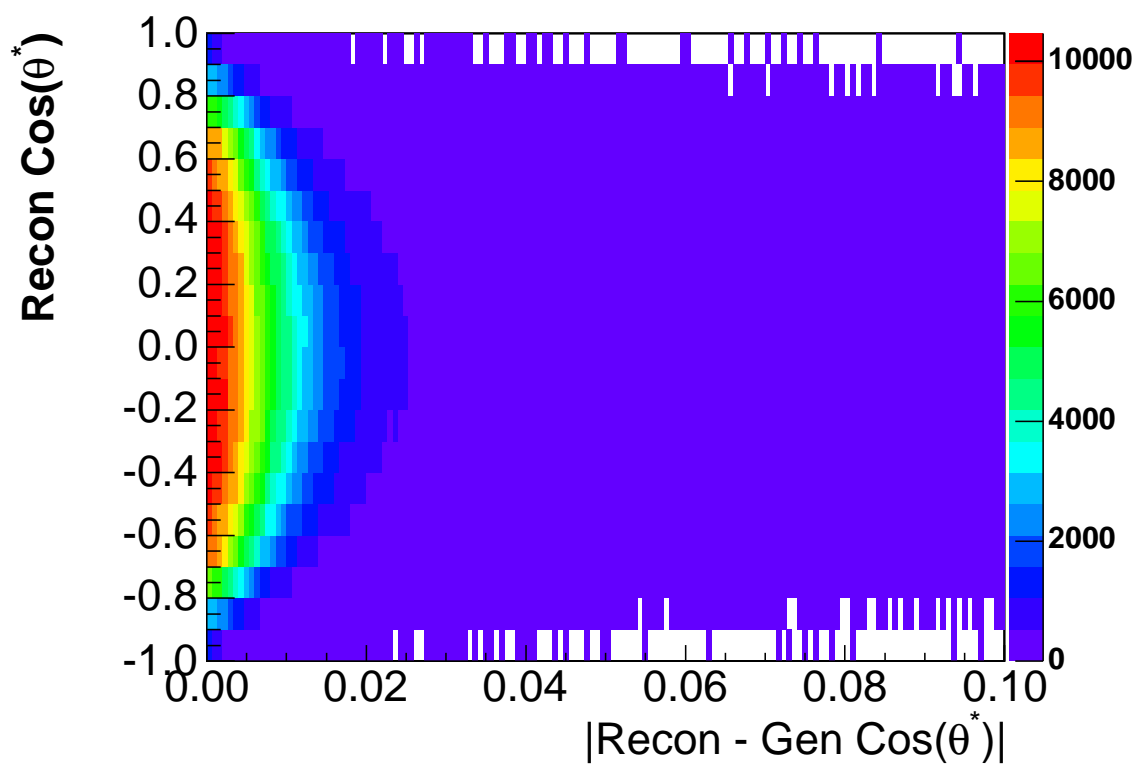


Figure 16: $\cos \theta^*$ resolution as it varies with $\cos \theta^*$ for L-polarized Monte Carlo.

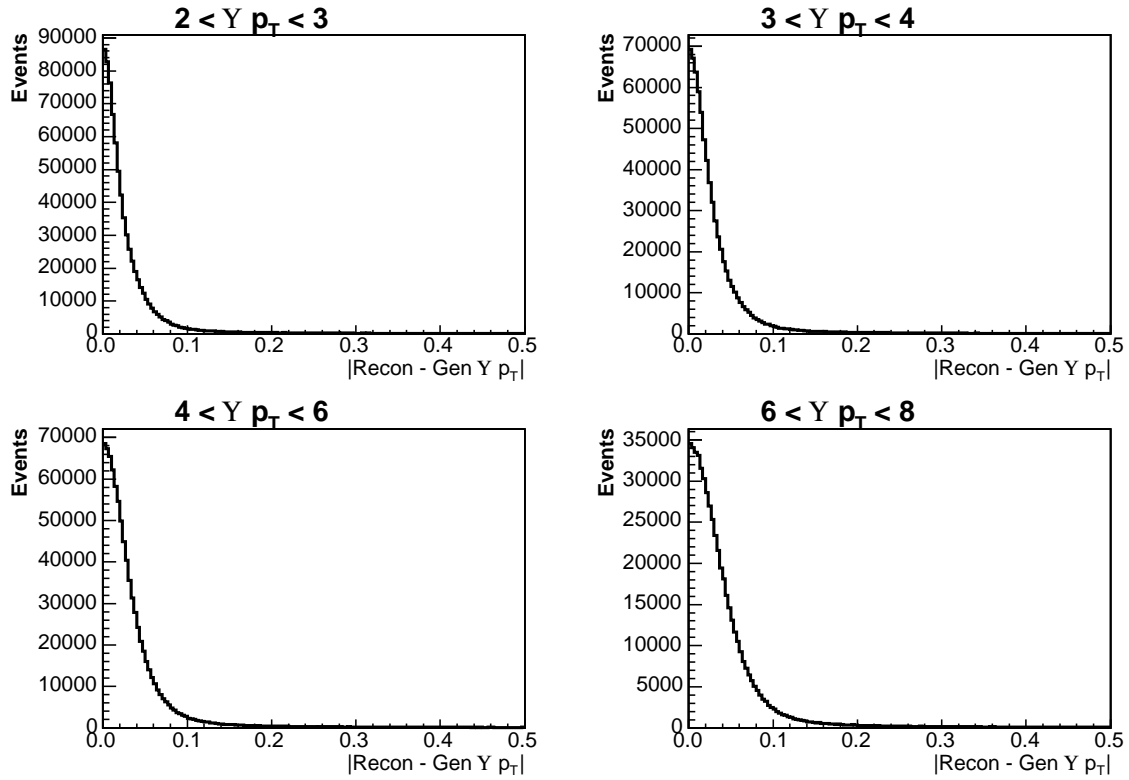


Figure 17: Absolute value of the difference between reconstructed $\Upsilon(1S)$ p_T and generator values for the first four p_T bins. The resolution shown is much smaller than the bin sizes, so event migration effects are considered negligible.

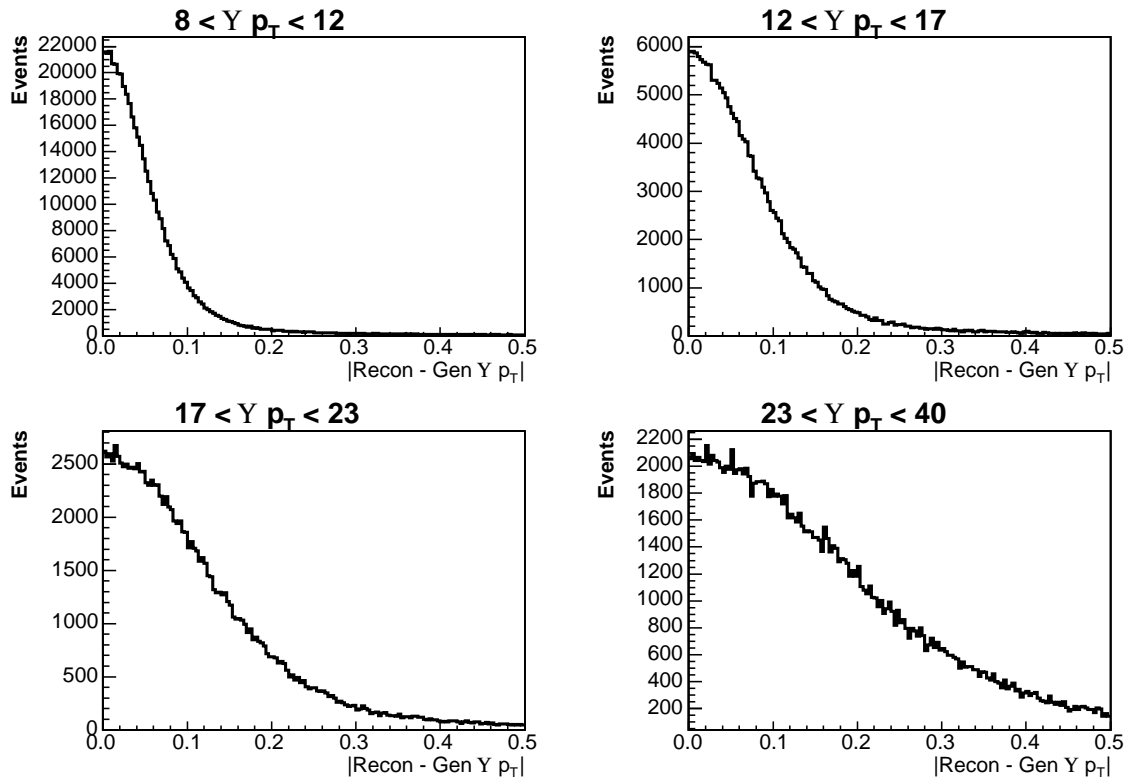


Figure 18: Absolute value of the difference between reconstructed $\Upsilon(1S)$ p_T and generator values for the last four p_T bins. The resolution shown is much smaller than the bin sizes, so event migration effects are considered negligible.

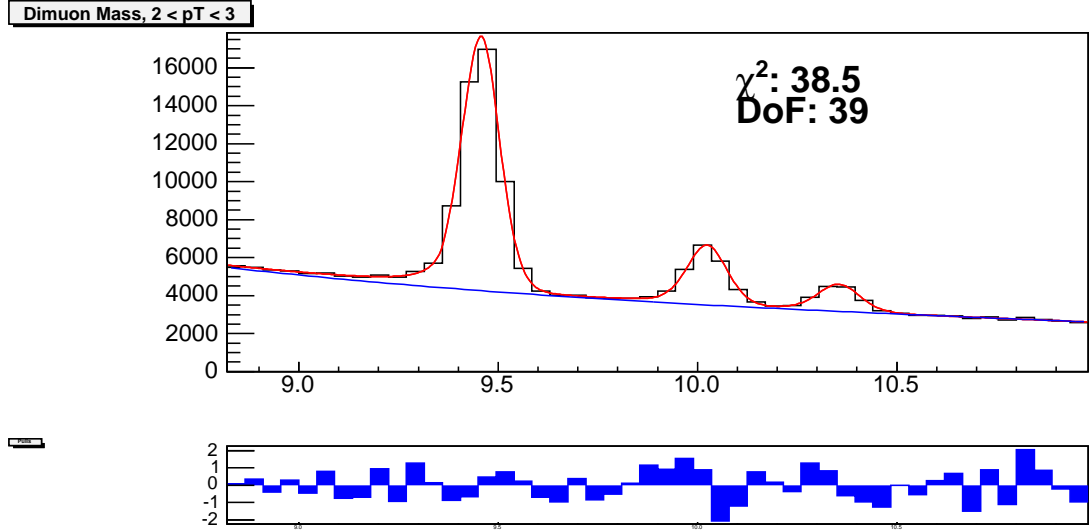


Figure 19: Mass fit in the first $\Upsilon(1S)$ p_T bin ($2\text{GeV}/c < p_T < 3\text{GeV}/c$), from which mass shifts and scale factors are extracted. Crystal Ball + Johnson SU functions are fit to each peak, and a third-order Chebyshev polynomial shape is applied to fit the background.

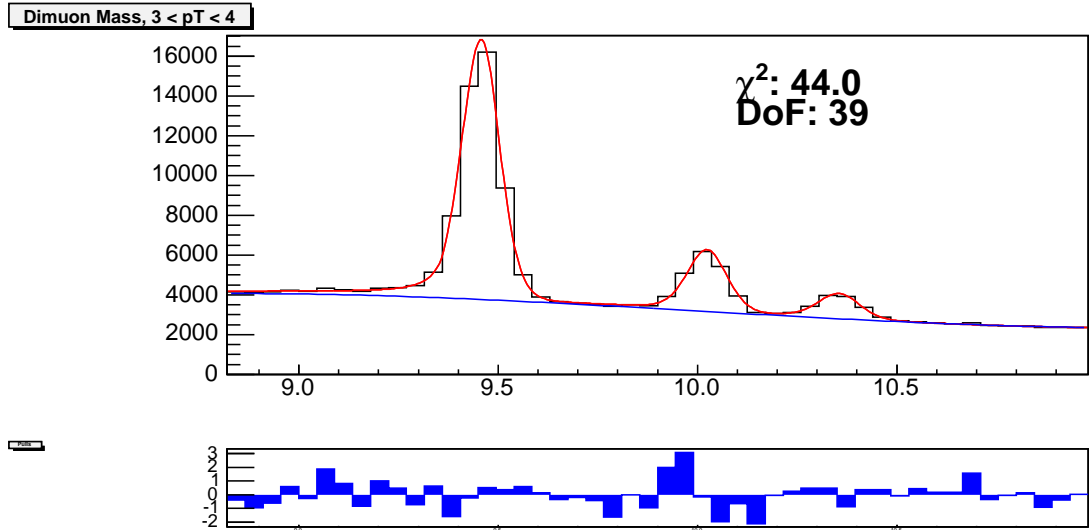


Figure 20: Mass fit in the second $\Upsilon(1S)$ p_T bin ($3\text{GeV}/c < p_T < 4\text{GeV}/c$), from which mass shifts and scale factors are extracted. Crystal Ball + Johnson SU functions are fit to each peak, and a third-order Chebyshev polynomial shape is applied to fit the background.

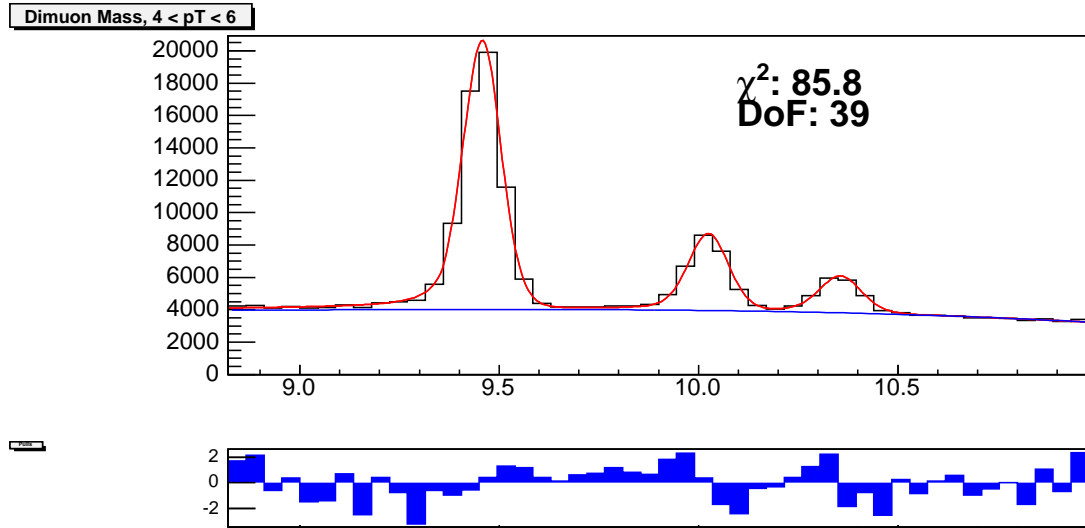


Figure 21: Mass fit in the third $\Upsilon(1S)$ p_T bin ($4\text{GeV}/c < p_T < 6\text{GeV}/c$), from which mass shifts and scale factors are extracted. Crystal Ball + Johnson SU functions are fit to each peak, and a third-order Chebyshev polynomial shape is applied to fit the background.

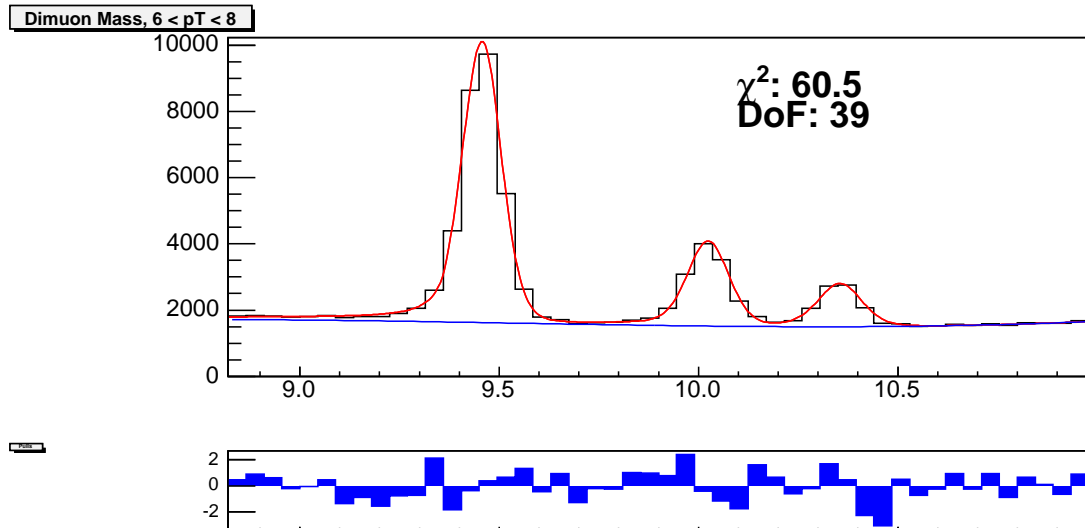


Figure 22: Mass fit in the fourth $\Upsilon(1S)$ p_T bin ($6\text{GeV}/c < p_T < 8\text{GeV}/c$), from which mass shifts and scale factors are extracted. Crystal Ball + Johnson SU functions are fit to each peak, and a third-order Chebyshev polynomial shape is applied to fit the background.

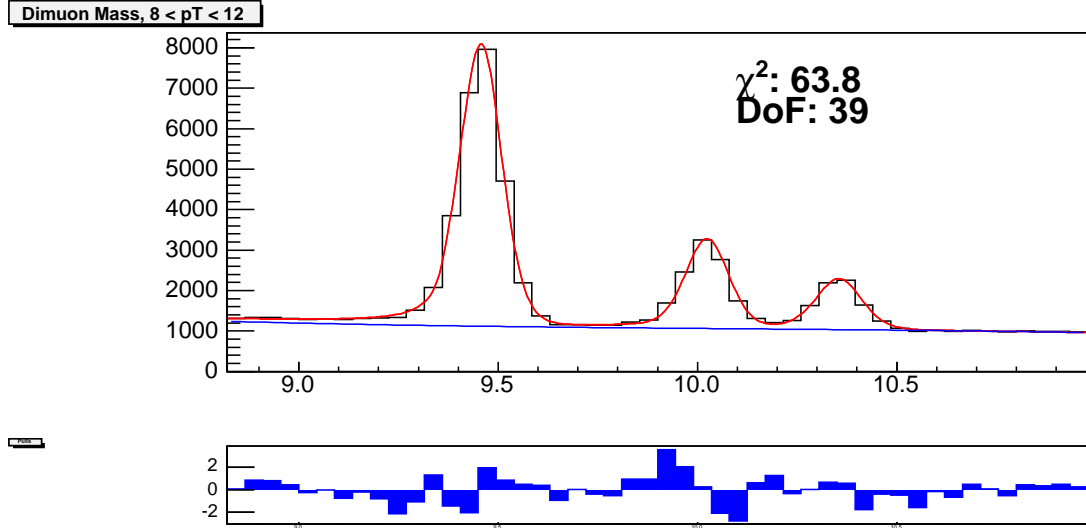


Figure 23: Mass fit in the fifth $\Upsilon(1S)$ p_T bin ($8\text{GeV}/c < p_T < 12\text{GeV}/c$), from which mass shifts and scale factors are extracted. Crystal Ball + Johnson SU functions are fit to each peak, and a third-order Chebyshev polynomial shape is applied to fit the background.

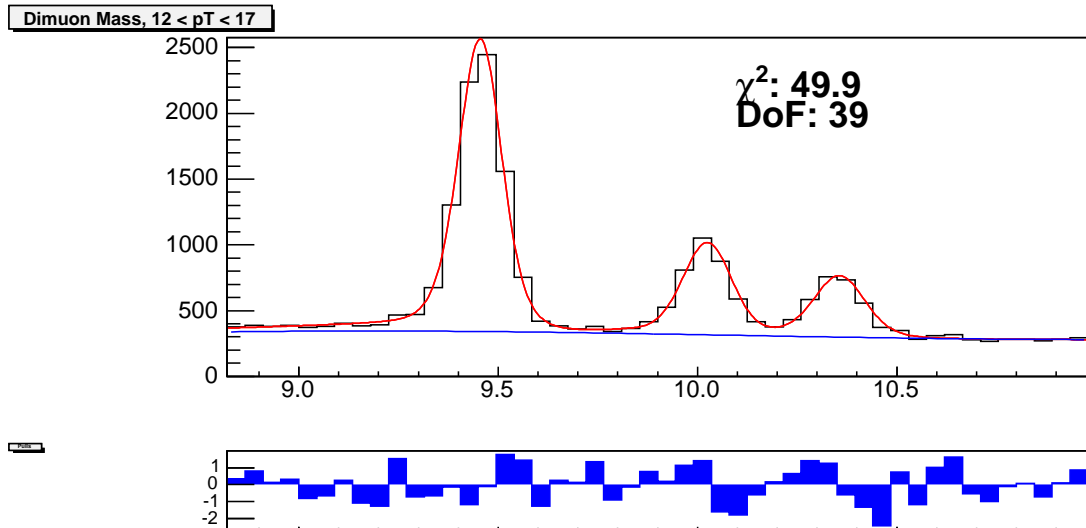


Figure 24: Mass fit in the sixth $\Upsilon(1S)$ p_T bin ($12\text{GeV}/c < p_T < 17\text{GeV}/c$), from which mass shifts and scale factors are extracted. Crystal Ball + Johnson SU functions are fit to each peak, and a third-order Chebyshev polynomial shape is applied to fit the background.

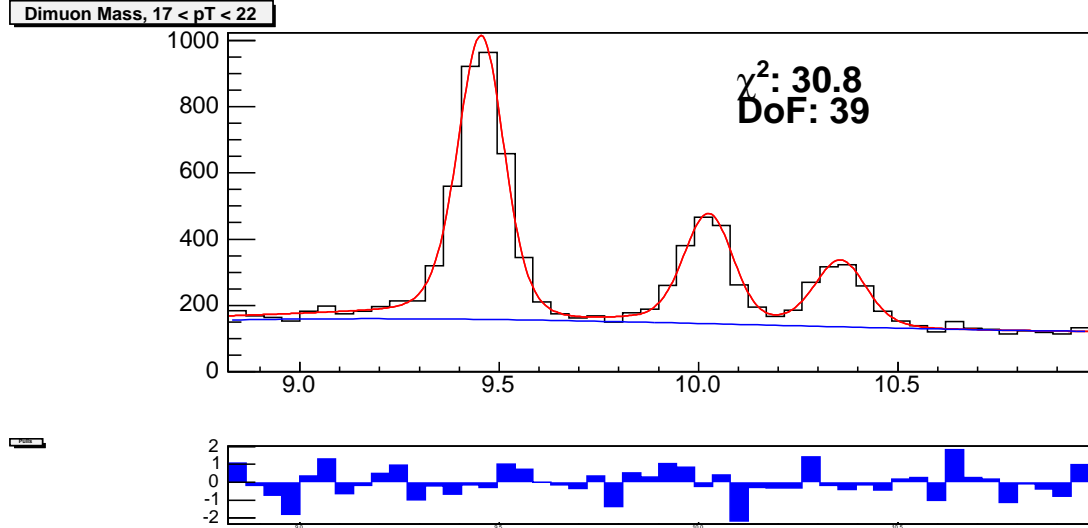


Figure 25: Mass fit in the seventh $\Upsilon(1S)$ p_T bin ($16\text{GeV}/c < p_T < 21\text{GeV}/c$), from which mass shifts and scale factors are extracted. Crystal Ball + Johnson SU functions are fit to each peak, and a third-order Chebyshev polynomial shape is applied to fit the background.

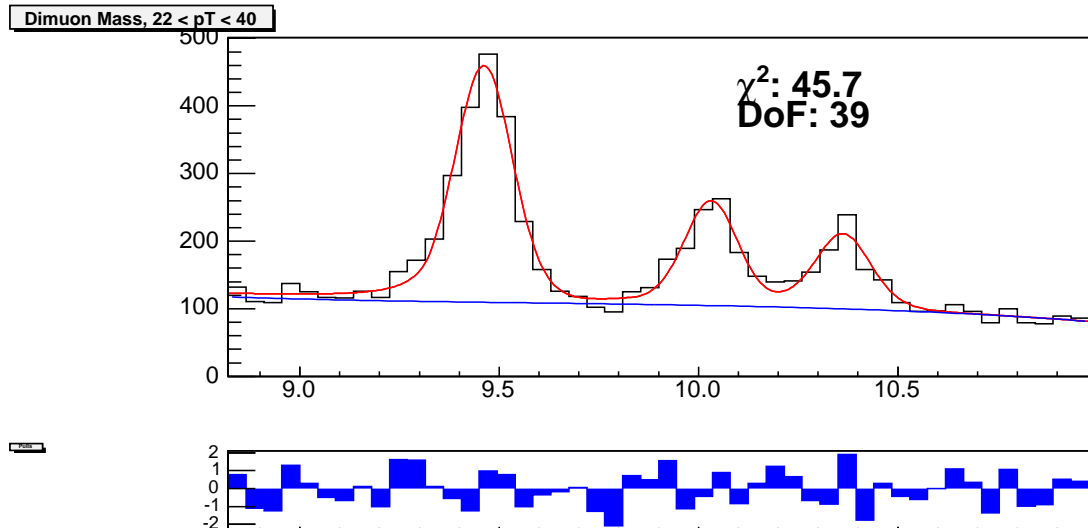


Figure 26: Mass fit in the eighth $\Upsilon(1S)$ p_T bin ($21\text{GeV}/c < p_T < 40\text{GeV}/c$), from which mass shifts and scale factors are extracted. Crystal Ball + Johnson SU functions are fit to each peak, and a third-order Chebyshev polynomial shape is applied to fit the background.

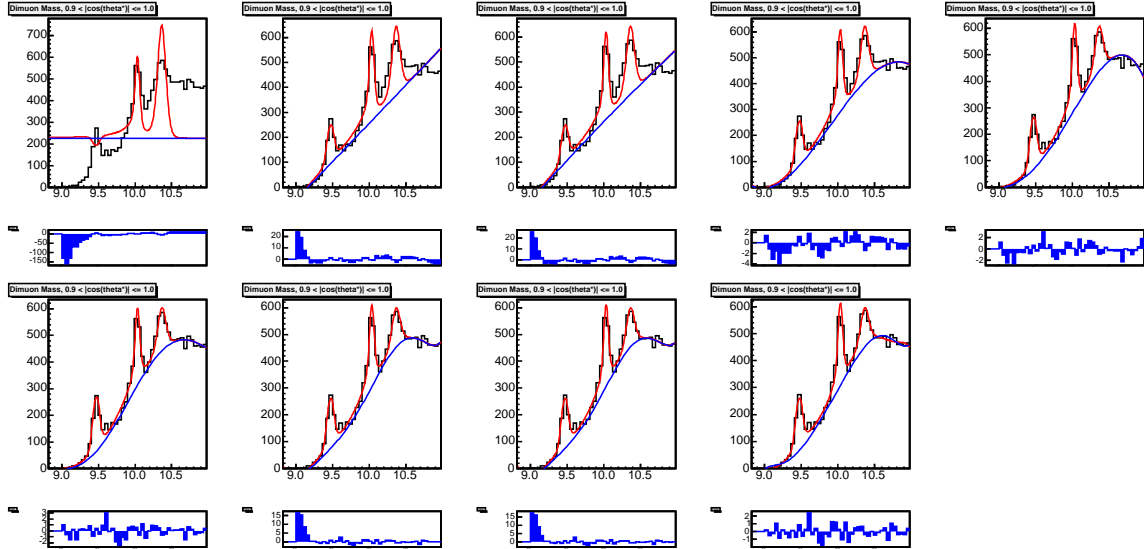


Figure 27: Mass fits for the $\Upsilon(1S)$, third p_T bin, tenth angular bin, using each Chebyshev Polynomial. This is a bin for which it may be difficult to choose the appropriate background shape, owing to its sparsely-populated lower bins and its curvature.

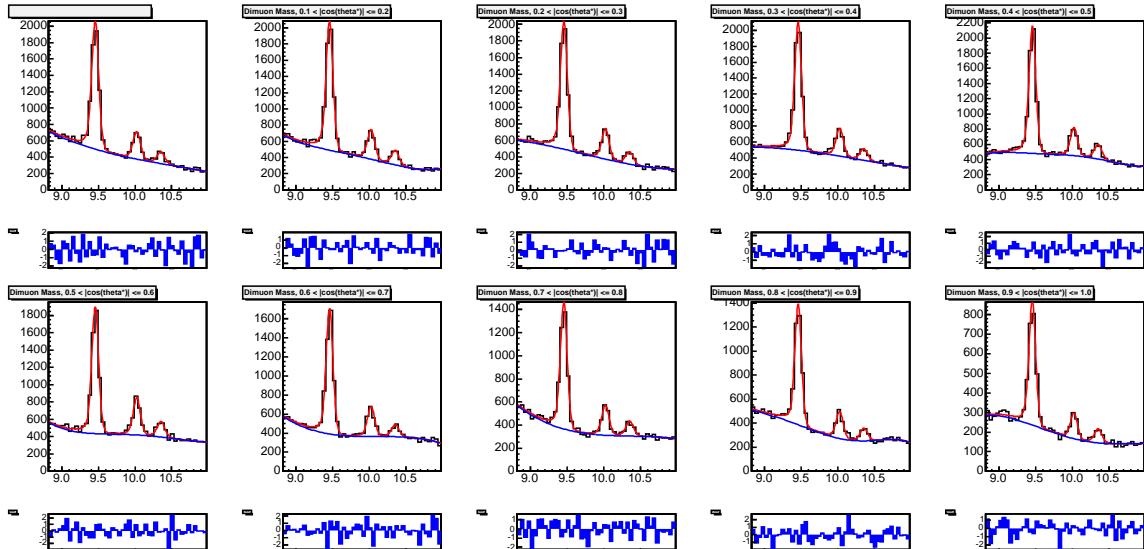


Figure 28: Mass fits in each $\cos \theta^*$ bin of the first $\Upsilon(1S)$ p_T bin ($2\text{GeV}/c < p_T < 3\text{GeV}/c$), from which signal distributions are extracted. Peak shapes are determined by Crystal Ball + Johnson SU functions fit to Monte Carlo, and background is modeled by a optimized Chebyshev polynomial.

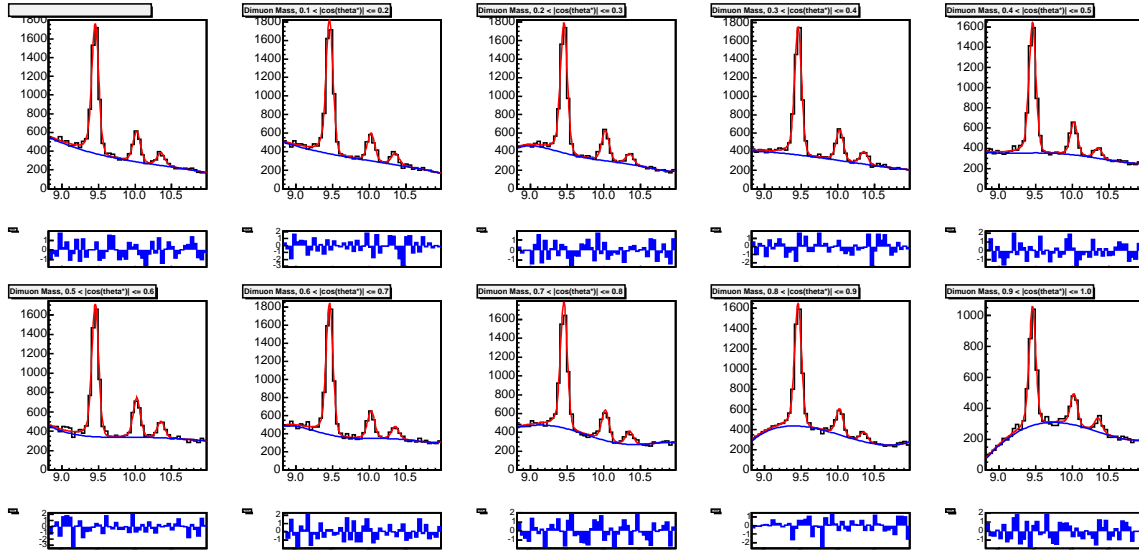


Figure 29: Mass fits in each $\cos \theta^*$ bin of the second $\Upsilon(1S)$ p_T bin ($3\text{GeV}/c < p_T < 4\text{GeV}/c$), from which signal distributions are extracted. Peak shapes are determined by Crystal Ball + Johnson SU functions fit to Monte Carlo, and background is modeled by a optimized Chebyshev polynomial.

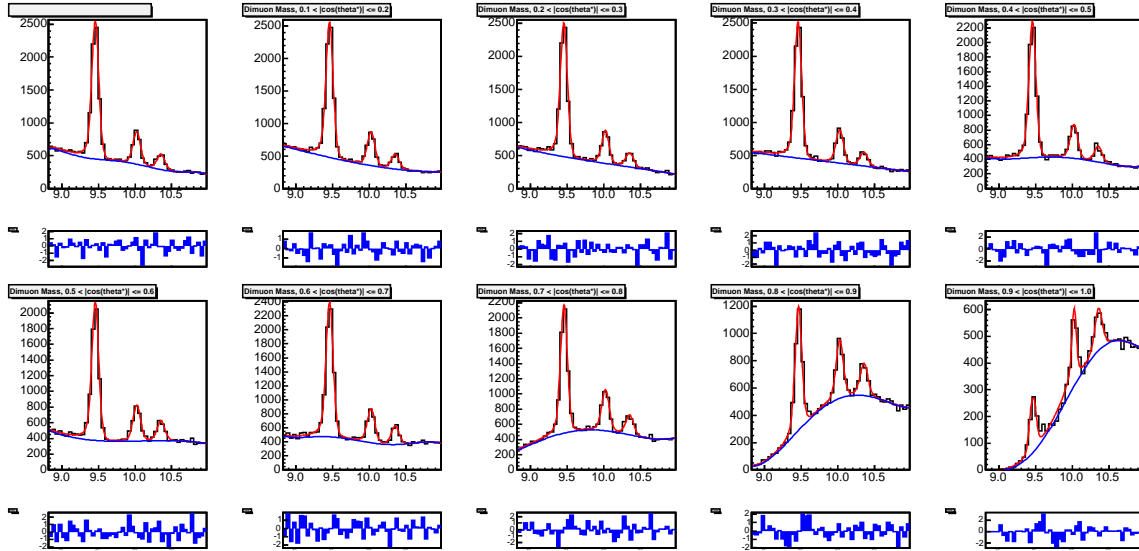


Figure 30: Mass fits in each $\cos \theta^*$ bin of the third $\Upsilon(1S)$ p_T bin ($4\text{GeV}/c < p_T < 6\text{GeV}/c$), from which signal distributions are extracted. Peak shapes are determined by Crystal Ball + Johnson SU functions fit to Monte Carlo, and background is modeled by a optimized Chebyshev polynomial.

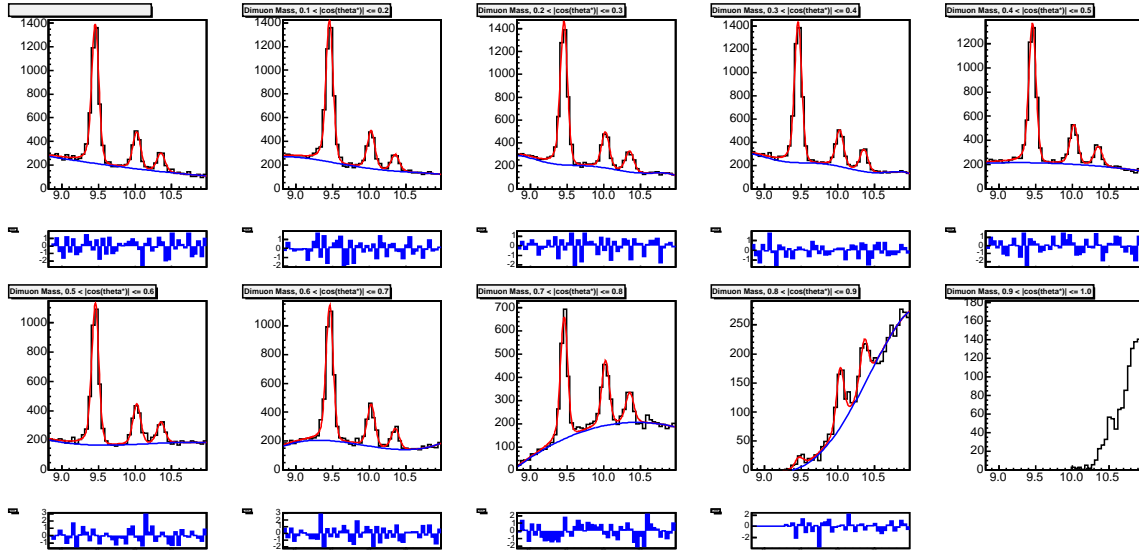


Figure 31: Mass fits in each $\cos \theta^*$ bin of the fourth $\Upsilon(1S)$ p_T bin ($6\text{GeV}/c < p_T < 8\text{GeV}/c$), from which signal distributions are extracted. Peak shapes are determined by Crystal Ball + Johnson SU functions fit to Monte Carlo, and background is modeled by a optimized Chebyshev polynomial.

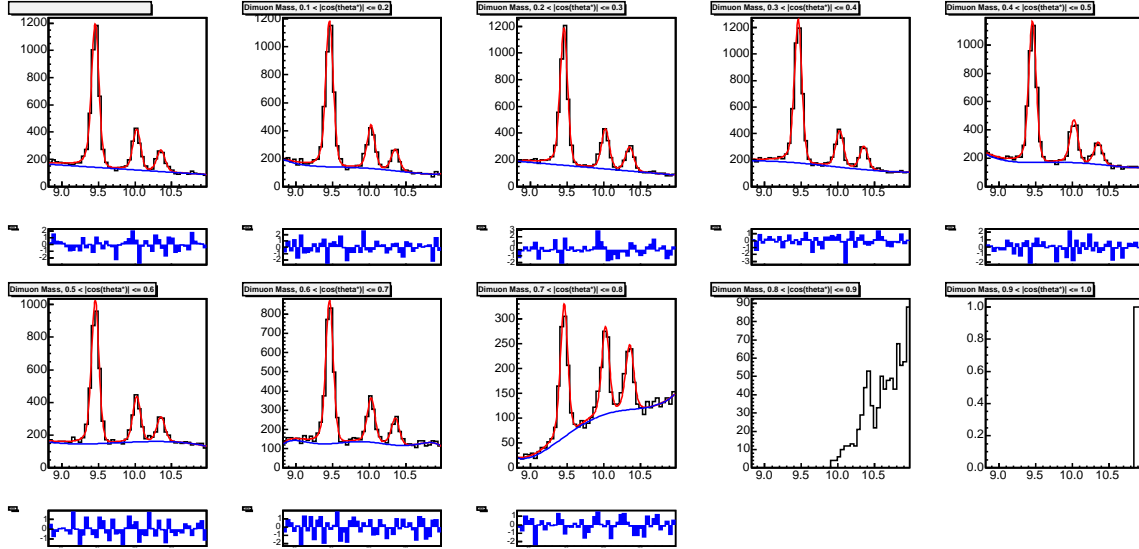


Figure 32: Mass fits in each $\cos \theta^*$ bin of the fifth $\Upsilon(1S)$ p_T bin ($8\text{GeV}/c < p_T < 12\text{GeV}/c$), from which signal distributions are extracted. Peak shapes are determined by Crystal Ball + Johnson SU functions fit to Monte Carlo, and background is modeled by a optimized Chebyshev polynomial.

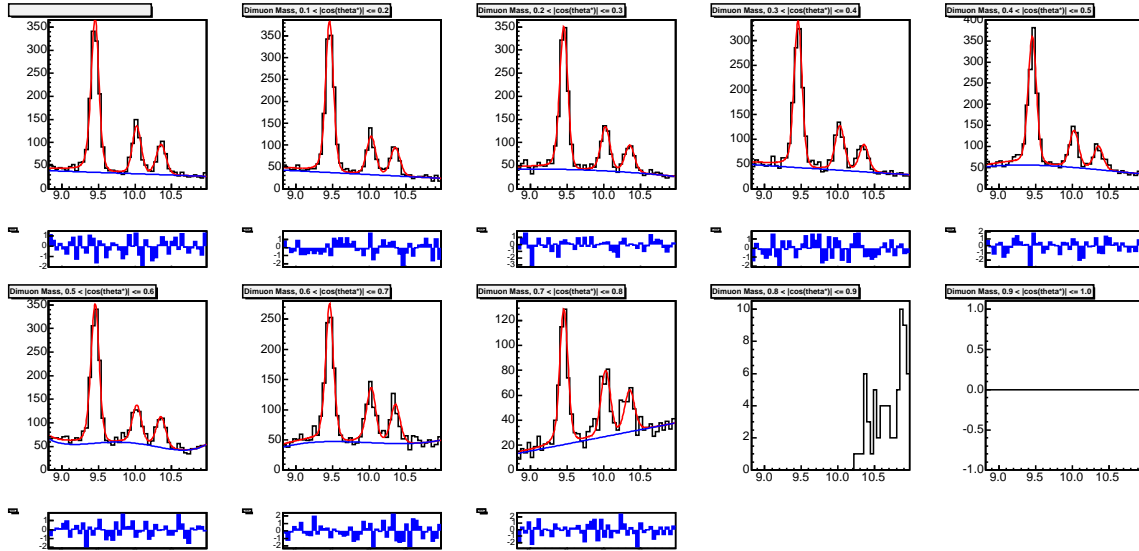


Figure 33: Mass fits in each $\cos \theta^*$ bin of the sixth $\Upsilon(1S)$ p_T bin ($12\text{GeV}/c < p_T < 16\text{GeV}/c$), from which signal distributions are extracted. Peak shapes are determined by Crystal Ball + Johnson SU functions fit to Monte Carlo, and background is modeled by a optimized Chebyshev polynomial.

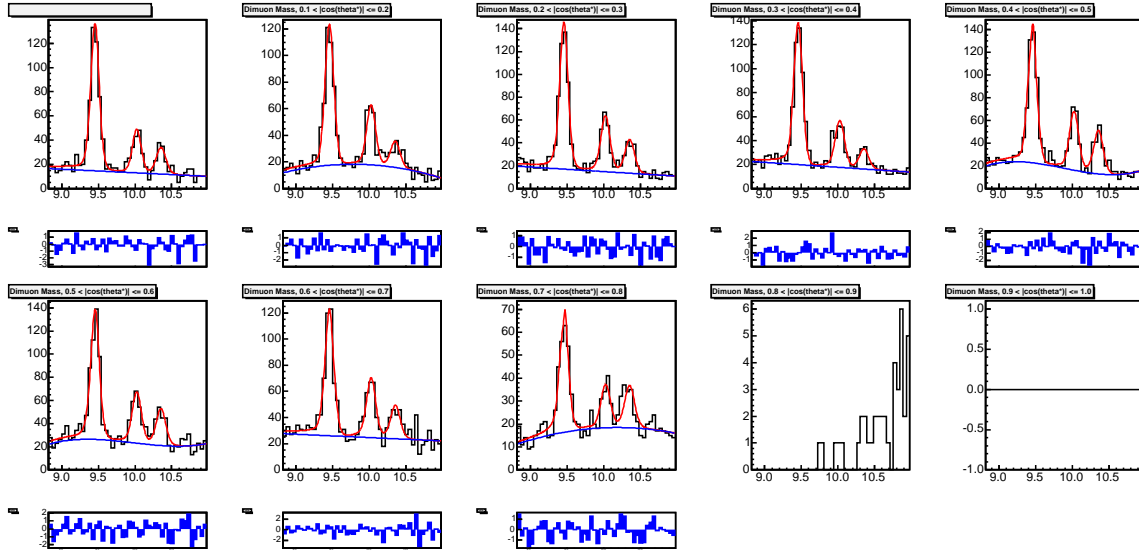


Figure 34: Mass fits in each $\cos \theta^*$ bin of the seventh $\Upsilon(1S)$ p_T bin ($16\text{GeV}/c < p_T < 21\text{GeV}/c$), from which signal distributions are extracted. Peak shapes are determined by Crystal Ball + Johnson SU functions fit to Monte Carlo, and background is modeled by a optimized Chebyshev polynomial.

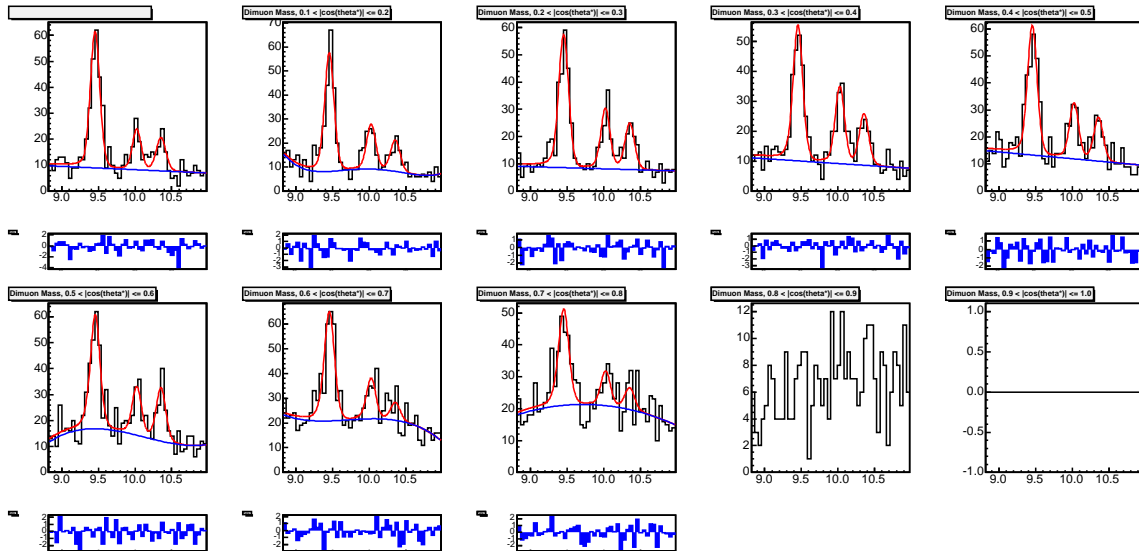


Figure 35: Mass fits in each $\cos \theta^*$ bin of the eighth $\Upsilon(1S)$ p_T bin ($21\text{GeV}/c < p_T < 40\text{GeV}/c$), from which signal distributions are extracted. Peak shapes are determined by Crystal Ball + Johnson SU functions fit to Monte Carlo, and background is modeled by a optimized Chebyshev polynomial.

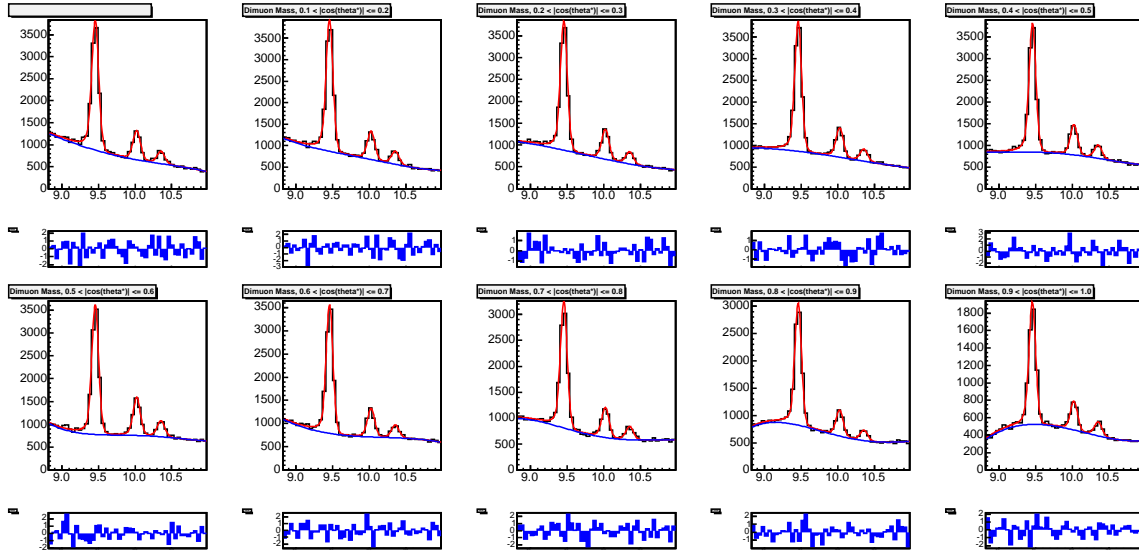


Figure 36: Mass fits in each $\cos \theta^*$ bin of the first $\Upsilon(2S)$ and $\Upsilon(3S)$ p_T bin ($2\text{GeV}/c < p_T < 4\text{GeV}/c$), from which signal distributions are extracted. Gaussian parameters for each peak are determined by fits to Monte Carlo, and the background is modelled by an optimized Chebyshev polynomial.

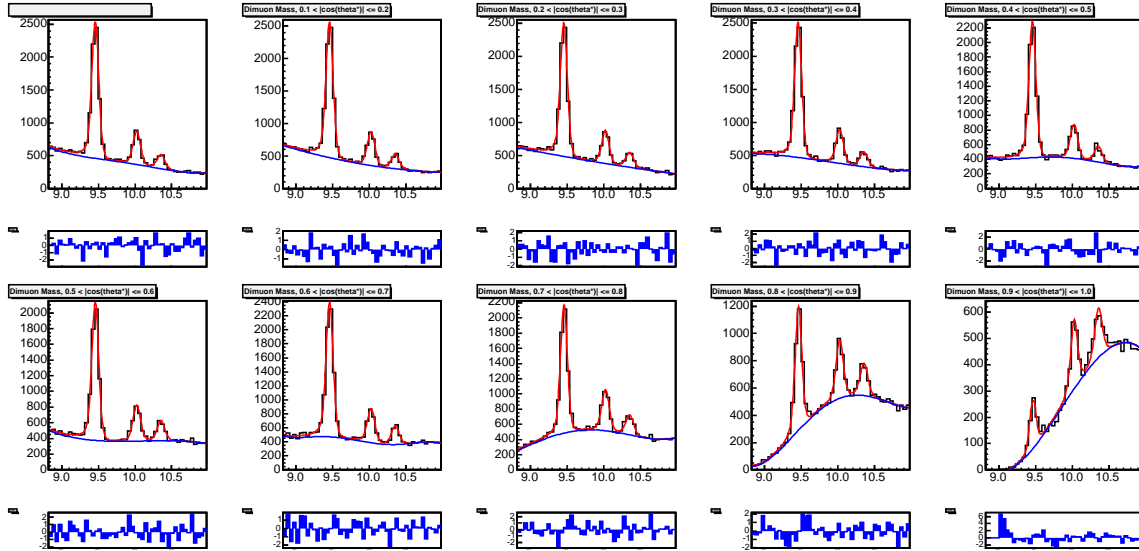


Figure 37: Mass fits in each $\cos \theta^*$ bin of the second $\Upsilon(2S)$ and $\Upsilon(3S)$ p_T bin ($4\text{GeV}/c < p_T < 6\text{GeV}/c$), from which signal distributions are extracted. Peak shapes are determined by Crystal Ball + Johnson SU functions fit to Monte Carlo, and background is modeled by a optimized Chebyshev polynomial.

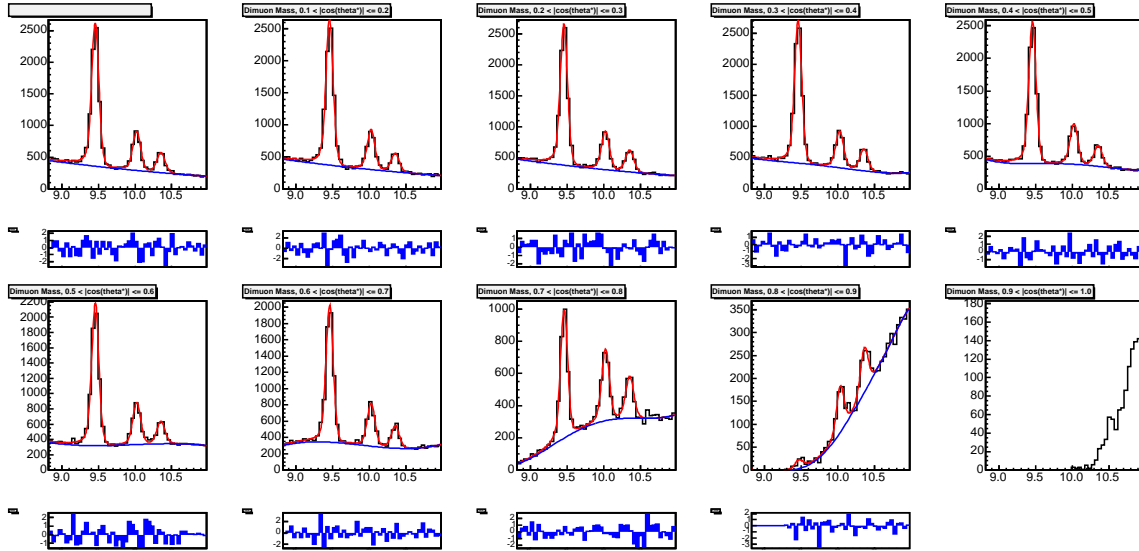


Figure 38: Mass fits in each $\cos \theta^*$ bin of the third $\Upsilon(2S)$ and $\Upsilon(3S)$ p_T bin ($6\text{GeV}/c < p_T < 12\text{GeV}/c$), from which signal distributions are extracted. Peak shapes are determined by Crystal Ball + Johnson SU functions fit to Monte Carlo, and background is modeled by a optimized Chebyshev polynomial.

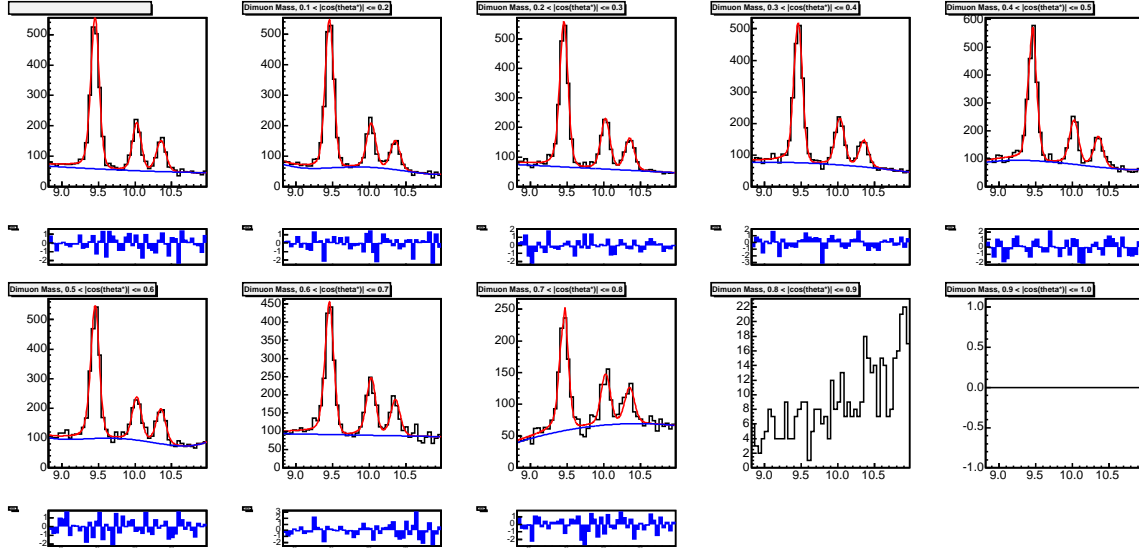


Figure 39: Mass fits in each $\cos \theta^*$ bin of the fourth $\Upsilon(2S)$ and $\Upsilon(3S)$ p_T bin ($12\text{GeV}/c < p_T < 40\text{GeV}/c$), from which signal distributions are extracted. Peak shapes are determined by Crystal Ball + Johnson SU functions fit to Monte Carlo, and background is modeled by a optimized Chebyshev polynomial.

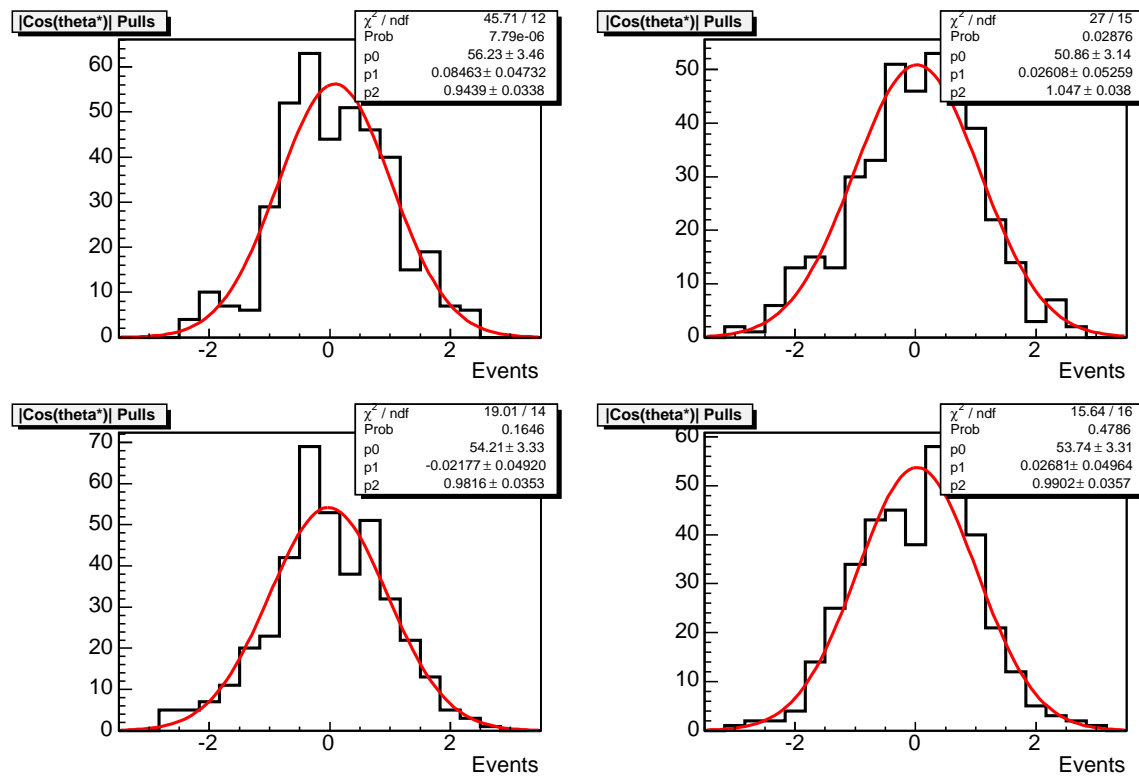


Figure 40: Pull distributions from polarization fitter for four trial values of η : 0.2 (top left), 0.4 (top right), 0.6 (bottom left), and 0.8 (bottom right).

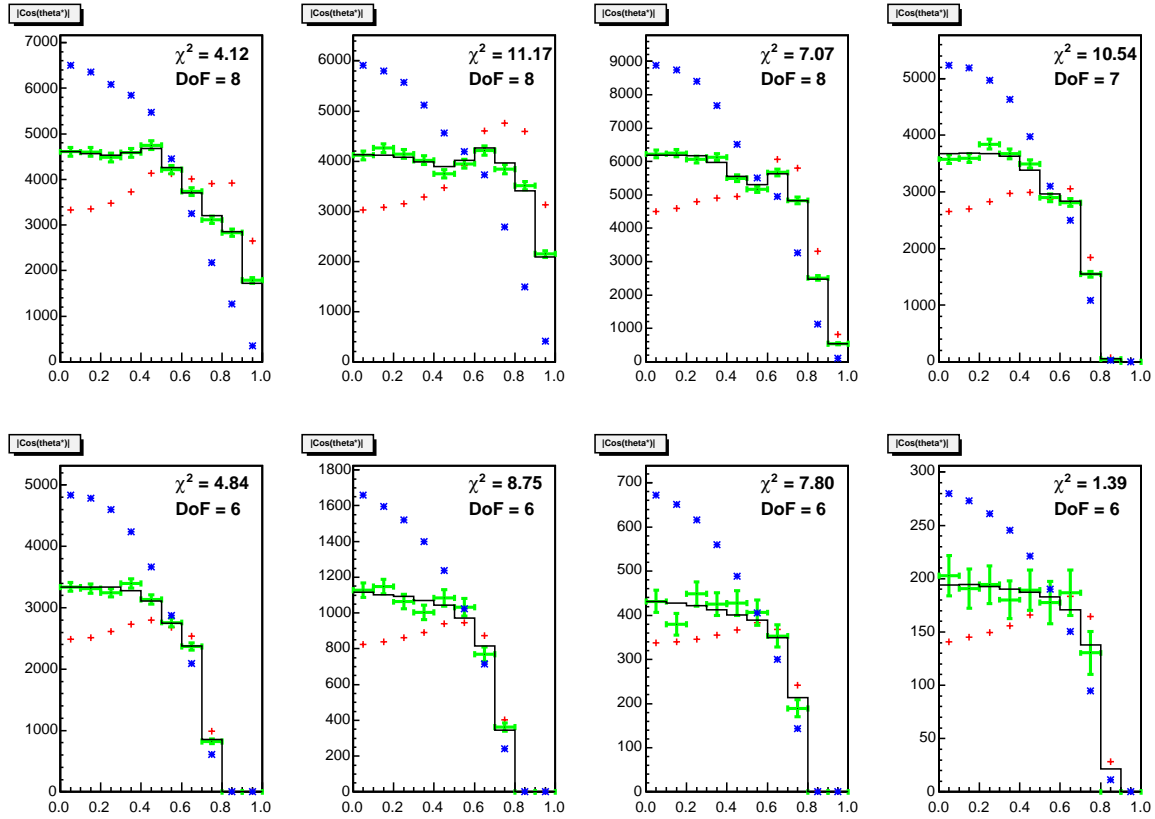


Figure 41: Polarization fits for $\Upsilon(1S)$, in each of the eight p_T bins. The data is shown in green with error bars. T and L templates are shown in red and blue points, respectively, while the best fit combination of the templates is indicated by the black line.

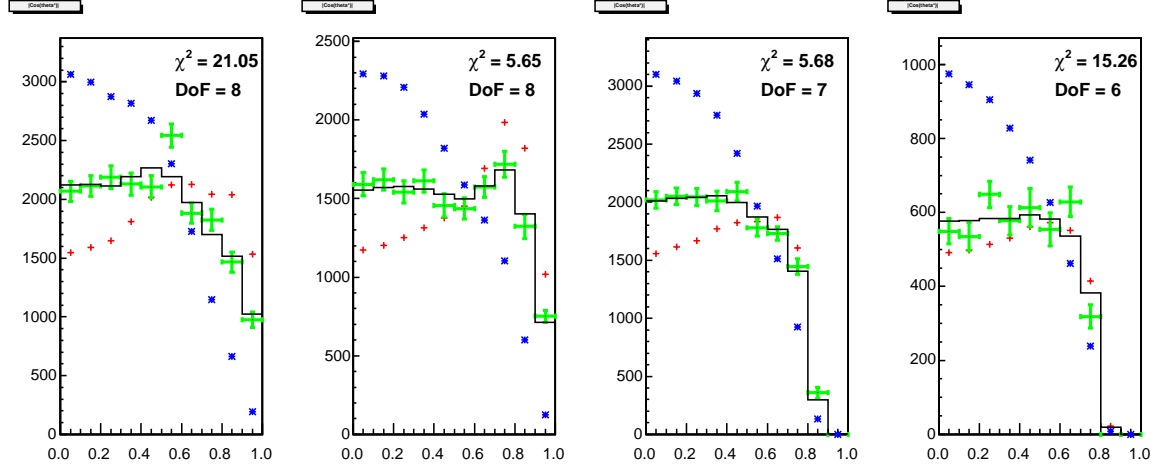


Figure 42: Polarization fits for $\Upsilon(2S)$, in each of the four p_T bins. The data is shown in green with error bars. T and L templates are shown in red and blue points, respectively, while the best fit combination of the templates is indicated by the black line.

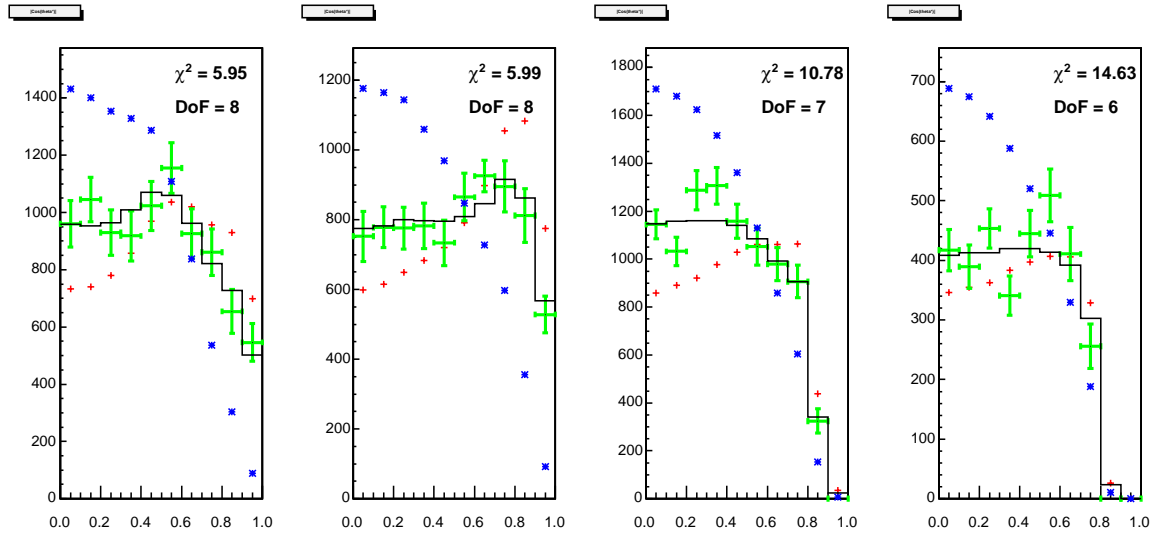


Figure 43: Polarization fits for $\Upsilon(3S)$, in each of the four p_T bins. The data is shown in green with error bars. T and L templates are shown in red and blue points, respectively, while the best fit combination of the templates is indicated by the black line.

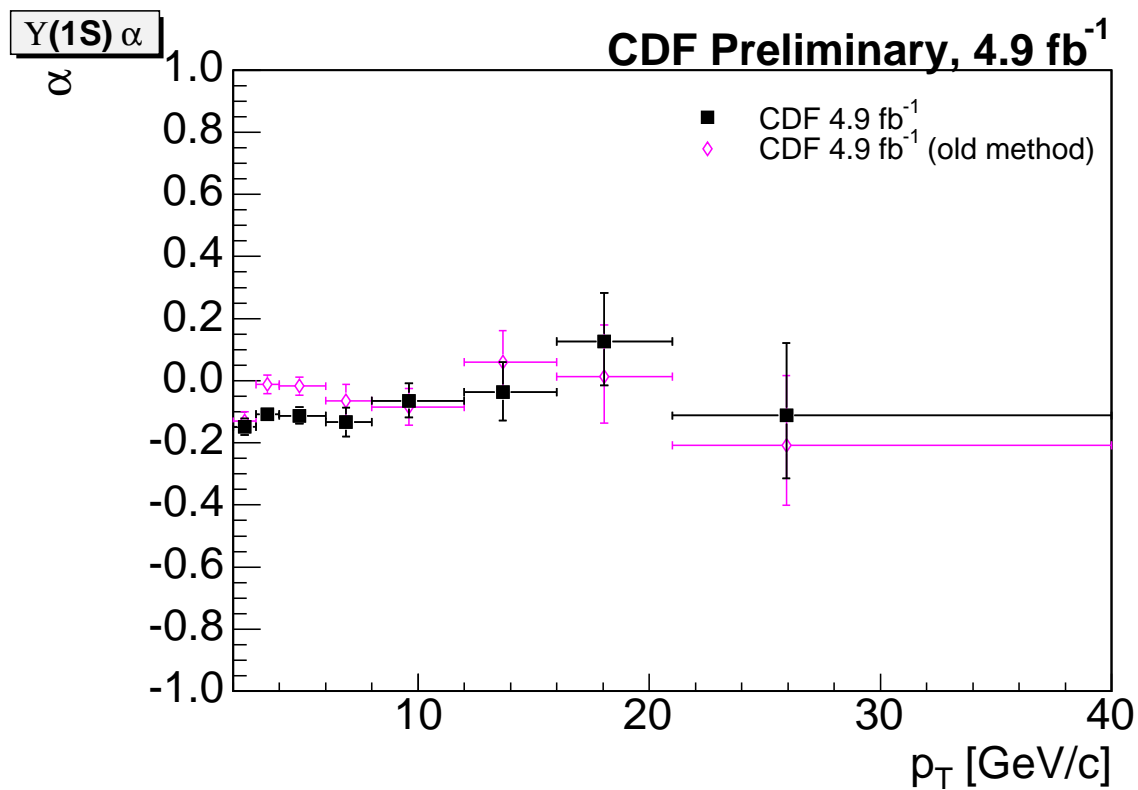


Figure 44: $\Upsilon(1S)$ polarization results using 4.9 fb^{-1} illustrating the results of the method from CDF9896 against the current method using the same data.

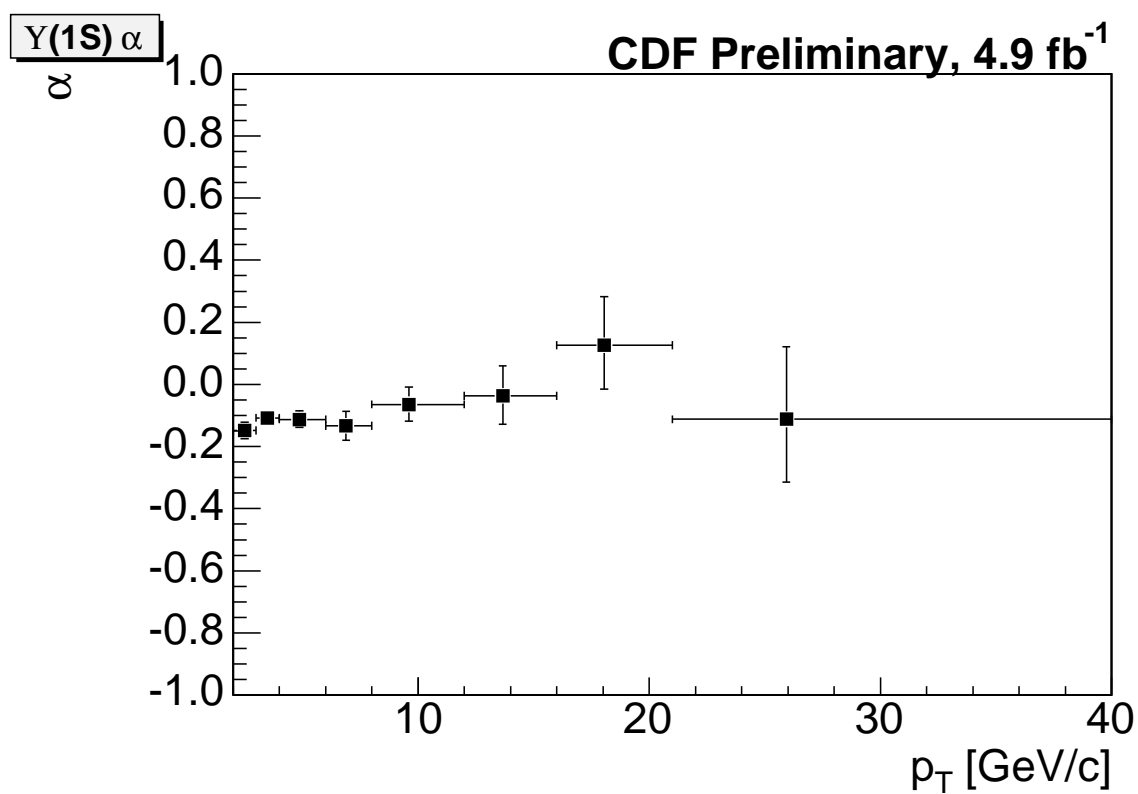
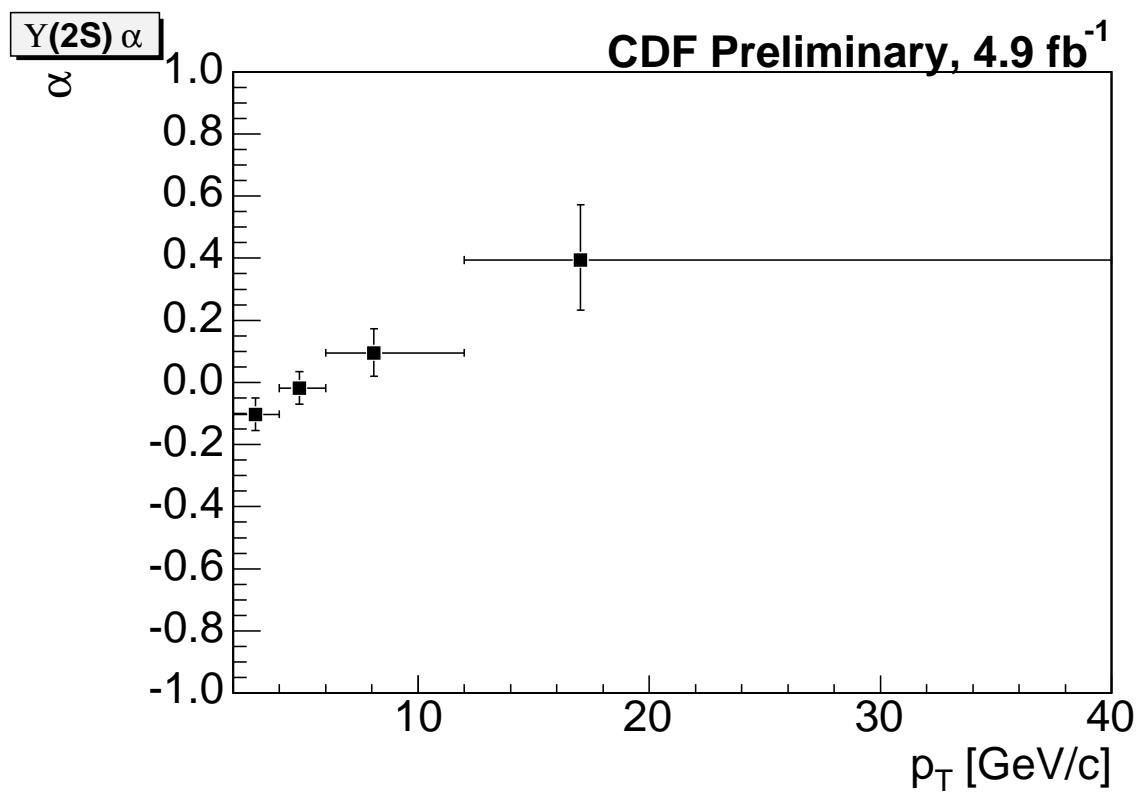


Figure 45: $\Upsilon(1S)$ polarization results.

Figure 46: $\Upsilon(2S)$ polarization results.

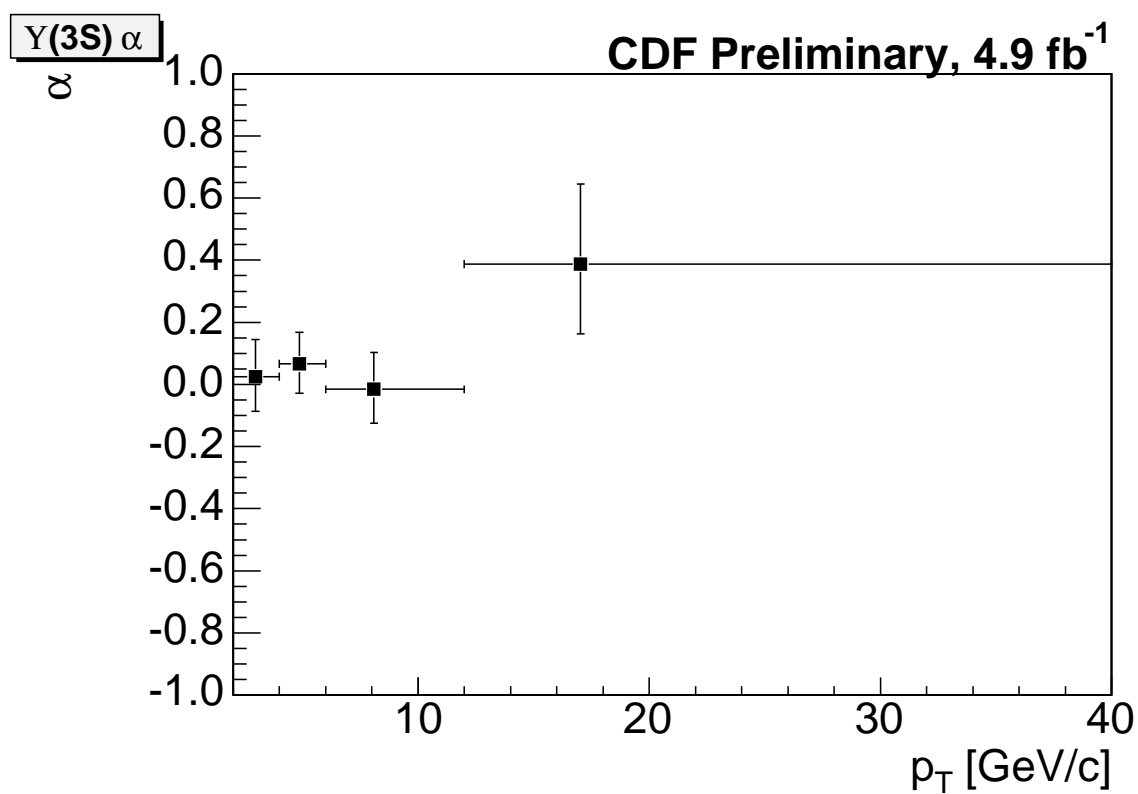


Figure 47: $\Upsilon(3S)$ polarization results.

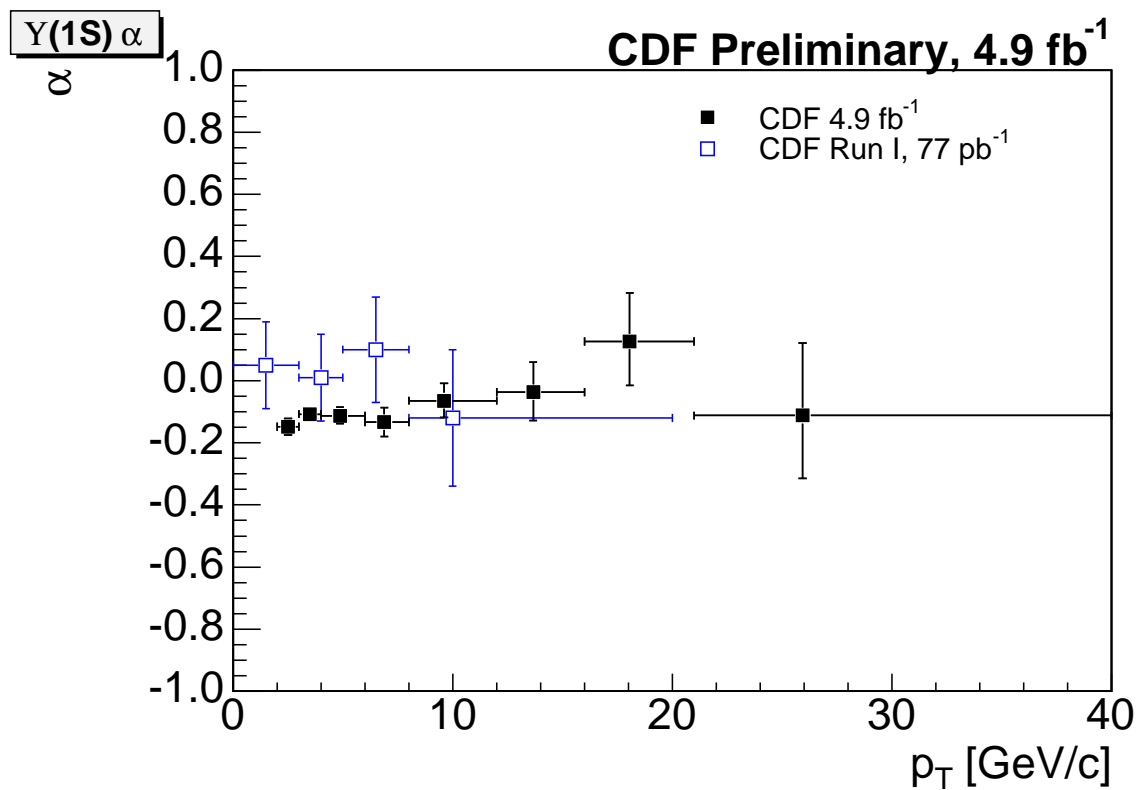


Figure 48: $\Upsilon(1S)$ polarization results show a slight low- p_T discrepancy with the CDF Run I measurement.

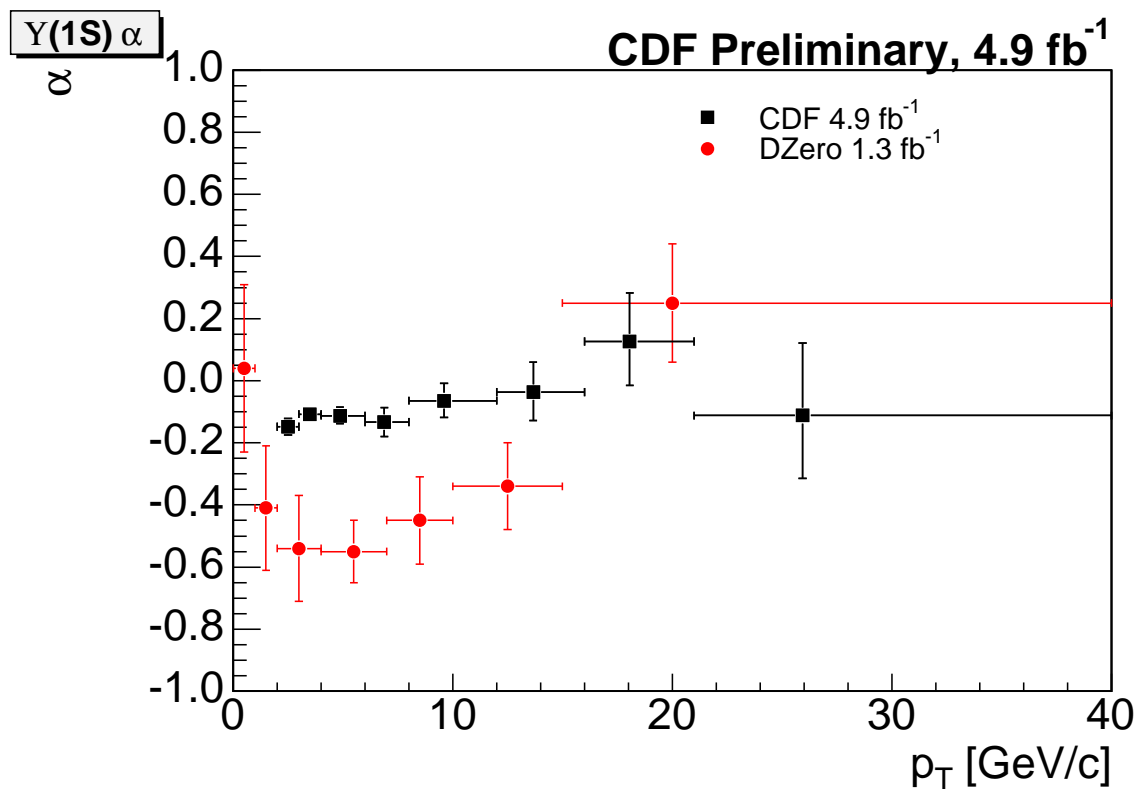


Figure 49: $\Upsilon(1S)$ polarization results stand in contrast to DZero measurements at low p_T , and become somewhat more consistent with increasing p_T .

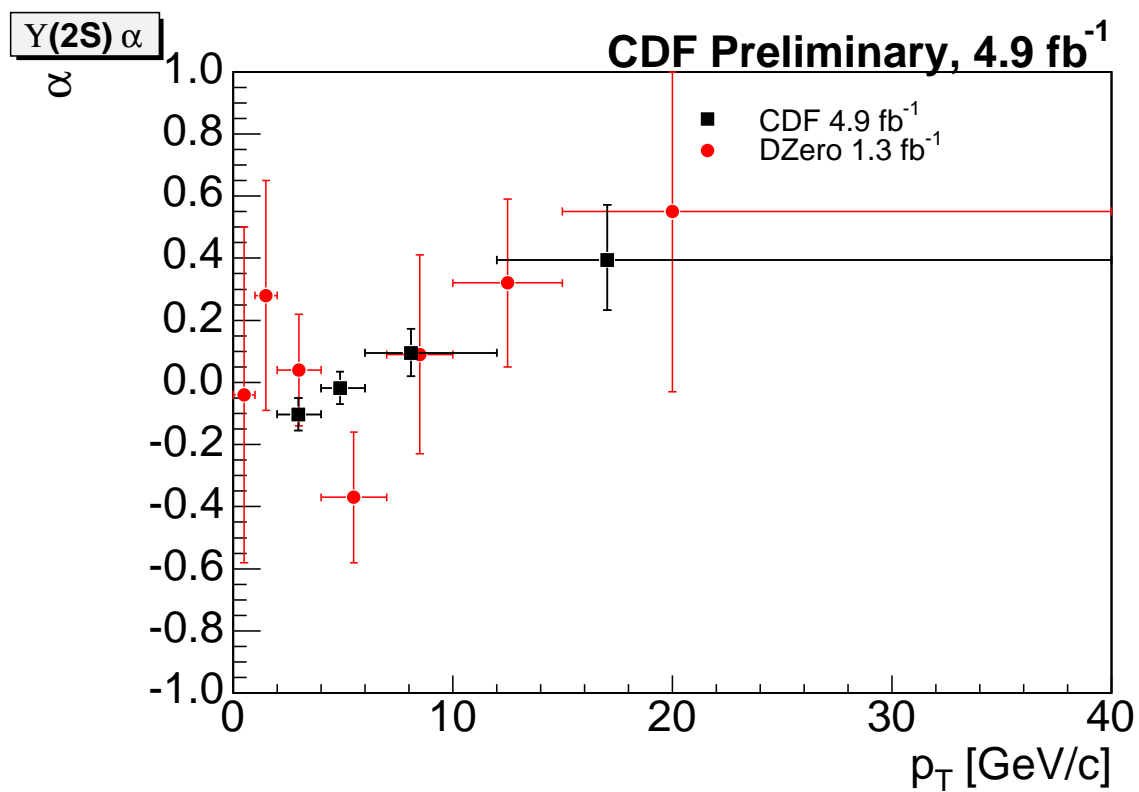


Figure 50: $\Upsilon(2S)$ polarization results are consistent with the DZero measurement.

8 Appendix A - Details of Monte Carlo Mass Fits

To illustrate the difference made by the tail function of the CB function, Fig. 51 shows successful fits results using two different fitting functions, JSU+G and JSU+CB, for $\Upsilon(1S)$ events generated with $|y| < 0.8$ and $3 < p_T < 4 GeV/c$. The histogram data are the same in both plots, including all events which survive production and cut selection, integrated over decay angles. The use of JSU+CB results in a much better χ^2 value for the fit, in accord with our observation above that it alone behaves well for all the mass fits in p_T and $\cos\theta^*$ bins.

In order to prepare for a study of possible mass shifts and width scale factors between data and Monte Carlo, we also made fits to data integrated over all decay angles in all p_T bins for the three $\Upsilon(nS)$ states. For the 1S and 3S cases the JSU+CB function gave a good fit to the integrated data as well as to the angle-binned data, as shown in the example of Fig. 51. However, in the 2S case, we observed some deviation between the Monte Carlo distribution and the bin integral of the JSU+CB fit function, indicating a discrepant PDF. The effect is subtle, but to ensure good behavior in the fit function for scale factor studies we defined a modified crystal ball function (MCB) for use in the 2S case by introducing a second Gaussian with the same centroid but different width and normalization. In Figure 52 one sees that using a JSU+MCB function improves the agreement between the Monte Carlo distribution and the fit compared to JSU+CB. The difference is small but noticeable for these statistics. The parametrization of the MCB is given in Eq. 7. The forms for both JSU+CB and JSU+MCB functions are well suited for mass shift and scale factor studies, described in the body of this note. Applying the MCB to the 1S and 3S distributions did not produce a significant improvement in the fit χ^2 . The plots showing the results of the maximum likelihood fits to the angle-integrated Monte Carlo events in p_T bins are shown in Figs. 53-55 for all three states.

The fit parameters for each p_T and $\cos\theta^*$ bin for each state are given in Tables B1-B3. The label for each column is $(p_T bin) - (\cos\theta^* bin)$. The column at left gives the name of the fit variable as it appears in the CB (first four entries) or JSU function definition. There are a pair of numbers for each entry: the fit value and its uncertainty. The mass centroids for the CB (E_t) and JSU (ϵ) are fixed in all fits, causing their uncertainties to be zero. Their values are determined by averaging the results of fits in all bins wherein these parameters have been allowed to float. The uncertainties in these parameters are always very small when they float.

².

²In Minuit all bins are used. In evaluating the fit we calculate χ^2 only for bins with population content > 25 . In all cases the peak bin population exceeds 6000 events/bin.

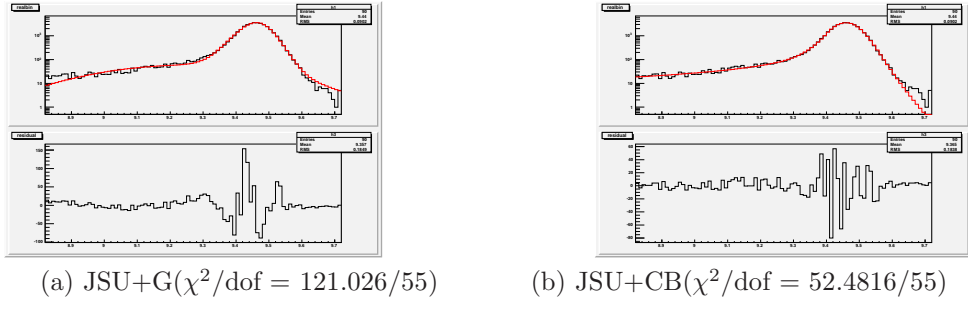


Figure 51: Fit function comparison for angle-integrated $\Upsilon(1S)$ mass distribution for $3 < p_T < 4$ GeV/c



Figure 52: Fit function comparison for $\Upsilon(2S)$ with $2 < p_T < 3$ GeV/c

9 Monte Carlo mass fit Results

The following tables describe fitting results for 1S, 2S and 3S states of upsilon. We apply JSU+CB for 1S and 3S, and JSU+MCB for 2S.

TABLE B1: $\Upsilon(1S)$

1S_10MeV	0_0	0_1	0_2	0_3	0_4	0_5	0_6	0_7	0_8	0_9	9.455
Et	9.455	9.455	9.455	9.455	9.455	9.455	9.455	9.455	9.455	9.455	9.455
0	0	0	0	0	0	0	0	0	0	0	0
sigma	0.0425089	0.038882	0.0411788	0.0413963	0.0401254	0.0409778	0.0402457	0.0426179	0.0396393	0.0330786	
n	0.00126944	0.00163081	0.00112434	0.00058379	0.00092477	0.00059822	0.00064427	0.00167435	0.00057791	0.00400483	
alpha	0.861583	1.11066	0.970489	0.992449	1.02875	0.942269	1.00726	0.840479	1.11715	0.87432	
0.0609162	0.0657177	0.0579229	0.0708235	0.0713722	0.0690353	0.0712068	0.090559	0.089384	0.186826		
0.180875	1.52522	1.73533	1.85772	1.75655	1.87728	1.82102	1.88804	1.79899	1.3277		
0.0787825	0.100161	0.10093	0.0419161	0.066118	0.0436722	0.0465132	0.112882	0.0439253	0.303074		
gamma	0.209741	0.17329	0.181144	0.114666	0.145696	0.0738587	0.0386369	0.274812	-0.226844	0.247094	
0.0298975	0.0293473	0.0471431	0.0688773	0.0450568	0.0883749	0.122295	0.0355258	0.37183	0.0278401		
delta	1.65888	2.19359	1.86026	1.2992	1.64155	1.29727	1.47136	1.54277	1.06891	4.05382	
0.228158	0.322157	0.346737	0.164842	0.205134	0.18809	0.249385	0.270192	0.183726	1.83465		
lamda	0.0666344	0.091333	0.0745187	0.0483414	0.0647098	0.04908	0.0545291	0.0565496	0.0340228	0.169468	
0.0116191	0.015732	0.0165737	0.00844095	0.00997748	0.00973175	0.0125165	0.0105802	0.0110062	0.0803961		
epsilon	9.4706	9.4706	9.4706	9.4706	9.4706	9.4706	9.4706	9.4706	9.4706	9.4706	9.4706
0	0	0	0	0	0	0	0	0	0	0	0
a_crystal	0.582759	0.511462	0.590063	0.71461	0.607444	0.766248	0.75842	0.587379	0.868392	0.30193	
0.0746312	0.070998	0.106369	0.0661638	0.0730565	0.0601129	0.078395	0.0910653	0.0634969	0.0926775		
chisq	43.1838	52.4812	62.2024	49.827	62.9288	57.743	54.8929	47.2233	50.0251	27.2671	
Bin	70	62	65	64	59	60	52	46	44	31	
MaximumX	9.46025	9.46001	9.46015	9.46116	9.46074	9.46037	9.46059	9.46029	9.46141	9.45865	

1S_10MeV	1_0	1_1	1_2	1_3	1_4	1_5	1_6	1_7	1_8	1_9	9.455
Et	9.455	9.455	9.455	9.455	9.455	9.455	9.455	9.455	9.455	9.455	9.455
0	0	0	0	0	0	0	0	0	0	0	0
sigma	0.040174	0.0389165	0.0438454	0.0399275	0.0429724	0.0413121	0.0412828	0.0404976	0.0482938	0.0394459	
n	0.00226208	0.00128043	0.00091725	0.00169598	0.00067608	0.00080105	0.00068322	0.00076347	0.00388304	0.00362961	
alpha	0.905437	1.15547	0.876667	1.01777	0.888587	0.855163	0.99855	1.20957	1.35879	0.799432	
0.0771792	0.0662775	0.061799	0.0759942	0.0660951	0.0639603	0.0923418	0.0810603	0.316553	0.233109		
0.164451	1.57014	1.85484	1.71813	1.92059	1.88388	1.83699	1.7	1.25579	1.67212		
0.119183	0.0728748	0.0655761	0.0915183	0.0460591	0.0523314	0.0547661	0.0543494	0.493496	0.241329		
gamma	0.180743	0.120256	0.156702	0.171382	0.100292	0.123245	0.0776814	0.0664577	0.294484	0.207197	
0.0258955	0.0392595	0.0573976	0.0381013	0.0590983	0.0630558	0.105968	0.121055	0.020046	0.036907		
delta	2.0417	2.33786	1.50931	1.90047	1.25923	1.51175	1.16821	1.62493	3.24239	2.09103	
0.351509	0.404935	0.228227	0.375672	0.144472	0.226763	0.219515	0.303637	0.792767	0.33765		
lamda	0.0878081	0.103291	0.0562999	0.0795927	0.045121	0.0583368	0.0443831	0.0629225	0.122184	0.0830137	
0.010836	0.0205184	0.0108161	0.0193004	0.00689335	0.0114213	0.0110989	0.0154411	0.033538	0.015425		
epsilon	9.4706	9.4706	9.4706	9.4706	9.4706	9.4706	9.4706	9.4706	9.4706	9.4706	9.4706
0	0	0	0	0	0	0	0	0	0	0	0
a_crystal	0.475808	0.584463	0.64982	0.58577	0.709483	0.686241	0.746865	0.728207	0.346219	0.337793	

1S_10MeV	2_0	2_1	2_2	2_3	2_4	2_5	2_6	2_7	3_0	3_1	3_2	9.455
Et	9.455	9.455	9.455	9.455	9.455	9.455	9.455	9.455	9.455	9.455	9.455	9.455
0	0	0	0	0	0	0	0	0	0	0	0	0
sigma	0.0414979	0.0425255	0.0412956	0.0408522	0.0417938	0.0420081	0.0415767	0.0416398	0.0407285	0.0387104	0.043403	
0.00087274	0.001224	0.0014349	0.00164165	0.00071563	0.00111608	0.00078165	0.00061252	0.00118149	0.0014798	0.00090965		
n	0.989245	0.896928	0.927184	0.995937	0.915738	0.952756	1.15554	1.23295	0.945176	0.978141	0.920011	
0.0562755	0.0550725	0.0571853	0.0620911	0.0639685	0.0594537	0.0680852	0.0807066	0.0739491	0.0727919	0.0868944		
alpha	1.77749	1.74713	1.7389	1.72594	1.87539	1.72696	1.7164	1.7947	1.76551	1.66463	1.84656	
0.0462831	0.0704808	0.0788231	0.0718905	0.0466196	0.0627307	0.0490549	0.0422128	0.0622802	0.0732943	0.055589		
gamma	0.0908545	0.17352	0.165311	0.143574	0.121356	0.161103	0.0682772	-0.0242764	0.0920377	0.114042	0.110444	
0.0509381	0.0265954	0.0295157	0.0336733	0.0512056	0.0333947	0.0738749	0.0911325	0.0424114	0.0337292	0.0509844		
delta	1.6115	1.6996	1.79554	1.94261	1.47048	1.67836	1.546	1.33214	2.02119	2.47875	1.38262	
0.204416	0.181998	0.270491	0.362114	0.18279	0.169253	0.210584	0.13121	0.307784	0.490395	0.157581		
lamda	0.0674308	0.0707555	0.0766364	0.0838888	0.0507945	0.0671744	0.0627251	0.0489618	0.0931732	0.116825	0.0586413	
0.0110231	0.00965653	0.0141754	0.0196409	0.00953748	0.00870737	0.0111477	0.00712784	0.0167642	0.0262024	0.00870731		
epsilon	9.4706	9.4706	9.4706	9.4706	9.4706	9.4706	9.4706	9.4706	9.4706	9.4706	9.4706	
0	0	0	0	0	0	0	0	0	0	0	0	
a_crystal	0.666838	0.542945	0.575115	0.602333	0.68652	0.572042	0.692524	0.733765	0.604021	0.553561	0.646821	
0.0612401	0.0650349	0.0679236	0.0606921	0.0608609	0.0622679	0.0727168	0.0534158	0.0619466	0.0600742	0.0644066		
chisq	89.5586	69.3082	70.9565	69.0584	60.8943	69.1303	77.6858	64.4182	44.1457	61.3344	59.8081	
Bin	76	78	76	72	73	72	65	54	59	62	59	
MaximumX	9.46041	9.46086	9.46003	9.45968	9.4603	9.46112	9.46072	9.46244	9.45966	9.45907	9.46111	
1S_10MeV	3_3	3_4	3_5	3_6	3_7	4_0	4_1	4_2	4_3	4_4	4_5	9.455
Et	9.455	9.455	9.455	9.455	9.455	9.455	9.455	9.455	9.455	9.455	9.455	
0	0	0	0	0	0	0	0	0	0	0	0	
sigma	0.0404472	0.043002	0.0446679	0.0433679	0.039491	0.0417605	0.0417328	0.0466099	0.0477213	0.0433253	0.0461749	
0.00222502	0.00082186	0.0007922	0.00065904	0.00133104	0.00185918	0.00136481	0.00068395	0.00120013	0.00184838	0.00117393		
n	0.978555	0.99126	0.962447	1.10602	2.22503	0.886358	0.973029	0.84052	0.845139	0.843975	0.789224	
0.084351	0.0865602	0.0853293	0.0934322	0.034751	0.076685	0.0940518	0.0825284	0.0863962	0.0867226	0.0883743		
alpha	1.6946	1.83486	1.84253	1.85859	1.57165	1.58532	1.75044	1.943	1.85656	1.86744	1.91108	
0.11837	0.0525572	0.0539255	0.0459701	0.0797359	0.11673	0.0673033	0.0504429	0.0897816	0.0866809	0.0812861		
gamma	0.137485	0.0884843	0.112091	-0.239487	-0.105843	0.174465	0.133917	0.116386	0.199393	0.114983	0.163022	
0.0349153	0.0854788	0.0748618	0.277783	0.489768	0.0236774	0.0374613	0.0633035	0.0359642	0.0467579	0.0524176		
delta	2.0555	1.43021	1.23502	1.04398	1.72715	2.23903	2.04479	1.13765	1.37889	1.93093	1.52864	
0.460569	0.236289	0.185608	0.148922	0.225981	0.292558	0.348228	0.150916	0.208022	0.455675	0.2717676		
lamda	0.0936983	0.0589543	0.0458519	0.0336161	0.0494647	0.10437	0.10246	0.0449803	0.0505045	0.0901303	0.064269	
0.0243854	0.0127196	0.00952631	0.00956644	0.0145751	0.0153832	0.0210574	0.00828558	0.0105861	0.0257863	0.0141506		
epsilon	9.4706	9.4706	9.4706	9.4706	9.4706	9.4706	9.4706	9.4706	9.4706	9.4706	9.4706	
0	0	0	0	0	0	0	0	0	0	0	0	
a_crystal	0.540164	0.717204	0.704235	0.838502	0.854984	0.42422	0.574157	0.724868	0.590515	0.60312	0.62834	
0.0836566	0.0822053	0.0750216	0.0588319	0.0246468	0.0702804	0.0636903	0.0616237	0.0874225	0.082911	0.0982503		
chisq	74.2719	41.5369	37.9468	38.9658	34.8621	86.2724	56.9153	51.2187	57.2525	48.319	76.2578	
Bin	56	56	49	47	32	58	54	58	53	51	49	
MaximumX	9.45975	9.46042	9.46235	9.46413	9.463	9.46012	9.45875	9.46195	9.46185	9.45978	9.46089	
1S_10MeV	4_6	4_7	5_0	5_1	5_2	5_3	5_4	5_5	5_6	5_7	6_0	9.455
Et	9.455	9.455	9.455	9.455	9.455	9.455	9.455	9.455	9.455	9.455	9.455	
0	0	0	0	0	0	0	0	0	0	0	0	
sigma	0.0441602	0.0308923	0.088509	0.0441242	0.0518952	0.0466031	0.101048	0.0439797	0.0612643	0.0458825	0.0812936	
0.00160097	0.00957508	0.0187178	0.00422741	0.0139128	0.00324452	0.0220763	0.0369955	0.00220055	0.0173389			
n	0.835066	20	0.946546	0.266817	0.513344	0.332216	3.83901	20	0.494242	2.76062	20	
0.122254	10.0795	1.22942	0.178837	0.258233	0.156424	13.626	17.2274	0.16168	2.00847	13.2744		
alpha	1.79286	0.270219	0.452263	1.86304	1.15021	2.07558	0.32246	0.0443491	1.89493	1.57005	0.189383	
0.0897331	0.106194	0.615994	0.292677	0.710669	0.160758	0.356062	0.0504218	0.159659	0.183719	0.114807		
gamma	0.170282	0.107396	0.290075	0.211418	0.236316	0.199835	0.246961	0.24055	0.221869	-1.0392	0.272783	
0.0382437	0.0374258	0.0148193	0.0262212	0.0254725	0.0435356	0.0145997	0.0218604	0.0420741	1.88291	0.0171436		
delta	1.6643	3.93777	2.43909	2.16502	3.21357	1.87209	5.01373	2.91111	3.0871	1.94433	3.11011	
0.213938	1.57342	0.338046	0.326244	0.704182	0.363418	2.65416	0.485324	1.8077	2.58085	0.666023		
lamda	0.0761513	0.172832	0.111375	0.1031	0.153067	0.0912441	0.235195	0.141372	0.110249	0.0895032	0.150369	
0.0116681	0.0704085	0.0150267	0.0168875	0.0345624	0.0200569	0.123673	0.0247834	0.064469	0.156692	0.0319208		
epsilon	9.4706	9.4706	9.4706	9.4706	9.4706	9.4706	9.4706	9.4706	9.4706	9.4706	9.4706	
0	0	0	0	0	0	0	0	0	0	0	0	
a_crystal	0.524995	0.150677	0.137408	0.271162	0.194672	0.489013	0.154814	0.106238	0.587867	0.896126	0.121904	
0.0852674	0.0377494	0.0440962	0.106247	0.0896036	0.125395	0.0351125	0.0121335	0.12701	0.0884158	0.0189622		
chisq	37.5855	38.6585	33.3664	36.1091	28.0814	29.7396	35.114	41.4951	32.8656	21.4503	30.9156	
Bin	43	26	33	32	29	32	30	29	28	21	28	
MaximumX	9.46043	9.46416	9.45919	9.46064	9.45982	9.45959	9.45941	9.45999	9.46187	9.45824	9.45859	

1S_10MeV	6_1	6_2	6_3	6_4	6_5	6_6	6_7	7_0	7_1	7_2	7_3	9.455
Et	9.455 0	9.455 0	9.455 0	9.455 0	9.455 0	9.455 0	9.455 0	9.455 0	9.455 0	9.455 0	9.455 0	9.455 0
sigma	0.0500843 0.0038774	0.0473122 0.00997278	0.05366 0.00179501	0.0553469 0.00113224	0.0414716 0.0190859	0.0252683 0.00668657	0.0531346 0.00278102	0.0536802 0.00191535	0.0806845 0.0185396	0.0565015 0.00279337	0.0551185 0.00612665	0.0551185 0.00612665
n	0.254132 0.181816	0.442937 0.349175	0.856061 0.184889	0.590918 0.156511	20 19.9655	1.44231 0.965243	1.48375 0.658283	0.339814 0.187795	0.7886 0.787176	0.80375 0.219516	0.380445 0.191674	0.380445 0.191674
alpha	2.10952 0.21112	1.75985 0.358802	1.91518 0.105679	2.10021 0.0918492	0.0895978 0.0750264	0.356265 0.271351	1.59674 0.178783	2.28101 0.190882	0.564918 0.884003	1.74689 0.21351	1.73643 0.284869	1.73643 0.284869
gamma	0.205859 0.0439862	0.186309 0.0430521	0.0116132 0.252564	0.00940167 0.166214	0.234307 0.021184	0.151884 0.0268375	-0.991244 0.623858	0.164203 0.0456266	0.243178 0.01379	0.208237 0.0274585	0.224816 0.020313	0.224816 0.020313
delta	2.80945 0.780168	2.05243 0.545326	141.961 109.702	1.27875 0.769118	2.47493 0.410986	82.3024 100.869	0.745743 0.285505	1.74797 0.490011	3.4668 0.679135	3.95237 1.76376	2.39954 0.300317	2.39954 0.300317
lamda	0.144515 0.041814	0.103774 0.0325946	5.19223 17.2689	0.030205 0.0212566	0.125746 0.0216406	4.40917 10.668	0.0138241 0.010725	0.10465 0.0312013	0.184076 0.0359463	0.230308 0.105332	0.138261 0.0198335	0.138261 0.0198335
epsilon	9.4706 0	9.4706 0	9.4706 0	9.4706 0	9.4706 0	9.4706 0	9.4706 0	9.4706 0	9.4706 0	9.4706 0	9.4706 0	9.4706 0
a_crystal	0.468368 0.171229	0.288717 0.157212	0.86457 0.0878045	0.897538 0.040957	0.10222 0.0170581	0.183232 0.0371368	0.880582 0.0292779	0.63477 0.119271	0.134417 0.0585757	0.482081 0.153894	0.262744 0.107126	0.262744 0.107126
chisq	27.8596	16.9807	31.6659	26.5808	51.6933	37.7721	16.9159	47.6453	76.1845	46.2103	63.2609	
Bin	28	28	29	28	29	27	23	37	38	37	37	
MaximumX	9.45858	9.46104	9.46019	9.46603	9.46011	9.45914	9.47467	9.45803	9.45859	9.45726	9.45856	

1S_10MeV	7_4	7_5	7_6	7_7	9.455
Et	9.455 0	9.455 0	9.455 0	9.455 0	9.455 0
sigma	0.0540902 0.00225972	0.0465043 0.0149628	0.0545578 0.00950304	0.033615 0.0293988	
n	0.379633 0.205791	0.123568 0.269655	0.404124 0.372404	20 12.8994	
alpha	2.18521 0.148024	1.10022 0.58995	1.3547 0.539208	0.0555888 0.0606488	
gamma	0.16584 0.0429816	0.187535 0.0195727	0.211028 0.0223925	0.180957 0.0216329	
delta	1.86547 0.409605	2.34236 0.356756	2.54852 0.428265	2.72467 0.516696	
lamda	0.115183 0.0279253	0.136231 0.0230079	0.156432 0.0296599	0.166169 0.0322726	
epsilon	9.4706 0	9.4706 0	9.4706 0	9.4706 0	
a_crystal	0.573633 0.135028	0.11169 0.0442043	0.175914 0.0992047	0.100379 0.0162621	
chisq	52.0618	56.1031	58.1132	44.3912	
Bin	39	38	36	35	
MaximumX	9.45814	9.46089	9.45871	9.46028	

TABLE B2: $\Upsilon(2S)$

2S_10MeV	0_0	0_1	0_2	0_3	0_4	0_5	0_6	0_7	0_8	1_0	1_1
Et	10.03	10.03	10.03	10.03	10.03	10.03	10.03	10.03	10.03	10.03	10.03
0	0	0	0	0	0	0	0	0	0	0	0
sigma	0.0431504	0.0432583	0.042693	0.0421808	0.0410493	0.0415879	0.0405585	0.0425495	0.0409204	0.0434407	0.0431602
1.08E-05	0.00048331	1.31E-05	0.00069226	0.00049241	0.000440433	0.00072954	0.00048739	0.00083853	1.00E-05	0.00057227	
n	0	0	0	0	0	0	0	0	0	0	0
0	0	0	0	0	0	0	0	0	0	0	0
alpha	3.08486	3.14191	3.1376	3.03658	3.28431	3.17897	3.12401	3.01052	3.04843	3.33112	3.55249
0.0652814	0.0336269	0.0010585	0.0451666	0.0480095	0.0385632	0.0450216	0.0388398	0.057985	0.347671	0.103784	
gamma	0.721057	0.672115	0.738222	0.617866	1.21048	0.680024	0.837054	0.657496	0.913361	0.973997	1.33515
0.125162	0.0685898	0.080589	0.101773	0.223911	0.0578043	0.161941	0.0905023	0.154038	0.318561	0.342127	
delta	0.922577	0.838586	0.88047	1.01796	0.855318	0.797609	1.00998	1.03499	1.06919	0.746449	0.780589
0.0779458	0.0428174	0.0356364	0.0869509	0.066512	0.0425898	0.110115	0.0807621	0.166276	0.151663	0.0843903	
lamda	0.0418537	0.0379772	0.0418092	0.0504143	0.034387	0.0356949	0.0482565	0.0476648	0.0483178	0.0373486	0.0332723
0.00518048	0.00322987	0.00315991	0.00667706	0.00406436	0.00314064	0.00769146	0.00577663	0.0109204	0.00968982	0.00643178	
epsilon	10.0366	10.0366	10.0366	10.0366	10.0366	10.0366	10.0366	10.0366	10.0366	10.0366	10.0366
0	0	0	0	0	0	0	0	0	0	0	0
a_crystal	0.75096	0.721855	0.760121	0.736834	0.827955	0.725569	0.772188	0.718573	0.782115	0.810193	0.84919
0.0350431	0.0251671	0.0238486	0.0443406	0.0232446	0.0216751	0.0419369	0.0367593	0.0339819	0.0364213	0.0257633	
R	0.0243435	0.0274591	0.0173022	0.0105012	0.0566179	0.0718431	0.0486294	0.0226634	0.0319623	0.0468311	
0.0100142	0.0184357	0.00842074	0.0124123	0.0182458	0.0369737	0.0224605	0.00428987	0.0174003	0.0127925	0.0209108	
B	1.9522	1.82155	2.13385	2.37521	1.83659	1.50599	1.8942	5.16021	2.20262	1.93124	1.92406
0.234752	0.328857	0.352253	0.631185	0.120744	0.17096	0.190528	10.0786	0.508634	0.285338	0.210999	
chisq	59.223	57.7239	57.2987	54.0267	63.7416	48.2564	59.1487	46.7767	58.4144	53.8196	60.2948
Bin	65	67	65	66	65	66	64	62	62	62	60
MaximumX	10.0269	10.0274	10.0272	10.0274	10.0263	10.0277	10.0267	10.0268	10.0262	10.0272	10.0266
2S_10MeV	1_2	1_3	1_4	1_5	1_6	1_7	2_0	2_1	2_2	2_3	2_4
Et	10.03	10.03	10.03	10.03	10.03	10.03	10.03	10.03	10.03	10.03	10.03
0	0	0	0	0	0	0	0	0	0	0	0
sigma	0.0418625	0.0429914	0.0420672	0.0427183	0.0431847	0.0425095	0.0434346	0.0453571	0.0452802	0.0450949	0.043571
0.00044902	9.90E-06	0.0009254	1.84E-05	0.00076384	0.00067497	0.00020699	0.00087167	0.00084124	5.40E-05	0.00062946	
n	0	0	0	0	0	0	0	0	0	0	0
0	0	0	0	0	0	0	0	0	0	0	0
alpha	3.19383	3.17454	3.16023	3.19775	3.00017	3.0406	3.06919	3.17587	3.40708	2.90117	2.9072
0.0678918	0.118007	0.0911642	0.126462	0.0486054	0.0504282	0.0103858	0.098211	0.114423	0.00287788	0.01857	
gamma	0.768813	0.681697	0.900831	0.685969	0.50618	0.517031	1.10256	0.695462	0.888483	0.447341	0.466528
0.100244	0.144755	0.25716	0.170709	0.0661273	0.0593448	0.330332	0.100564	0.177325	0.0362107	0.0409053	
delta	0.781919	0.878994	0.983544	0.875786	1.12112	0.17561	1.19533	0.731127	0.715348	1.18817	1.17296
0.0659165	0.10181	0.191243	0.126295	0.117863	0.109199	0.147628	0.0677753	0.0596822	0.0654867	0.0955376	
lamda	0.0357842	0.0467606	0.0539645	0.0455764	0.0561059	0.0555572	0.0618291	0.0338096	0.0377763	0.0624564	0.0630654
0.00485128	0.00673328	0.0144005	0.00885	0.0086559	0.00820871	0.0072297	0.00445398	0.00533186	0.00528045	0.00764481	
epsilon	10.0366	10.0366	10.0366	10.0366	10.0366	10.0366	10.0366	10.0366	10.0366	10.0366	10.0366
0	0	0	0	0	0	0	0	0	0	0	0
a_crystal	0.751167	0.745189	0.82038	0.777508	0.67211	0.690941	0.838462	0.723249	0.789	0.642309	0.646018
0.0297709	0.0438397	0.0461808	0.0466616	0.0435313	0.0356982	0.0395553	0.031449	0.0355093	0.0287949	0.0325668	
R	0.193946	0.012702	0.0590167	0.0288638	0.00096211	0.00085157	0.0667499	0.0648581	0.0391613	0.0126164	0.0676609
0.0906709	0.0142409	0.0395968	0.0272069	0.00209307	0.00144768	0.0129331	0.0544544	0.0234724	0.0199079	0.0555263	
B	1.42652	2.20256	1.74629	1.77387	19.9964	19.9997	1.90925	1.55705	1.95206	1.90318	1.49915
0.124092	0.931889	0.287496	0.600385	12.6888	13.4752	0.101303	0.263776	0.278198	0.768768	0.22686	
chisq	41.055	51.6413	69.0625	44.2405	67.3314	65.2356	72.6467	72.4215	63.1134	58.8979	90.0363
Bin	63	61	61	57	59	56	65	65	64	67	65
MaximumX	10.0272	10.0275	10.0274	10.0278	10.0273	10.0276	10.0266	10.0276	10.0272	10.0273	10.0272
2S_10MeV	2_5	2_6	2_7	3_0	3_1	3_2	3_3	3_4	3_5	3_6	3_7
Et	10.03	10.03	10.03	10.03	10.03	10.03	10.03	10.03	10.03	10.03	10.03
0	0	0	0	0	0	0	0	0	0	0	0
sigma	0.0449813	0.0445685	0.0426519	0.0493109	0.0509833	0.0526345	0.0518424	0.0505866	0.0502951	0.0486928	0.0543039
0.00059694	6.85E-06	0.00139896	0.00043835	6.91E-05	0.00070015	0.00044135	0.00013703	0.00074098	0.00077447	8.49E-06	
n	0	0	0	0	0	0	0	0	0	0	0
0	0	0	0	0	0	0	0	0	0	0	0
alpha	3.45043	3.118	3.05095	3.58567	3.33339	3.0547	2.93578	2.96419	2.94387	2.83088	2.92472
0.104736	0.00027074	0.0785518	0.0563691	0.00466063	0.0783245	0.0157195	0.0044835	0.0395919	0.0182104	0.0003197	
gamma	0.996248	0.663236	0.451967	1.60253	0.89035	0.545657	0.645563	0.624237	0.45176	0.435629	1.95655
0.245627	0.0978163	0.0928704	0.273508	0.229974	0.068322	0.097571	0.17969	0.0654716	0.0517512	0.450649	
delta	0.733418	0.913502	0.168694	0.720789	0.745497	0.891769	90.484	1.81101	1.59957	116.793	107.351
0.0652852	0.0566886	0.157108	0.064171	0.0656017	0.118092	126.29	0.429801	0.272253	141.649	153.676	
lamda	0.0365413	0.0473141	0.0605859	0.0297523	0.0521833	0.0533204	8.72966	0.151316	0.113981	9.73996	7.89166
0.00543114	0.00534386	0.0134318	0.00588505	0.00817993	0.00960858	12.6347	0.0445616	0.0265722	14.0528	13.9124	
epsilon	10.0366	10.0366	10.0366	10.0366	10.0366	10.0366	10.0366	10.0366	10.0366	10.0366	10.0366
0	0	0	0	0	0	0	0	0	0	0	0
a_crystal	0.809794	0.754223	0.723454	0.874101	0.841967	0.732612	0.878065	0.816483	0.719901	0.722587	0.953678
0.0373696	0.0344399	0.064346	0.0123589	0.0322211	0.029238	0.0162424	0.0555961	0.0521205	0.0319562	0.00788406	
R	0.0325894	0.0305214	0.139406	0.0571149	0.0420094	0.00275824	0.00446565	0.0401591	0.00676674	0.00861737	0.0154991
0.0164171	0.015327	0.137089	0.011852	0.0113236	0.00151894	0.00205826	0.00223266	0.0041935	0.00535289		
B	2.18864	2.01228	1.44835	2.14223	2.06186	20	20	2.04125	19.9993	18.8192	4.23468
0.354937	0.335782	0.267828	0.125858	0.222769	9.74546	10.5285	0.24061	13.631	15.6603	2.22824	
chisq	74.1556	67.6876	54.3778	201.689	160.385	243.752	153.181	251.178	224.806	266.49	147.41
Bin	60	58	44	68	67	66	65	63	62	62	45
MaximumX	10.0269	10.0273	10.0282	10.0257	10.0276	10.0272	10.0289	10.028	10.0273	10.0278	10.0295

TABLE B3: $\Upsilon(3S)$

3S_10MeV	0_0	0_1	0_2	0_3	0_4	0_5	0_6	0_7	1_0	1_1	1_2	10.24
Et	10.24	10.24	10.24	10.24	10.24	10.24	10.24	10.24	10.24	10.24	10.24	0
0	0	0	0	0	0	0	0	0	0	0	0	0
sigma	0.131138	0.123773	0.117747	0.00747787	0.104525	0.101703	0.132745	0.0936172	0.135424	0.121338	0.144584	
0.0074282	0.0109735	0.0107926	0.00276833	0.0152727	0.0186231	0.00928483	0.0191259	0.0146831	0.0120812	0.00986487		
n	0.656961	0.903889	2.74543	1.78474	1.06476	1.29653	0.52392	0.798513	0.715752	0.718482	0.348573	
0.213463	0.351665	1.79132	0.599531	0.383493	0.449781	0.278413	0.231222	0.397996	0.287417	0.188325		
alpha	0.95651	0.788834	0.598201	0.0441861	0.79143	0.674293	1.09177	0.743729	0.781603	0.801022	1.04583	
0.120243	0.154453	0.12412	0.0187703	0.181047	0.162843	0.19587	0.137441	0.195729	0.146754	0.158934		
gamma	0.139911	0.134121	0.148165	0.167034	0.144831	0.145093	0.150428	0.13673	0.137796	0.1254	0.137644	
0.00732875	0.00777999	0.0079153	0.00662949	0.00873285	0.00934391	0.0081943	0.0113123	0.00956701	0.00956207	0.00897168		
delta	3.09886	2.72556	2.94553	2.9253	2.93727	3.04273	2.82449	2.70925	2.85894	2.60603	2.83108	
0.255701	0.203882	0.24794	0.219043	0.235309	0.264345	0.226452	0.217971	0.275097	0.204525	0.246906		
lamda	0.140281	0.123301	0.131565	0.132121	0.131287	0.135472	0.122516	0.118729	0.132387	0.119841	0.130703	
0.0120068	0.00950341	0.0113665	0.0103171	0.0108288	0.012077	0.0102117	0.0100492	0.0131705	0.00985965	0.011916		
epsilon	10.365	10.365	10.365	10.365	10.365	10.365	10.365	10.365	10.365	10.365	10.365	
0	0	0	0	0	0	0	0	0	0	0	0	
a_crystal	0.107136	0.100943	0.0985144	0.0623782	0.0958815	0.0950568	0.104128	0.0981458	0.0984659	0.097258	0.0997721	
0.00356066	0.00470151	0.00482795	0.00212745	0.0055398	0.00631323	0.00421651	0.00593366	0.00524442	0.00469695	0.0041718		
chisq	53.0012	64.0797	58.6867	52.5547	65.6288	58.6813	52.0823	51.5601	61.846	61.4986	72.3201	
Bin	61	60	59	58	60	57	51	47	49	50	49	
MaximumX	10.359	10.3594	10.3588	10.3582	10.3588	10.3588	10.359	10.3594	10.3591	10.3597	10.3591	
3S_10MeV	1_3	1_4	1_5	1_6	1_7	2_0	2_1	2_2	2_3	2_4	2_5	10.24
Et	10.24	10.24	10.24	10.24	10.24	10.24	10.24	10.24	10.24	10.24	10.24	0
0	0	0	0	0	0	0	0	0	0	0	0	
sigma	0.1355	0.115475	0.138047	0.098614	0.101724	0.136706	0.142415	0.13303	0.137282	0.138962	0.136929	
0.00777053	0.0124587	0.0170835	0.01426	0.0186551	0.00625259	0.00647423	0.00678506	0.00733995	0.00667998	0.00806886		
n	0.316243	0.660078	1.0448	0.519395	0.529886	1.03578	1.76539	0.62725	1.70662	0.823569	1.03411	
0.16239	0.255489	0.850135	0.16561	0.280767	0.406632	0.929997	0.1752	0.712712	0.289151	0.425813		
alpha	1.21663	0.921276	0.66769	0.885918	1.02479	0.810448	0.714581	0.945742	0.739111	0.891361	0.786458	
0.133004	0.140823	0.235871	0.137982	0.233176	0.132018	0.125731	0.0988468	0.104586	0.1206	0.132844		
gamma	0.125387	0.125095	0.148638	0.129253	0.114696	0.141993	0.142035	0.130291	0.136363	0.130804	0.151513	
0.00907716	0.010588	0.0101297	0.0112898	0.0119003	0.0063107	0.00621479	0.00665381	0.00663305	0.00671126	0.00715125		
delta	3.93795	2.59407	2.45138	2.75859	3.18967	2.90908	2.77575	3.04516	2.65219	3.03632	3.00422	
0.599715	0.204897	0.218375	0.246443	0.349977	0.213286	0.191898	0.221001	0.166505	0.232159	0.241001		
lamda	0.18012	0.11594	0.110163	0.124767	0.143213	0.13995	0.131425	0.147019	0.126408	0.14595	0.142411	
0.0282423	0.00962088	0.0101196	0.0116444	0.016266	0.0105831	0.0093502	0.0110422	0.00822789	0.0115364	0.0117616		
epsilon	10.365	10.365	10.365	10.365	10.365	10.365	10.365	10.365	10.365	10.365	10.365	
0	0	0	0	0	0	0	0	0	0	0	0	
a_crystal	0.10957	0.101056	0.0993347	0.102279	0.101364	0.105068	0.107198	0.104678	0.103087	0.104965	0.102113	
0.00393668	0.00473124	0.00706751	0.00492753	0.00620767	0.00368526	0.00388922	0.00315267	0.00371206	0.0034395	0.00382723		
chisq	52.4905	44.2343	45.0259	38.2215	51.7069	73.2499	71.1438	87.1666	69.6056	82.9732	74.3465	
Bin	46	45	47	46	42	75	76	74	73	73	69	
MaximumX	10.3593	10.3598	10.3591	10.3594	10.3599	10.3586	10.3588	10.359	10.359	10.359	10.3583	
3S_10MeV	2_6	2_7	3_0	3_1	3_2	3_3	3_4	3_5	3_6	3_7	10.24	
Et	10.24	10.24	10.24	10.24	10.24	10.24	10.24	10.24	10.24	10.24	10.24	0
0	0	0	0	0	0	0	0	0	0	0	0	
sigma	0.105113	0.12569	0.160193	0.170715	0.157542	0.163827	0.099753	0.179572	0.136496	0.186843		
0.0124535	0.00898073	0.00705072	0.00920554	0.00618268	0.00983351	0.0137841	0.00647636	0.0149218	0.0127427			
n	0.703579	0.598036	2.08632	0.700243	0.189268	7.84182	0.701684	0.00378975	0.549241	4.82E-08		
0.175133	0.216442	1.46607	0.357988	0.134133	12.9053	0.185409	0.0983485	0.241934	0.04303			
alpha	0.905751	1.10469	0.698835	0.918181	1.32613	0.586246	0.889396	1.50944	0.755058	1.40911		
0.111604	0.12599	0.123473	0.14828	0.134311	0.121162	0.12945	0.112427	0.158471	0.0804943			
gamma	0.117731	0.10965	0.0997866	0.113455	0.0904699	0.11033	0.0467575	0.120002	0.094372	0.114558		
0.00954408	0.00836495	0.00651669	0.00669588	0.00681714	0.00707409	0.0098548	0.00745061	0.00897148	0.009693			
delta	2.5706	2.82842	3.84161	3.48808	3.17137	2.78256	2.62309	2.94113	2.55212	2.68685		
0.158173	0.213022	0.464436	0.350287	0.245917	0.21695	0.152266	0.241429	0.186486	0.236648			
lamda	0.120244	0.133273	0.21284	0.189919	0.173007	0.151436	0.143189	0.161603	0.141386	0.154544		
0.00776173	0.0105033	0.0262163	0.0195051	0.0139014	0.0120662	0.00875042	0.0137328	0.0106717	0.0141384			
epsilon	10.365	10.365	10.365	10.365	10.365	10.365	10.365	10.365	10.365	10.365	10.365	
0	0	0	0	0	0	0	0	0	0	0	0	
a_crystal	0.102245	0.0909992	0.108912	0.103496	0.11232	0.104106	0.094818	0.123254	0.0878408	0.108632		
0.00420835	0.00346863	0.00387648	0.00353897	0.0033016	0.00461743	0.00429607	0.00376248	0.00529634	0.00489767			
chisq	67.8845	58.3913	256.797	243.691	231.161	238.57	190.803	189.973	165.869	121.668		
Bin	63	51	76	73	76	69	69	71	56	51		
MaximumX	10.3598	10.3601	10.3595	10.359	10.3601	10.3594	10.3621	10.3588	10.3601	10.3591		

TABLE B4: Parameters for angle-integrated pt bins

1S_10MeV		pt_0	pt_1	pt_2	pt_3	pt_4	pt_5	pt_6	pt_7		
Et		9.455 0	9.455 0								
sigma	0.0411922 0.00023169	0.0417284 0.0002686	0.0420343 0.00026501	0.0425716 0.00038451	0.0455928 0.00045105	0.0831717 0.00320212	0.0863095 0.00340639	0.0564572 0.00113931			
n	0.961239 0.0231309	0.996901 0.0238562	1.01112 0.0213303	0.994826 0.0298568	0.915354 0.0317881	2.19683 0.764054	3.28123 1.71469	0.976207 0.0604198			
alpha	1.83529 0.0147152	1.80615 0.0157288	1.78561 0.0144254	1.79183 0.0193263	1.8387 0.0224807	0.528178 0.13589	0.455861 0.113523	1.84212 0.0495863			
gamma	0.125697 0.0197401	0.10986 0.0203579	0.102297 0.0159247	0.0856344 0.0207283	0.125295 0.0183133	0.257087 0.0053341	0.253507 0.00575364	0.145859 0.0188484			
delta	1.4022 0.0478093	1.4434 0.0520427	1.51871 0.044157	1.5596 0.0604725	1.45923 0.0656859	3.23262 0.292419	3.18451 0.31949	1.80295 0.185264			
lamda	0.0533452 0.00258642	0.0557802 0.00286524	0.0609806 0.00247154	0.0665943 0.00354603	0.0630328 0.00395261	0.148433 0.0130847	0.155406 0.0153146	0.10746 0.0135122			
epsilon	9.4706 0										
a_crystal	0.702284 0.020533	0.687711 0.021865	0.653872 0.0190031	0.652677 0.0239443	0.639265 0.0272383	0.155396 0.0179159	0.146831 0.0165612	0.610775 0.0510626			
chisq	118.329	145.669	152.771	110.114	118.636	72.2151	77.9992	128.419			
Bin	78	78	77	80	82	83	80	83			
MaximumX	9.46073	9.46103	9.46115	9.46078	9.46109	9.45973	9.45925	9.45885			
2S_10MeV		pt_0	pt_1	pt_2	pt_3	3S_10MeV		pt_0	pt_1	pt_2	pt_3
Et		10.03 0	10.03 0	10.03 0	10.03 0	Et		10.24 0	10.24 0	10.24 0	10.24 0
sigma	0.0418525 4.12E-06	0.0424482 4.39E-06	0.0439852 3.91E-06	0.0495952 4.41E-06	sigma		0.133286 0.0015994	0.135607 0.00212532	0.143584 0.00145849	0.161836 0.00166898	
n	0 0	0 0	0 0	0 0	n		0.97296 0.120702	1.03573 0.167906	0.921574 0.117788	1.26647 0.238968	
alpha	3.0814 0.00014987	3.14908 0.00018104	3.07781 0.00015891	2.89692 0.00026493	alpha		0.855101 0.0406802	0.853179 0.0521789	0.885276 0.0403668	0.798778 0.046505	
gamma	0.690706 0.0149185	0.682025 0.0154209	0.661013 0.0184667	0.442158 0.0137433	gamma		0.151357 0.00239141	0.130448 0.00286726	0.135035 0.002232	0.0982616 0.00245412	
delta	0.928447 0.0130275	0.882559 0.019512	0.92875 0.0223082	1.39973 0.0699951	delta		0.0859653 0.0136308	0.83961 0.128986	2.83961 0.139006	2.92058 0.166132	
lamda	0.0435133 0.00110476	0.045313 0.00188723	0.0500297 0.00216033	0.101467 0.00743588	lamda		0.136308 0.00396264	0.128986 0.00406134	0.13006 0.00353769	0.139006 0.00498217	
epsilon	10.0366 0	10.0366 0	10.0366 0	10.0366 0	epsilon		10.365 0	10.365 0	10.365 0	10.365 0	
a_crystal	0.738343 0.00592092	0.75891 0.00661158	0.754037 0.0078237	0.732545 0.0103607	a_crystal		0.106717 0.00115661	0.102195 0.00143291	0.105698 0.0011236	0.109904 0.00139285	
R	0.0374741 0.00484135	0.065833 0.0121667	0.0779581 0.0103158	0.0614813 0.0131848	chisq		123.479 82	99.5111 83	119.033 83	269.086 87	
B	1.75212 0.0650247	1.52956 0.0643942	1.63025 0.0542262	1.59119 0.068585	Bin						
chisq	89.9629	89.6683	106.403	186.721	MaximumX		10.3587	10.3595	10.359	10.3598	
Bin	66	66	67	71							
MaximumX	10.0271	10.0275	10.0273	10.0277							

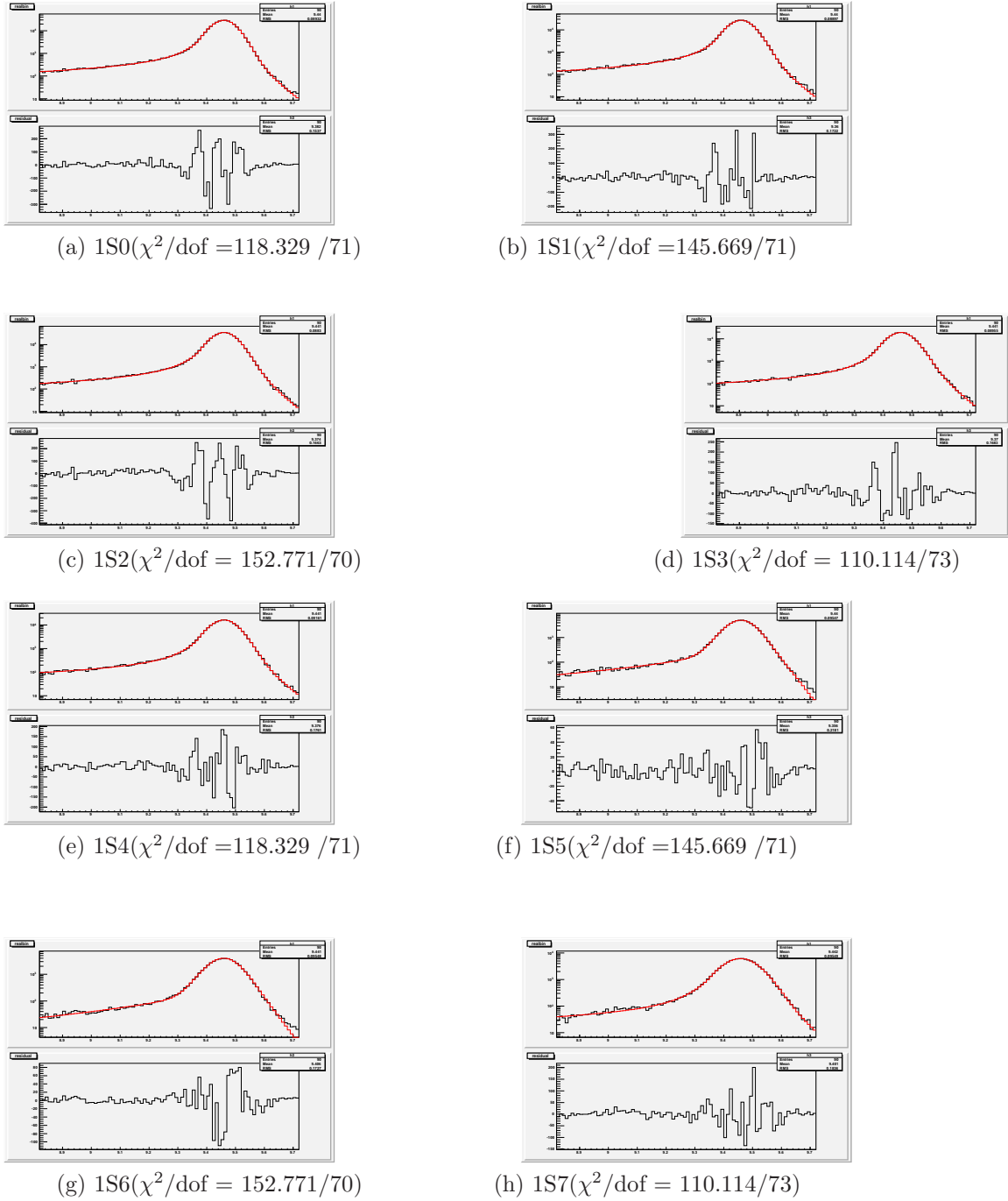
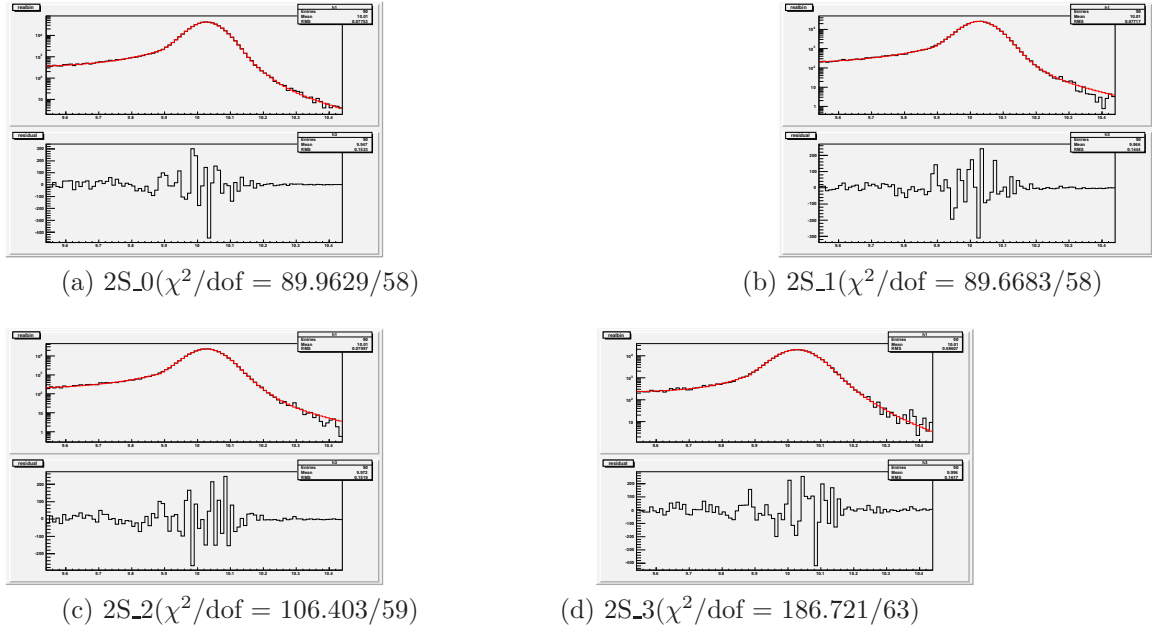
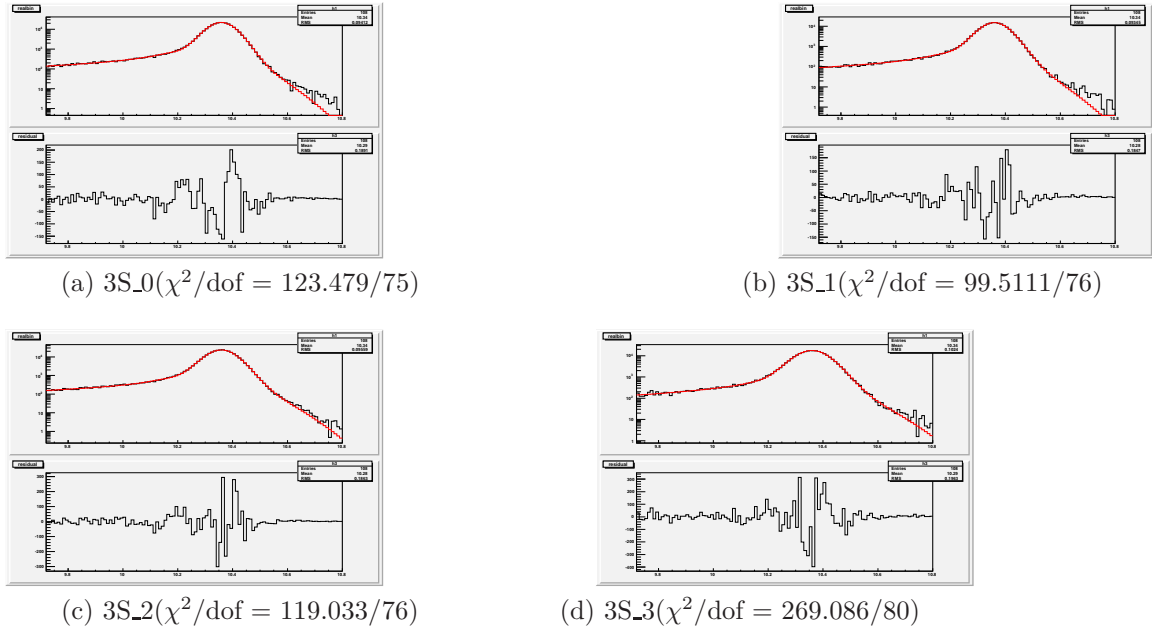


Figure 53: Angle-Integrated Y(1S) Monte Carlo Mass Fits

10 Appendix B Signal and Background Yield Tables

The $\Upsilon(nS)$ yields in $\cos\theta^*$ and $p_T(\Upsilon)$ bins are given below.

Figure 54: Angle-integrated 2S Monte Carlo Mass Distribution in p_T binsFigure 55: Angle-integrated 3S Monte Carlo Mass Distribution in p_T bins

References

[1] M. Kramer, “Quarkonium Production at High-Energy Colliders”, arXiv:hep-ph/0106120. 2

- [2] CDF Collaboration, F. Abe *et al.*, "J/ ψ and $\psi(2S)$ Production in $ppbar$ collisions at $\sqrt{s} = 1.8$ TeV," PRL **79** 572 (1997). 2
- [3] V.A. Khoze, A.D. Martin, M.G. Ryskin, and W.J. Stirling, "Inelastic J/ ψ and Υ hadroproduction," Eur. Phys. J. C **39** 163-171 (2005). 3, 20
- [4] CDF Collaboration, D. Acosta *et al.*, "Measurement of the J/ ψ Meson and b -Hadron Production Cross Sections in $ppbar$ Collisions at $\sqrt{s} = 1960$ GeV," PRD **71** 032001 (2005). 2
- [5] CDF Collaboration, T. Affolder *et al.*, "Measurement of J/ψ and $\psi(2S)$ Polarization in $ppbar$ collisions at $\sqrt{s} = 1.8$ TeV," PRL **85** 2886 (2000). 3
- [6] Sean Fleming, *et al.*, "Power Counting and Effective Field Theory for Charmonium," PRD **64** 036002 (2001). 3
- [7] P. Artoisenet, *et al.*, "Upsilon production at the Tevatron and the LHC", arXiv:0806.3282. 3, 20
- [8] J. Heinrich. Personal communication. March 2011. 11
- [9] E. Braaten, J. Lee, "Polarization of Upsilon(nS) at the Tevatron," PRD **63** 071501 (2000). 3
- [10] D. Glenzinski, M. Herndon, T. Kamon, V. Krutelyov, C.-J. Lin, C. Plager, N. Wisniewski, "Measurement of Level-1, 2, and 3 Low- p_T DiMuon Trigger Efficiencies for the $B_s^0 \rightarrow \mu^+\mu^-$ Analysis," CDF-7314 (2005). 6
- [11] CDF Collaboration, A. Abulencia, *et al.*, "Polarization of J/ ψ and $\psi(2S)$ Mesons Produced in $p\bar{p}$ Collisions at $\sqrt{s} = 1.8$ TeV" Phys. Rev. Lett. **99** 132001 (2007). 3
- [12] R. Cropp, K. Sumorok, W. Trischuk, "A Measurement of Prompt J/ ψ Polarization," CDF-5029 (1999).
- [13] R. Cropp, "A Measurement of the Polarization of J/ ψ Mesons Produced in High-Energy $p\bar{p}$ Collisions," CDF-5400 (2000).
- [14] K. Chung, M.J. Kim, J. Russ, "A Measurement of the Prompt J/ ψ Spin Alignment in CDF Run II Data," CDF-8212 (2006).
- [15] CDF Collaboration, D. Acosta, *et al.*, "Upsilon Production and Polarization in $p\bar{p}$ Collisions at $\sqrt{s} = 1.8$ TeV", Phys. Rev. Lett. **88** 161802 (2002). 15, 19
- [16] DZero Collaboration, V.M. Abazov, *et al.*, "Measurement of the Polarization of the $\Upsilon(1S)$ and $\Upsilon(2S)$ States in $p\bar{p}$ Collisions at $\sqrt{s} = 1.96$ TeV", Phys. Rev. Lett. **101** 182004 (2008). 19

$p_T(\Upsilon)$	$\cos \theta^*$	Yield	σ_{yield}	Background	σ_{bkg}	Order	Yield Systematic	χ^2/dof
2-3	0.0-0.1	4606	96	2441	35	3	26	52.5/41
	0.1-0.2	4602	97	2437	35	4		41.7/40
	0.2-0.3	4482	95	2409	35	3		41.0/41
	0.3-0.4	4586	95	2435	35	3		36.3/41
	0.4-0.5	4751	98	2386	35	5		47.8/39
	0.5-0.6	4213	92	2150	34	4	38	48.4/40
	0.6-0.7	3736	86	1921	32	3		48.4/41
	0.7-0.8	3110	80	1800	30	3		40.8/41
	0.8-0.9	2830	80	1847	30	5		39.5/39
	0.9-1.0	1788	63	1144	23	4		35.2/40
3-4	0.0-0.1	4118	88	1842	31	3	22	33.4/41
	0.1-0.2	4261	89	1846	31	3	18	49.0/41
	0.2-0.3	4143	87	1905	31	5		30.7/39
	0.3-0.4	4019	86	1790	30	3	18	37.8/41
	0.4-0.5	3749	85	1744	30	4		37.1/40
	0.5-0.6	3948	86	1692	30	4	22	50.9/40
	0.6-0.7	4209	92	1928	32	5		41.3/39
	0.7-0.8	3842	91	2158	34	5		49.2/39
	0.8-0.9	3511	85	2130	33	3		26.3/41
	0.9-1.0	2151	67	1397	25	4		43.4/40
4-6	0.0-0.1	6226	113	2198	51	6	12	33.5/38
	0.1-0.2	6246	106	2350	35	3		26.7/41
	0.2-0.3	6057	103	2362	35	3		38.7/41
	0.3-0.4	6076	104	2297	35	3		40.9/41
	0.4-0.5	5498	100	2075	39	4		48.9/40
	0.5-0.6	5164	96	1841	34	3		46.0/41
	0.6-0.7	5672	105	2238	35	5		45.4/39
	0.7-0.8	4834	96	2352	35	4		47.9/40
	0.8-0.9	2510	70	1367	33	4		40.7/40
	0.9-1.0	536	34	386	16	6	32	52.1/38
6-8	0.0-0.1	3577	75	1046	24	2	9	52.6/42
	0.1-0.2	3596	80	1098	25	4		36.6/40
	0.2-0.3	3841	87	1068	25	6		30.6/38
	0.3-0.4	3672	85	1143	25	6		20.9/38
	0.4-0.5	3493	74	1048	24	2		45.0/42
	0.5-0.6	2895	70	829	22	3		37.3/41
	0.6-0.7	2810	70	992	24	3		48.1/41
	0.7-0.8	1548	51	641	17	2	19	48.2/42
	0.8-0.9	n.d.	n.d.					
	0.9-1.0	n.d.	n.d.					

Table 11: $\Upsilon(1S)$ yields - lowest four bins

$p_T(\Upsilon)$	$\cos \theta^*$	Yield	σ_{yield}	Background	σ_{bkg}	Order	Yield Systematic	χ^2/dof
8-12	0.0-0.1	3346	70	671	21	2		41.0/42
	0.1-0.2	3312	74	705	20	4		52.6/40
	0.2-0.3	3244	70	791	22	1		43.5/43
	0.3-0.4	3395	75	869	23	3		33.7/41
	0.4-0.5	3134	73	845	23	4		39.3/40
	0.5-0.6	2760	68	722	21	3		33.0/41
	0.6-0.7	2368	60	658	20	6		48.2/38
	0.7-0.8	822	40	290	13	4		35.7/40
	0.8-0.9	n.d.	n.d.					
	0.9-1.0	n.d.	n.d.					
12-16	0.0-0.1	1134	41	165	11	2		30.2/42
	0.1-0.2	1149	41	184	11	1		34.9/43
	0.2-0.3	1063	40	203	11	2		37.8/42
	0.3-0.4	985	41	224	12	3		45.4/41
	0.4-0.5	1077	47	273	14	3		40.6/41
	0.5-0.6	1032	50	288	13	4		28.5/40
	0.6-0.7	769	40	230	13	3		48.2/41
	0.7-0.8	362	23	108	8	1		54.7/43
	0.8-0.9	n.d.	n.d.					
	0.9-1.0	n.d.	n.d.					
16-21	0.0-0.1	425	26	76	7	3		47.0/41
	0.1-0.2	380	25	83	8	2		53.4/42
	0.2-0.3	448	28	80	7	1		31.3/43
	0.3-0.4	425	26	103	8	1		32.2/43
	0.4-0.5	427	28	111	8	3		41.5/41
	0.5-0.6	406	28	128	9	3		47.6/41
	0.6-0.7	353	25	124	9	1		50.7/43
	0.7-0.8	189	20	76	7	2		35.0/42
	0.8-0.9	n.d.	n.d.					
	0.9-1.0	n.d.	n.d.					
21-40	0.0-0.1	203	19	46	6	1		54.0/43
	0.1-0.2	191	18	43	6	4		44.3/40
	0.2-0.3	194	18	43	5	1		42.7/43
	0.3-0.4	180	19	50	6	1		39.7/43
	0.4-0.5	189	19	67	7	1		47.8/43
	0.5-0.6	178	20	82	7	3		51.2/41
	0.6-0.7	187	21	102	8	3		50.9/41
	0.7-0.8	131	20	102	8	2		55.3/42
	0.8-0.9	n.d.	n.d.					
	0.9-1.0	n.d.	n.d.					

Table 12: $\Upsilon(1S)$ yields - highest four bins

$p_T(\Upsilon)$	$\cos \theta^*$	Yield	σ_{yield}	Background	σ_{bkg}	Order	Yield	Systematic	χ^2/dof
2-4	0.0-0.1	2069	87	3819	46	3	12	26	50.2/41
	0.1-0.2	2114	88	3846	46	2			57.2/42
	0.2-0.3	2189	92	3889	46	4			24.4/40
	0.3-0.4	2129	90	4189	48	3			33.8/41
	0.4-0.5	2106	94	4444	49	4			52.4/40
	0.5-0.6	2593	97	4295	49	4			37.7/40
	0.6-0.7	1883	86	4111	48	3			42.9/41
	0.7-0.8	1824	88	3691	44	4			49.2/40
	0.8-0.9	1465	84	3658	45	4			34.4/40
	0.9-1.0	975	65	2643	37	3			37.1/41
4-6	0.0-0.1	1592	72	2042	34	4	13	5	40.0/40
	0.1-0.2	1621	68	2032	34	2			27.4/42
	0.2-0.3	1542	69	2189	35	2			39.6/42
	0.3-0.4	1612	70	2189	35	3			40.9/41
	0.4-0.5	1456	73	2375	43	4			4.9/40
	0.5-0.6	1437	68	2117	36	3			45.9/41
	0.6-0.7	1573	65	2319	37	5			45.4/39
	0.7-0.8	1718	81	2889	40	4			47.9/40
	0.8-0.9	1323	75	3024	43	4			40.7/40
	0.9-1.0	751	37	1783	50	6			64.7/38
6-12	0.0-0.1	2017	71	1662	32	2	5		55.2/41
	0.1-0.2	2049	72	1717	33	2			72.4/41
	0.2-0.3	2044	72	1769	34	2			44.2/41
	0.3-0.4	2011	83	1900	35	6			33.4/38
	0.4-0.5	2091	81	2104	36	4			38.3/40
	0.5-0.6	1780	70	1929	35	3			40.1/41
	0.6-0.7	1731	59	1689	33	3			55.3/41
	0.7-0.8	1445	67	1767	35	4			45.2/40
	0.8-0.9	358	47	481	20	7			35.8/37
	0.9-1.0	n.d.	n.d.						
12-40	0.0-0.1	549	32	298	15	1	4		35.3/43
	0.1-0.2	535	38	342	16	4			34.9/40
	0.2-0.3	649	35	350	17	1			26.6/43
	0.3-0.4	577	39	391	17	2			38.4/42
	0.4-0.5	613	41	458	18	3			49.8/41
	0.5-0.6	555	44	512	20	4			42.3/40
	0.6-0.7	629	40	530	20	1			52.0/43
	0.7-0.8	319	34	393	17	2			50.2/42
	0.8-0.9	n.d.	n.d.						
	0.9-1.0	n.d.	n.d.						

Table 13: $\Upsilon(2S)$ yields

$p_T(\Upsilon)$	$\cos \theta^*$	Yield	σ_{yield}	Background	σ_{bkg}	Polynomial Order	Yield Systematic	χ^2/dof
2-4	0.0-0.1	960	81	3796	38	3		40.2/41
	0.1-0.2	1045	76	3849	38	2		53.7/42
	0.2-0.3	930	79	4017	27	4		27.7/40
	0.3-0.4	918	82	4101	29	3		33.8/41
	0.4-0.5	1023	86	4463	40	4		52.4/40
	0.5-0.6	1155	88	4295	55	4		37.7/40
	0.6-0.7	926	85	4111	54	3		42.9/41
	0.7-0.8	861	80	3716	38	4		49.2/40
	0.8-0.9	654	76	3658	48	4		34.4/40
	0.9-1.0	546	66	2643	40	3		37.1/41
4-6	0.0-0.1	752	63	2046	28	4		40.0/40
	0.1-0.2	778	59	2038	28	2		27.4/42
	0.2-0.3	776	60	2233	21	2		39.6/42
	0.3-0.4	782	65	2212	21	3		40.9/41
	0.4-0.5	734	65	2375	39	4		40.9/40
	0.5-0.6	865	68	2117	40	3		45.9/41
	0.6-0.7	925	45	2416	24	5		45.4/39
	0.7-0.8	895	74	2889	44	4		40.7/40
	0.8-0.9	812	78	3024	46	4		40.7/40
	0.9-1.0	528	52	1783	65	6		27.7/38
6-12	0.0-0.1	1144	60	1707	19	3		55.2/42
	0.1-0.2	1033	59	1774	19	2		72.4/42
	0.2-0.3	1288	64	1825	20	2		44.2/42
	0.3-0.4	1306	76	1962	20	4		36.0/40
	0.4-0.5	1158	71	2027	22	4		38.3/40
	0.5-0.6	1052	70	1930	19	3		40.1/41
	0.6-0.7	980	63	1689	36	3		55.3/40
	0.7-0.8	906	65	1767	37	4		45.2/40
	0.8-0.9	324	51	481	9	7		35.8/37
	0.9-1.0	n.d.	n.d.					
12-40	0.0-0.1	417	31	308	9	1		34.7/43
	0.1-0.2	389	36	312	9	4		34.9/40
	0.2-0.3	453	33	340	9	1		26.6/43
	0.3-0.4	341	33	370	10	2		38.4/42
	0.4-0.5	445	39	440	11	3		49.8/41
	0.5-0.6	509	44	513	11	4		42.3/40
	0.6-0.7	410	36	517	11	1		52.0/43
	0.7-0.8	256	34	357	11	2		50.2/42
	0.8-0.9	n.d.	n.d.					
	0.9-1.0	n.d.	n.d.					

Table 14: $\Upsilon(3S)$ yields